Monolith Loop Reactors for Fischer-Tropsch Synthesis

Doctoral Thesis
(Dissertation)

to be awarded the degree of

Doctor of Engineering (Dr.-Ing.)

submitted by

Dipl.-Ing. Robert Güttel

from Löbau

approved by the Faculty of

Mathematics/Computer Science and Mechanical Engineering,
Clausthal University of Technology.

Date of submission
October 21, 2008

Date of oral examination
February 16, 2009

Chairperson of the Board of Examiners

Prof. Dr.-Ing. Hubert Schwarze

Chief Reviewer

Prof. Dr.-Ing. Thomas Turek

Reviewer

Prof. Dr.-Ing. Georg Schaub
Universität Karlsruhe (TH)

Prof. Dr. Freek Kapteijn
Delft University of Technology

„Das also war des Pudels Kern!“

J. W. von Goethe, Faust I

Zusammenfassung

Aufgrund steigender Erdölpreise und sinkender Erdölreserven ist die Fischer-Tropsch-Synthese (FTS) weltweit wieder in den Fokus von Forschung und Entwicklung gerückt. Mit diesem Prozess können flüssige Kohlenwasserstoffe als Treibstoff aus prinzipiell jeder Kohlenstoffquelle erzeugt werden. Die wesentlichen Herausforderungen für die technische Umsetzung dieser stark exothermen Reaktion sind in der effizienten Wärmeabfuhr und der Reduktion der Stoffübergangswiderstände zu sehen. Die bisher technisch eingesetzten Suspensionsblasensäulen- (SBC) und Rohrbündelreaktoren (FBR) mit suspendiertem oder regellos gepacktem Katalysator weisen eine Reihe von Nachteilen auf. Insbesondere die notwendige Abtrennung des Katalysators von dem Produkt in der Suspensionsblasensäule und der hohe Druckverlust und die ineffiziente Wärmeabfuhr im Festbettreaktor limitieren die Effizienz des Gesamtverfahrens. Der Einsatz von neuartigen, strukturierten Katalysatoren, wie monolithischen Wabenkörpern, kann diese Nachteile eliminieren. Außerdem kann der äußere Stofftransport intensiviert werden, indem das vorteilhafte Regime der Kolbenströmung in den Minikanälen eingestellt wird.

Gegenstand dieser Arbeit ist der Einsatz von wabenförmigen struktuierten Katalysatoren in einer Schlaufenreaktoranordnung unter Kreislaufführung der Flüssigkeit für die Fischer-Tropsch-Synthese. Innerhalb der Kanäle soll Kolbenströmung vorliegen, um von dem verbesserten äußeren Stofftransport profitieren zu können. Zur Einschätzung dieses neuartigen Konzeptes sollen Vergleichsversuche mit suspendiertem pulverförmigen Katalysator in einem Rührkesselreaktor durchgeführt werden.

Im Vorfeld der Experimente wurden Simulationen durchgeführt, welche verschiedene Reaktorkonzepte für die Tieftemperatur-FTS vergleichen. Es wurden die etablierten SBC und FBR, sowie neuartige Monolithschlaufen- (MLR) und Mikrowandreaktoren (μR) berücksichtigt. Die verschiedenen Reaktoren wurden anhand der Katalysator- und Reaktorproduktivität miteinander verglichen. Außerdem wurde die Reaktorleistung bewertet und Leistungsverluste durch Wärme- und Stofftransportwiderstände quantifiziert. Es wurde festgestellt, dass SBC und μR die größte Katalysatorproduktivität erreichen. Hinsichtlich der Reaktorproduktivität nähert sich der MLR jedoch dem Niveau des SBC an, was in dem höheren Katalysatorinhalt begründet ist. Die Produktivität im MLR kann weiter gesteigert werden durch die Reduktion der Temperaturerhöhung. Damit ist der MLR zu dem SBC aus Sicht der Simulationsergebnisse konkurrenzfähig.

Zur Untersuchung von Wabenkörpern in einem Schlaufenreaktor wurde ein geeigneter Versuchsaufbau im Labormaßstab realisiert. Die Versuchsanlage besteht aus einem Rohrreaktor zum Einsatz von monolithischen Wabenkörpern und einem Rührkesselre-

aktor zur Untersuchung pulverförmiger Katalysatoren. Die Gas- und Flüssigphase kann separat im Kreislauf geführt werden, um verschiedene Strömungsregime in den Kanälen des Wabenkörpers einstellen zu können. Weiterhin wurde eine gaschromatographische Analytik aufgebaut, welche die Analyse der Gasphase sowie der flüssigen Produkte ermöglicht. Damit kann sowohl der CO–Umsatz und die CH_4–Selektivität, als auch die Kettenwachstumswahrscheinlichkeit ermittelt werden.

Außerdem ist eine Methode erarbeitet worden, welche die Herstellung von vergleichbaren waben- und pulverförmigen Katalysatoren auf Kobaltbasis ermöglicht. Die wabenförmigen Trägerstrukturen wurden mit einem pulverförmigen Katalysatorvorläufer beschichtet, welcher bereits die Aktivkomponenten Co und Re enthält. Damit kann eine gleichmäßige Verteilung des Aktivmaterials innerhalb der Kanäle gewährleistet werden. Aus dem Überstand der Beschichtungsprozedur wurde aus dem Katalysatorvorläufer Pulverkatalysator hergestellt. Ein Vergleich der waben- und pulverförmigen Katalysatoren zeigt vergleichbare strukturelle Eigenschaften. Jedoch wurden Unterschiede in der Verteilung des aktiven Materials gefunden, welche in weiterführenden Arbeiten reduziert werden können.

Abschließend wurden Versuche durchgeführt, die eine Bewertung der Wabenkatalysatoren im Schlaufenreaktor gegenüber suspendierten Katalysatoren ermöglichen. Aus den erhaltenen experimentellen Ergebnissen kann geschlussfolgert werden, dass die Raum-Zeit-Ausbeute in der FTS durch den Einsatz von wabenförmigen Katalysatoren in einer Schlaufenreaktoranordnung verbessert werden kann. Die wesentliche Ursache für diese Verbesserung kann in dem intensivierten äußeren Stofftransport gesehen werden. Weiterführende Versuche können einen entscheidenden Beitrag zur Übertragung dieser Technologie in den industriellen Maßstab leisten.

Diese Arbeit stellt einen ersten Beitrag zur Untersuchung von Wabenkörpern in einer Schlaufenreaktoranordnung für die FTS dar. Es konnte gezeigt werden, dass diese Anordnung Vorteile gegenüber Suspensionsreaktoren hinsichtlich des äußeren Stofftransports aufweist. Allerdings stellt der notwendige Kreislauf der Flüssigkeit eine Herausforderung für die technische Umsetzung dar. Weiterführende Untersuchungen können zu einer Minimierung des Aufwands für die Kreislaufführung führen und gleichzeitig die Stofftransporteigenschaften weiter verbessern.

Summary

Due to increasing oil prices and decreasing oil reserves the worldwide research interest in Fischer-Tropsch synthesis (FTS) increases. This process allows the production of liquid hydrocarbons for fuel from any carbon source in principle. The essential challenges for the technical realization of this highly exothermic reaction are the need for efficient heat removal and the reduction of mass transfer resistances. Multi tubular fixed-bed reactors (FBRs) and slurry bubble column reactors (SBCs) currently applied in industrial scale exhibit a number of disadvantages. Especially the need for catalyst separation in the slurry bubble column and the high pressure drop and inefficient heat removal in the fixed-bed reactor limit the performance of the total process. The application of novel structured catalysts, such as monolithic honeycombs, could eliminate these disadvantages. Furthermore, the external mass transfer can be intensified, by operating in the favorable slug flow regime inside the mini-channels.

The objective of this work is the application of structured honeycomb catalysts for Fischer-Tropsch synthesis in a loop-reactor alignment under recirculation of the liquid phase. Within the channels the slug flow regime is established to profit from the intensified external mass transfer. For evaluation of this novel reactor concept comparing experiments were carried out with suspended powder catalyst in a stirred tank reactor.

Prior to experiments a simulation study was carried out to compare various reactor concepts for low-temperature FTS. The established SBCs and FBRs, as well as the novel monolith loop reactors (MLRs) and micro reactors (μRs) were considered in this study. The different reactors were compared by catalyst and reactor productivity. Furthermore the reactor efficiency was evaluated and the efficiency losses due to heat and mass transfer resistances were quantified. It was revealed, that SBC and μR offer the highest catalyst productivity. However, with respect to the reactor productivity the MLR can compete with the SBC, due to the relatively high catalyst inventory. The productivity of the MLR can further be improved by reduction of the temperature increase.

Furthermore an adequate experimental setup in laboratory scale was realized, which allows for investigation of honeycombs in a loop-reactor alignment. The setup consists of a tubular reactor for investigation of monolithic honeycombs and a stirred tank reactor for application of powder catalyst. Gas and liquid phase can be recycled separately to adjust different flow regimes inside the honeycomb channels. Moreover, an analytical system was established to analyze the gas phase and the liquid products. This allows for determining the CO conversion and CH_4 selectivity, as well as the chain growth probability.

In addition, a method was developed, which allows for preparation of comparable

cobalt based honeycomb and powder catalysts. The monolithic honeycomb carriers were coated with a powder catalyst precursor, which already contains the active material Co and Re. This allows for an even distribution of active material inside the channels. The final powder catalyst was prepared from the excess of the coating slurry. A comparison between honeycomb and powder catalyst reveals similar structural characteristics. However, differences were observed in the distribution of active material, which could be improved in future work.

Finally, experiments were carried out for evaluation of honeycomb catalysts in the loop-reactor against suspended powder catalyst. The experimental results revealed, that the space-time-yield for Fischer-Tropsch synthesis could be increased by applying honeycomb catalysts in a loop-reactor alignment. The essential reason for this enhancement could be attributed to the intensified external mass transfer. Additional experiments could contribute importantly to the scale-up of this technology to industrial scale.

This work represent the first step in the research on MLRs for FTS. It can be shown, that the monolith loop-reactor alignment exhibits advantages compared to reactors with suspended catalysts with respect to external mass transfer. However, the main challenge for technical realization is the required external recycle of the liquid phase. Additional research can minimize the efforts for the liquid recycle and further improve the mass transfer characteristics.

Acknowledgement

I would like to express my deep gratitude to Prof. Dr.-Ing. Thomas Turek for the opportunity to carry out my doctoral thesis about this very interesting and challenging topic under his supervision. I am especially grateful for the demanding and constructive scientific discussions as well as his confidence in me and the project, which essentially contributed to the successful course of my graduation. In addition, I would like to thank Prof. Dr.-Ing. Georg Schaub from Universität Karlsruhe and Prof. Dr.-Ing. Ulrich Kunz for their valuable comments and suggestions regarding my work. Moreover, I would like to thank Prof. Dr.-Ing. Thomas Turek, Prof. Dr.-Ing. Georg Schaub and Prof. Dr. Freek Kapteijn for undertaking to be examiners.

I would especially thank my dear colleague and friend Dipl.-Ing. Christian Perbandt for his personal and scientific support and motivation during our shared time at Clausthal University of Technology. I would also like to thank my colleague and friend Dipl. Chem. Markus Maly for his scientific support in the first stage of my research. Furthermore, I cordially thank my former diploma students Markus Rose and Jens Knochen, who contributed greatly to this thesis. I would like to thank Dipl.-Ing. Jens Knochen in particular, for the enormous engagement in performing experiments for my doctoral theses. Additionally, I would like to express my thanks to the old hands at the institute Dipl.-Ing. Christoph Greve and Dr.-Ing. Jan Siebert for their sincere colleagueship and their help for my first steps at Clausthal University of Technology. Moreover, I would like to thank my colleague Dipl.-Ing. Christian Eisenbeis for his personal support during my work. I also thank Dipl.-Ing. Stefan Pinnow for his helpful support realizing this dissertation in LaTeX.

Furthermore I would like to thank Roland Schmidt and his colleagues from our workshop for the competent support in construction of the experimental setup. In addition, I would like to thank Dr. Anton Nagy from Integrated Lab Solutions GmbH for the support and kind motivation, which were very helpful in realizing the experimental setup. Furthermore, I thank our laboratory technician Hans Langer for his logistic talent. Thanks also go to all the people of our institute who contributed to this work.

I would like to thank my family and my friends, in particular my parents, my sister and my grandparents for their belief and support throughout my education. I especially thank my father, who shared his experience of his doctoral thesis with me and substantially, together with my mother, contributed to my motivation to do a doctorate. Finally, I would like to express my sincere thank to my girlfriend for her support and patience as well as for her encouragement and motivation during times of a petulant experimental setup.

Contents

1 Introduction

1.1 General introduction and motivation

The Fischer-Tropsch synthesis (FTS) is an almost 100 year old process to produce hydrocarbons for approximately 22 to 25 $\$\,\mathrm{bbl}^{-1}$ from any carbon source (Dry, 2001). Since the oil price has risen during the last years from 18.86 $\$\,\mathrm{bbl}^{-1}$ in 1997 to 69.04 $\$\,\mathrm{bbl}^{-1}$ in 2007 (BMWi, 2008) and further to more than 100 $\$\,\mathrm{bbl}^{-1}$ in 2008[1], the interest in FTS increased again. The German BMWi (2008) estimates the world oil resources to $\approx 165\,000\,\mathrm{Mt}$ ($\approx 1300\,\mathrm{Gbbl}$, with oil density of $800\,\mathrm{kg\,m}^{-3}$), which allows sustaining the current production levels for 42 years. For this reason alternative routes for production of liquid fuels play an important role. The OPEC estimates that the total oil production will increase from $10.6\,\mathrm{Mt\,d}^{-1}$ ($83.3\,\mathrm{Mbbl\,d}^{-1}$) in 2005 to $15\,\mathrm{Mt\,d}^{-1}$ ($117.6\,\mathrm{Mbbl\,d}^{-1}$) in 2030. The production is partly covered by producing liquid fuels from coal (CTL) or natural gas (GTL). In 2005 the CTL/GTL capacity was between 6.4 and $19\,\mathrm{kt\,d}^{-1}$ ($50 - 150\,\mathrm{kbbl\,d}^{-1}$) and will increase to between 64 and $190\,\mathrm{kt\,d}^{-1}$ ($500 - 1500\,\mathrm{kbbl\,d}^{-1}$) in 2030 (OPEC, 2007). The lower limit of this value seems not reasonable, since the available CTL/GTL capacity will already achieve $423\,\mathrm{kbbl\,d}^{-1}$ by 2010 (Guettel et al., 2008). With a reasonable CTL/GTL capacity of $1500\,\mathrm{kbbl\,d}^{-1}$ and an oil price of 100 $\$$ in 2030, the value of the synthetic liquid products will be about $150\,\mathrm{M\$\,d}^{-1}$ or $54\,\mathrm{G\$\,a}^{-1}$. It is obvious, that even small improvements of processes for the production of liquid fuels have a high effect on process efficiency and financial benefit. Both arguments are a strong driving force for research in improving FTS.

The challenge of FTS is that the reaction is highly exothermic on the one hand, which requires a good temperature management in the reactor. On the other hand, mass transfer resistances between the fluid phases and the solid catalyst, as well as inside the catalyst play an important role. In industrial application two reactor types are used,

[1] Brent, September 10, 2008

the slurry bubble column reactor (SBC) and the multi-tubular fixed-bed reactor (FBR) in trickle-flow operation mode. Both reactors exhibit several disadvantages. The SBC suffers from the need of separation of the fine powder catalyst from the liquid products, while the FBR suffers from high pressure drop, low catalyst utilization and challenging heat removal (Guettel et al., 2008).

The aim of the proposed research is to investigate the possibility of improving the Fischer-Tropsch (FT) technology significantly by applying an advantageous novel reactor system based on structured catalysts. In this thesis the monolithic honeycomb catalyst was investigated. This structure is characterized by a large number of parallel channels with a characteristic diameter of about 1 mm. The advantages are the high geometric surface area, the low pressure drop and the fixed catalyst bed. Under FT conditions gas-liquid two-phase flow will be present inside the channels, which could form different flow regimes depending on gas and liquid velocity. The slug or Taylor-flow regime is preferred, as it provides high mass transfer rates and low axial backmixing (Bauer, 2007). However, the main challenges can be seen in the manufacturing of robust catalysts with high activity and long life time at acceptable costs on the one hand and an even distribution of gas and liquid phase over the cross section on the other hand. First experimental and theoretical investigations revealed, that honeycomb catalysts are applicable in the FTS and that potential for process intensification exists (Hilmen et al., 2001, 2005; de Deugd, 2004).

1.2 Objectives and thesis structure

The objective of this work is the benchmark of monolithic honeycomb catalysts for FTS. Therefore this novel reactor system was compared to the well known slurry stirred tank reactor (STR) in the same experimental setup. Because the STR is a standard system in chemical engineering research, the obtained results can be transferred to the SBC.

The structure of the thesis is shown in Figure 1.1. The experimental work is supported by simulation studies, which reveal the significance of the research efforts on structured monolithic reactors compared to reactors established in industrial practice. Furthermore, the design of the experimental setup is based on the simulation results. The experimental work is divided in three basic tasks. Firstly, an experimental setup was built, which allows the comparison of the monolithic honeycomb catalyst in slug

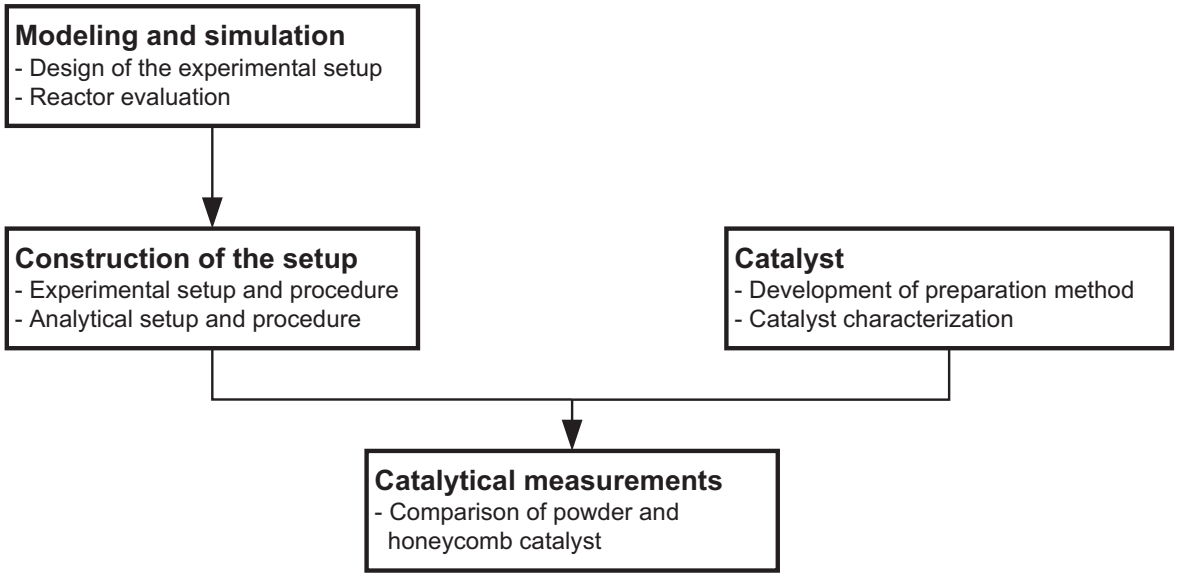

Figure 1.1: Overview of the tasks and thesis structure.

flow regime with the STR. This task also includes the setup of an analytical system to analyze the gas and the liquid phase for the estimation of the conversion and product distribution. Furthermore honeycomb and powder catalysts with comparable properties were prepared and characterized. For this purpose a preparation method was developed, which fulfills this requirement. Finally, comparing experiments were performed using the monolithic honeycomb and the powder catalyst. The results regarding the achieved reaction rate and reaction rate constant, as well as the activation energy were compared, which allows drawing conclusions on the effectiveness of the mass transfer.

The thesis document starts in chapter 2 with a review of the background of the relevant aspects. The following chapter provides a simulation study to underline the significance of research in novel monolithic honeycomb reactors for FTS against conventional SBC and FBR. Chapter 4 describes the preparation of comparable powder and monolithic catalysts. The following chapter explains the experimental and analytical setup and procedures. Chapter 6 discusses the results of the comparing experiments. Finally, general conclusions and suggestions for future work are given in chapter 7.

2 Background

2.1 Fischer-Tropsch synthesis

2.1.1 Overview

The FTS converts synthesis gas to hydrocarbons. Figure 2.1 shows the overall process for production of synthetic fuels based on FTS. In principle any carbon source can be used as raw material for synthesis gas production. The broad range of FTS products can be processed to the desired hydrocarbon fractions. The FT reaction is highly exothermic and requires the use of heterogeneous catalysts in a temperature range between 200 and 350 °C under elevated pressure (Frohning et al., 1992). Since its discovery by Fischer and Tropsch in the second decade of the 20^{th} century, FTS went through phases of rapid evolution and stagnation. This development was on the one hand caused by different economic assessment in times of changing oil prices. On the other hand specific political conditions in countries like Germany during World War II and South Africa during the Apartheid played an important role. However, in view of decreasing oil reserves and rising oil prices it is generally expected that FTS will gain great importance within the next decades for the production of synthetic fuels and petrochemical base materials from natural gas, coal, and biomass (Steynberg and Dry, 2004).

In principle different reactor technologies are suitable for performing the highly exothermic FTS. Several of these concepts have already been proven on laboratory, pilot plant, and industrial scale (Davis, 2005). One can distinguish between the so-called high temperature process, where gaseous products are formed in moving bed reactors and the low temperature process in which liquid products are also present under reaction conditions. In these more advanced low temperature processes multitubular FBR and SBC are employed industrially (Dry, 2002). However, both reactor technologies exhibit certain disadvantages. The multitubular FBR suffers from high pressure drop, low catalyst utilisation and insufficient heat removal, whereas the SBC

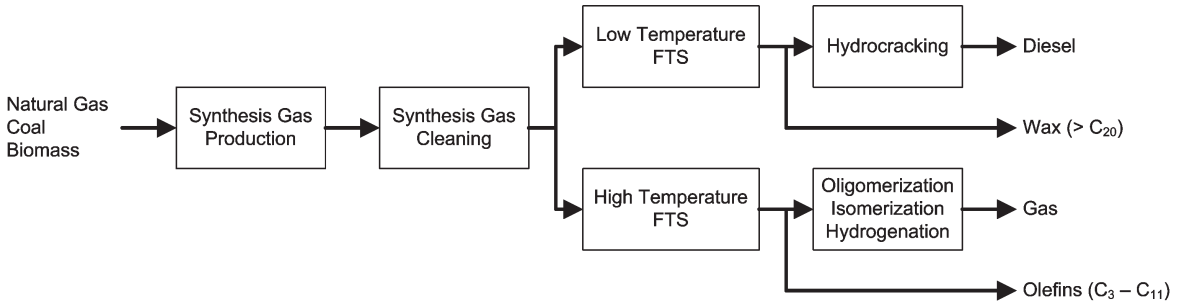

Figure 2.1: Overall process for production of liquid fuels by FTS (Guettel et al., 2008).

faces the need for catalyst separation and highly demanding scale-up. These drawbacks lead to investigations towards improved reactor technologies that might become industrially applicable in a medium and long term perspective.

For intensification of mass transfer between synthesis gas, liquid products and solid catalysts alternative catalyst geometries like honeycombs, structured packings and foams have been developed. An enhancement of mass transfer characteristics while maintaining isothermal operation can be achieved by using micro reactors (μRs). Finally, the coupling of FTS reaction with separation of the inhibiting product water using membrane reactors will be discussed. The present chapter starts with the historical development of FTS reactor technologies revealing a surprising diversity of applied reactor types. Based on the state of the art for low temperature FTS, chances and challenges of emerging reactor technologies will be critically discussed.

2.1.2 Historical development

The FTS has its origin in Germany at the beginning of the 20th century, where groundbreaking progress for several processes under elevated pressure was made. Haber and Bosch developed the ammonia synthesis in 1908, Bergius worked on the direct hydrogenation of coal in 1913, and at the beginning of the second decade, methanol synthesis was achieved on technical scale by BASF. Based on previous work by BASF (BASF, 1913), Fischer and Tropsch began to develop the synthesis of hydrocarbons from synthesis gas at the Kaiser Wilhelm Institut für Kohlenforschung in Mülheim (Ruhr), Germany, in 1920 (Fischer and Tropsch, 1923). This new process was filed as patent in 1925 (Fischer and Tropsch, 1925).

Table 2.1: Existing plants and plants under construction for FTS (values in $kt\,a^{-1}$ calculated with assumed average product density of $800\,kg\,m^{-3}$) (Guettel et al. (2008), updated).

Company	Site	Capacity [bpd ($kt\,a^{-1}$)]	Raw material	Date of commissioning
Existing plants				
Sasol	Sasolburg	2500 (120)	Coal	1955
Sasol	Secunda	85 000 (4000)	Coal	1980
Sasol	Secunda	85 000 (4000)	Coal	1982
MossGas	Mossel Bay	30 000 (1400)	Natural gas	1992
Shell	Bintulu	12 500 (580)	Natural gas	1993
Sasol/Qatar Petroleum	Qatar	34 000 (1600)	Natural gas	2006
Under construction				
Shell	Qatar	140 000 (6500)	Coal	2010
SasolChevron	Escravos	34 000 (1600)	Natural gas	2010

As early as 1935, the first commercial plants were installed by Ruhrchemie in Oberhausen, Germany. In the 1940s, the total German production capacity of liquid fuels on FTS basis reached $600\,kt\,a^{-1}$ in 9 plants operating with cobalt catalysts (Dry, 1990). In all cases, the synthesis gas was produced from coal (Steynberg and Dry, 2004). In addition, nearly $3\,Mt\,a^{-1}$ liquid fuels were produced by direct coal liquefaction according to the Bergius-Pier process. During World War II, further FTS plants based on Ruhrchemie licenses were built in Japan.

After World War II, interest in further development of FTS remained strong. Ruhrchemie and Lurgi developed a fixed bed process based on iron catalysts. These so-called ARGE reactors were installed for the first time in Sasolburg, South Africa, in 1955. In the USA, remarkable effort for the development of commercial FTS processes was also undertaken. Between 1951 and 1957, a FTS pilot plant was operated in Brownsville, Texas (Davis, 2005). The development in the USA was focussed on fluidized bed reactors for high temperature FTS, as it was subsequently applied in the South African industry.

In the mid-1950s, it became evident that FTS was uneconomical at the extremely low oil prices of that time. The "oil era" began and except in South Africa, all other developments in FTS were stopped. Until the first oil crisis in the 1970s, FTS was almost exclusively developed further in South Africa. The current production capacity in South Africa amounts to approx. $9\,Mt\,a^{-1}$ (200 000 bpd barrel per day). As raw

material for synthesis gas production, coal (Sasol), and to an increasing extent, natural gas (PetroSA) are used. Different processes and reactor technologies have been used in South Africa. Stationary and circulating fluidized bed reactors are used for the high-temperature process to produce more olefinic products with short chain lengths. The modern low-temperature process for the manufacture of waxy products has been performed in SBC since the 1990s.

In 1973, Shell began the development of the ShellMiddle Destillate Synthesis (SMDS). This process is based on the FBR technology and employs cobalt catalysts. In 1993, a FTS plant based on natural gas with a capacity of 12 500 bpd was placed into operation in Bintulu, Malaysia (Sie, 1998). The current, most economic way to produce synthesis gas is the direct usage of natural gas that is obtained as by-product from oil production and whose transportation would be too expensive. This production of liquid products from natural gas (Gas To Liquid, GTL) is currently being realized on industrial scale at several sites. Commissioning of a plant with a capacity of 70 000 bpd built by Sasol and Qatar Petroleum occurred in June 2006 in Qatar (Fleisch, 2006). Further large-scale industrial plants in Escravos, Nigeria (SasolChevron), and Qatar (Shell, Qatar Petroleum) are under construction. After finishing these projects, the worldwide capacity for FTS fuels will increase to almost $30\,\mathrm{Mt\,a^{-1}}$ in 2010 (Schaub et al., 2006) (Table 2.1).

Besides natural gas, the usage of coal for synthesis gas production has intensively been discussed. Particularly coal-rich countries like the USA and China intend to apply indirect coal liquefaction (Coal To Liquid, CTL) by conversion of synthesis gas using FTS (Hao et al., 2007). These economically understandable developments may be discussed critically in view of the possible consequences for anthropogenic climate change. Because of its insufficient hydrogen content, especially the use of coal gives rise to additional CO_2 emissions during the production of liquid hydrocarbons (Schaub, 2006). In the long term, a CO_2 neutral way could be the production of synthesis gas from biomass and its subsequent liquefaction by FTS (Biomass To Liquid, BTL).

2.1.3 Reaction

The basic FT reaction can be described as formation of paraffinic or olefinic chains (Equations 2.1 and 2.2):

$$\mathrm{nCO} + (2\,\mathrm{n} + 1)\,\mathrm{H_2} \longrightarrow \mathrm{C_nH_{2n+2}} + \mathrm{nH_2O} \tag{2.1}$$

$$\mathrm{nCO} + 2\,\mathrm{nH_2} \longrightarrow \mathrm{C_nH_{2n}} + \mathrm{nH_2O} \tag{2.2}$$

The main reaction (Equation 2.1) is highly exothermic with a reaction enthalpy of $\approx -150\,\mathrm{kJ\,mol^{-1}}$ converted CO. The co-product, H_2O, can be converted with CO to carbon dioxide and hydrogen in the water/gas shift reaction; see Equation 2.3:

$$\mathrm{CO} + \mathrm{H_2O} \rightleftharpoons \mathrm{CO_2} + \mathrm{H_2} \tag{2.3}$$

Undesirable side reactions are the formation of methane (Equation 2.4) and the Boudouard reaction (Equation 2.5). In addition, alcohols can be formed in small amounts (Equation 2.6).

$$\mathrm{CO} + 3\,\mathrm{H_2} \rightleftharpoons \mathrm{CH_4} + \mathrm{H_2O} \tag{2.4}$$

$$2\,\mathrm{CO} \rightleftharpoons \mathrm{C} + \mathrm{CO_2} \tag{2.5}$$

$$\mathrm{nCO} + 2\,\mathrm{nH_2} \longrightarrow \mathrm{C_nH_{2n+2}O} + (\mathrm{n}-1)\,\mathrm{H_2O} \tag{2.6}$$

2.1.4 Product distribution

Anderson (1956) considered the FTS as an ideal polymerization reaction with the monomer $-CH_2-$. Following this approach, the distribution of mole fractions x_n and mass fractions x_m of products can be described as a function of the number of carbon atoms n_c in the chain and the chain growth probability α using the Anderson-Schulz-Flory distribution (Equations 2.7 and 2.8) (Unruh, 2006). The dependency of the logarithmic molar fraction of one component on the chain length of this component can be displayed in the ASF plot (Figure 2.2). In the ideal case the ASF plot shows a straight line with the slope α. The mass and mole specific product composition with increasing chain growth probability is shown in (Figure 2.3). The production of long

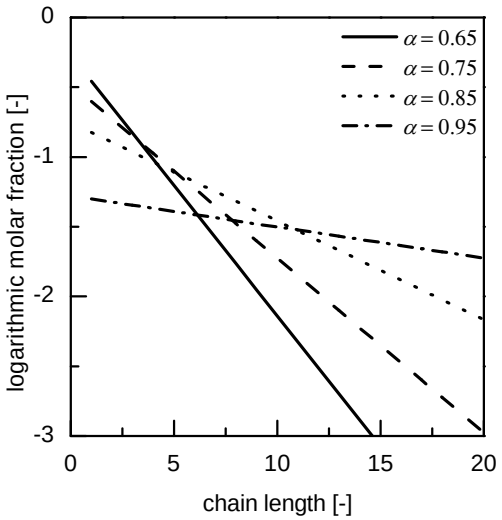

Figure 2.2: ASF plot for different chain growth probabilities (Unruh (2006), redrawn).

hydrocarbon chains ($\alpha > 0.9$) is favored, which can be cracked and isomerized to the desired product.

$$x_n = (1-\alpha)\,\alpha^{n_c-1} \tag{2.7}$$

$$x_m = n_c\,(1-\alpha)^2\,\alpha^{n_c-1} \tag{2.8}$$

In reality, significant deviations from the ideal polymerization behavior are observed. Usually the methane mole fraction is higher, while the ethene/ethane mole fractions are lower than calculated. Furthermore, the real product distribution is characterized by an increase in the chain growth probability in the range of C_8 to C_{12} (Riedel, 2002).

2.1.5 Reaction kinetics

Because of the complex reaction mechanism, the wide range of involved components and the diversity of catalyst compositions several kinetic reaction rate expressions can be found in the literature (van der Laan and Beenackers, 1999). The kinetic approaches range from simple power law expressions (Post et al., 1989), over Langmuir-Hinshelwood-Hougen-Watson approaches (Yates and Satterfield, 1991; Riedel and Schaub, 2003) to complex micro kinetics of the elementary steps (Storsæter et al., 2006; Visconti et al., 2007).

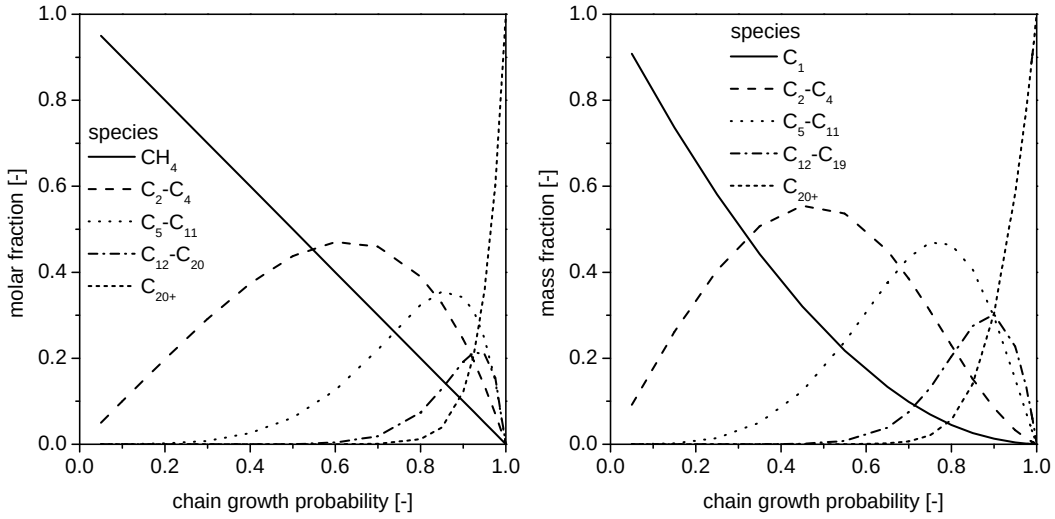

(a) molar fraction (b) mass fraction

Figure 2.3: Product distribution in FTS as a function of chain growth probability (Guettel et al., 2008).

The reaction rate of FTS is often influenced by pore diffusion processes because the pores are generally assumed to be filled with liquid products. Post et al. (1989) showed that the catalyst efficiency is significantly reduced at characteristic catalyst dimensions of more than 100 µm. However, since the activity of modern and future catalysts is higher than of the catalysts used by Post et al., internal mass transfer limitations can occure at significantly smaller characteristic dimensions. Furthermore, the selectivity can be negatively influenced by pore diffusion effects. Caused by the higher diffusion coefficient of hydrogen compared to carbon monoxide, the H_2/CO ratio inside the porous catalyst will increase. This leads to an increase of the chain termination probability and thus to a decrease in chain length of the products (Wang et al., 2001).

2.1.6 Catalysts

As FTS catalysts, metals from the VIII B group of the periodic table like iron, cobalt, and ruthenium can be used (van der Laan and Beenackers, 1999). Due to the high cost of ruthenium, solely iron and cobalt have industrial relevance. A disadvantage of iron catalysts is the kinetic inhibition by the co-product water, whereas an advantage is the activity for water/gas shift reaction that allows the use of carbon dioxide containing or

hydrogen depleted synthesis gas mixtures (Riedel, 2002). However, the water/gas shift reaction could also lead to a loss of carbon monoxide by formation of carbon dioxide. Compared to iron, cobalt catalysts are already active at lower reaction temperatures and have a durability of up to 5 years on stream compared to about 6 months in the case of iron (Davis, 2005). On the other hand, cobalt is more expensive than iron (van Steen and Claeys, 2008). In addition to the active component, different promoters (Pt, Pd, Ru, Re, K) can be employed (Oukaci et al., 1999). As carrier materials, alumina, silica, and titania – in earlier catalysts also ZnO – can be utilized (Fischer and Tropsch, 1923; Storsæter et al., 2005b). Typical chain growth probabilities are 0.5 – 0.7 for iron and 0.7 – 0.8 for cobalt (Dry, 1982). Currently, the development of cobalt catalysts is aimed at maximizing the chain growth probability to values of up to 0.95 (Sie, 1998).

2.2 Reactors for Fischer-Tropsch synthesis

Modern FT processes for the production of liquid fuels are low-temperature processes, where synthesis gas, liquid products, and solid catalysts are present. Reactors for high-temperature processes are not discussed in this chapter. Details concerning these reactors can be found in Steynberg and Dry (2004) and Davis (2005).

2.2.1 Reactors developed in Germany

The first industrial FT process was developed by Ruhrchemie in the third decade of the 20^{th} century. In this process, a FBR under atmospheric pressure was used which was cooled by evaporating water. In this "Normaldruck-Synthese", the catalyst was located between parallel plates, while the cooling water was transported in tubes. An enhancement was a process at medium pressure ("Mitteldruck-Synthese") developed by Fischer and Pichler, where multitubular reactors with the catalyst located in the gap of concentric tubes were used. A flow of cooling water inside the inner tubes as well as outside the outer tubes was used to remove the heat of reaction (Sie, 1998).

Another possibility for heat removal in FBRs is the application of sufficiently large gas recycles with external heat removal under adiabatic reactor operation. This mode of cooling was used in the "Michael" process by IG Farben. A hybrid between direct and indirect cooling of a FBR was used in the commercialized ARGE process after World War II. In this process, the water cooling system, known from atmospheric and medium

Table 2.2: Reactor technologies for low-temperature FTS investigated between 1935 and 1955 (Guettel et al., 2008).

Process	Reactor type	Cooling system
Ruhrchemie "Normaldruckverfahren"	FBR with catalyst between parallel plates	Water internal
Ruhrchemie "Mitteldruckverfahren"	FBR with catalyst in gap between concentric tubes	Water internal
IG Farben "Michael-Verfahren"	FBR	External gas recycle
ARGE "Hochlast-Synthese"	Multitubular FBR	Water internal + external gas recycle
Lurgi "Stufenofen"	Segmented FBR	Distributed feed of fresh gas + external gas recycle
BASF "Duftschmidt-Verfahren"	FBR	External liquid recycle
BASF "Schaumverfahren"	Suspension reactor with powder catalyst	External liquid recycle
"Rheinpreussen-Koppers-Synthese"	Suspension reactor with powder catalyst	Water internal + external liquid recycle

pressure processes, was combined with a recycle of gas at incomplete conversion (Sie, 1998; Davis, 2005). Besides the gas phase, also the liquid phase can be recycled for external heat removal which was investigated in the "Duftschmidt" process by BASF. Finally, the possibility of cooling by distributed feed of fresh synthesis gas to a segmented fixed bed was achieved by Lurgi in a multiple bed technology ("Lurgi-Stufenofen").

In addition to FBRs, also reactors with suspended catalysts are a viable option for gas-liquid reactions. BASF investigated the suitability of these reactors in the "Schaumverfahren" with iron catalysts at temperatures of about 250 °C. The reaction heat was removed externally by recycling of liquid. Early investigations by Fischer regarding the feasibility of suspended catalyst reactors were continued by Kölbel and coworkers during and after World War II (Schulz, 1999). After World War II, a first pilot plant was operated using an iron catalyst. Unlike the BASF "Schaumverfahren", this "Rheinpreußen-Koppers" synthesis was characterized by internal cooling with water.

The different reactor types for low-temperature FTS investigated in Germany between 1935 and 1955 are summarized in Table 2.2. The various possibilities can be grouped as follows:

- internal cooling in suspended reactors or FBRs
- external cooling by gas or liquid recycle in suspended reactors or FBRs
- direct cooling by distributed feed of fresh synthesis gas in staged FBRs

It is impressive to see how within a relatively short span and under difficult conditions, all reactor types were investigated, that are principally feasible for performing highly exothermic heterogeneously catalyzed gas-liquid reactions, although the fundamentals of heterogeneous catalysis and reaction engineering were not yet completely developed at that time.

2.2.2 State of the art and challenges

The medium pressure process ("Mitteldruck-Synthese") developed by Fischer and Pichler was commercialized by Ruhrchemie and Lurgi after World War II. In 1955, Sasol used this technology to build the first plants in Sasolburg, South Africa. These still used ARGE reactors are operated at 25 bar and at a temperature of 200 – 300 °C (Steynberg and Dry, 2004; Davis, 2005). They consist of 2052 parallel tubes with diameters of 4 cm (Figure 2.4a) (Davis, 2005; Schulz, 1999). The entire reactor is 12.8 m long, has a diameter of 2.95 m and a catalyst inventory of 40 m^3. Compared to the early German multitubular reactor technology, the ARGE reactors were operated with a recycle of unconverted synthesis gas to support the internal heat removal. In combination with higher reaction temperatures and pressures, this led to an increase of production capacity by a factor of 25 (Krishna and Sie, 2000).

In 1973, Shell began to develop the Shell Middle Distillate Synthesis (SMDS), which was also based on the FBR technology using cobalt catalysts. This technology was partly based on work by Gulf, who had successfully operated tubular reactors with a diameter of 2.54 cm and a length of 12.2 m over several months (Davis, 2005). Shell began building a plant with a capacity of 12 500 bpd in Bintulu, Malaysia, which was commissioned in 1993 (Davis, 2005; Sie, 1998).

Multitubular FBRs are widely applied to carry out exothermic reactions. They are easy to handle and to design because the parallel tubes behave very similarly. However, multitubular reactors exhibit disadvantages. To minimize the pressure drop, the catalyst dimension should be chosen between 1 and 3 mm (Sie, 1998). This leads to a

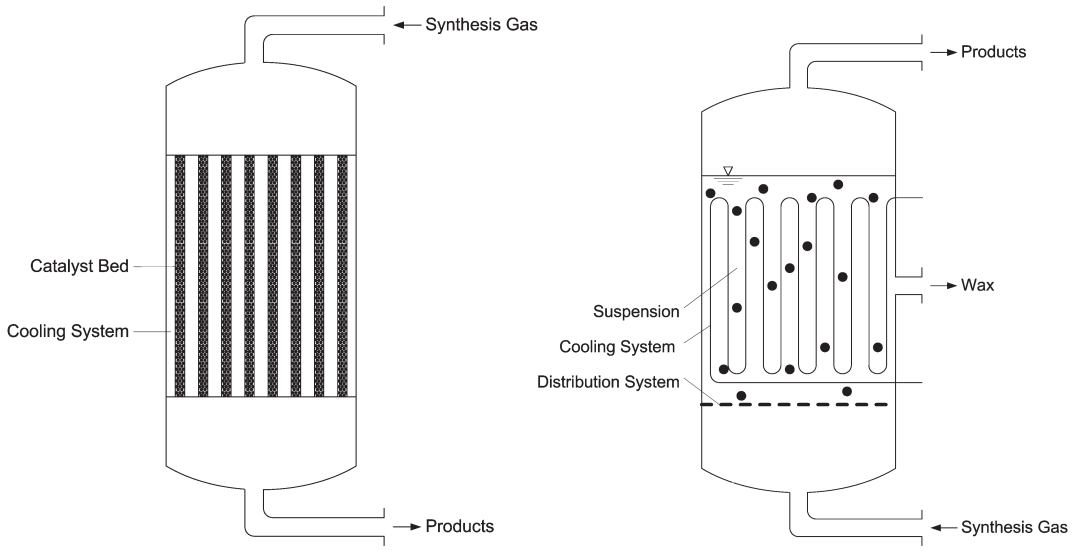

(a) multitubular fixed-bed reactor (b) slurry bubble column reactor

Figure 2.4: Technically established reactors for FTS (Guettel et al., 2008).

decrease of catalyst utilization and to undesirable effects on product selectivity. Furthermore, in tubes with diameters of several centimetres, as used in the industry, hot spot formation will occur. To prevent damage of the catalyst, the temperatures of both feed and cooling medium have to be chosen significantly lower than the maximal possible temperature. This gives rise to a decrease in reactor productivity. Moreover, the capital costs of multitubular reactors are relatively high.

The second reactor type which is industrially used for FTS is the SBC with suspended catalyst (Figure 4.6b). Sasol began the development of iron-based SBC in the eighth decade of the 20th century (Steynberg and Dry, 2004). Since the early nineties, a commercial plant based on the cobalt catalyst with a capacity of 2500 bpd has been operated in South Africa. Sasol and Qatar Petroleum recently commissioned a reactor in Qatar with a capacity of 11 000 bpd, a diameter of 11 m and a height of 60 m.

In SBC, fine catalyst powders with dimensions of 10 to 200 µm are used (Steynberg and Dry, 2004). Thus, the influence of internal mass transfer resistances are negligible and optimal activity and selectivity can be achieved. Internals assure efficient heat removal from the reactor that allows for a nearly isothermal operation. Due to the higher achievable catalyst fraction of up to 20 vol% (15 vol% in the FBR), the enhanced catalyst utilization and the higher average reactor temperature, the reactor productivity of a SBC should be higher than of a FBR. The possible influence of axial dispersion

in FTS bubble columns on productivity has been discussed controversially. While Fox (Fox, 1990) postulated a strong negative effect on the space-time-yield, Steynberg and Dry (Steynberg and Dry, 2004) saw no reason for such an assumption. The latter assessment appears to be more plausible because the backmixing of the inert liquid products should have no influence, while the residence time distribution of synthesis gas in a reactor with a sufficiently high length-to-diameter ratio should not significantly differ from ideal plug-flow behavior.

Nevertheless, two aspects decelerated the commercialization of SBC for FTS. Both separation of the solid catalyst from the liquid products and the scale-up of these reactors are major challenges for industrial use of SBC. For example the operation rate of the Oryx-GTL plant in Qatar, operated by Sasol and Qatar Petroleum, was constrained by the filtration of fine material[1]. Generally, time and cost intensive pilot-plant studies with reactors of different diameters have to be conducted for a successful scale-up. Only recently, adequate models for FTS in SBC have been developed that may facilitate scale-up in the future (van der Laan, 1999; Krishna and Sie, 2000; Krishna, 2000; Krishna and van Baten, 2003).

Advantages and disadvantages of both established reactor technologies are summarized in Table 2.3. It can be concluded that until now, no reactor concept is available that combines optimal features in all relevant aspects. An ideal reactor would have the following characteristics:

- fixed bed catalyst
- high catalyst efficiency due to short diffusion lengths
- highly efficient gas-liquid mass transfer
- isothermal operation at highest possible temperatures

The following chapter deals with strategies to achieve these aims and with other alternatives for process intensification in FTS currently under investigation.

2.2.3 Possibilities of process intensification

The specific drawbacks of the commercially established FBR and SBC reactors lead to investigations of improved reactor technologies that might become applicable in a

[1] Investor Insight, July 2007, Sasol.

Table 2.3: Advantages (+) and disadvantages (–) of established reactors for FTS (partly from Sie (1998)).

	FBR	SBC
Pore diffusion	–	+
Catalyst inventory in reactor	+	–
Gas-liquid mass transfer	+	–
Isothermal behavior	–	+
Catalyst exchange	–	+
Catalyst attrition	+	–
Need for liquid-solid separation	+	–
Scale-up	+	–
Reactor costs	–	+

medium and long term perspective. In this context this chapter deals with novel structured catalysts and reactors and membrane reactors.

Structured catalyst geometries are characterized by a non-randomly ordered fixed bed of catalysts. Important examples are catalytic packings, honeycomb or foam shaped catalysts, which are reviewed extensively by Pangarkar et al. (2008) with respect to hydrodynamic and heat and mass transfer characteristics. The main conclusion in this review is, that strucutred packings will overcome the disadvantages of lower catalyst inventories and higher costs over randomely packed beds in the near future. This work is focussed on honeycomb shaped structured catalysts applied in the so called monolith loop reactor (MLR), which will be discussed in detail later.

Metal-based structures for FTS were investigated by Meshcheryakov et al. (Meshcheryakov et al., 1999a,b). The monolithic carrier made of stainless steel was coated with catalyst. This catalytic packing was operated as gas lift reactor by feeding synthesis gas to the bottom. The liquid phase was circulating inside the reactor which was caused by vertical density differences.

Also possible, but not yet demonstrated, is the application of foams for FTS. Solid foams were originally developed as filters for molten metals. They are increasingly more often used as catalyst carrier materials in chemical engineering (Twigg and Richardson, 2002; Reitzmann et al., 2006). Foams are characterized by an open structure consisting of interconnected bridges and void spaces. Advantages are good axial and radial heat and mass transfer combined with a low pressure drop.

Another approach for process intensification during FTS is the use of μRs. As in honeycombs, the parallelization of a large number of small channels gives rise to good mass transfer characteristics. Furthermore, heat transfer is intensified to an extent, where isothermal operation even for highly exothermic reactions becomes possible (Klemm et al., 2003). μRs are especially suitable for modern highly active catalysts, which are under development for future FT processes.

Only a few results on the use of μRs for FTS have been reported until now. Scientific and patent literature concentrates on catalyst development (Wang et al., 2003a; Schanke et al., 1996; Wang et al., 2002; Guillou et al., 2007) and the benefits of the enhanced heat and mass transfer characteristics (Wang et al., 2005). The application of this new technology for the production of liquid fuels appears to be especially promising for decentralized and mobile applications. However, it has also been proposed for large-scale plants with capacities up to 50 000 bpd. It has been claimed that capital cost can be reduced significantly using μRs at high conversions and low methane selectivity (Jarosch et al., 2005).

A recent development concerns the use of membrane reactors in FTS. These reactors may also have potential in small or medium plants for future off-shore or BTL applications. Four concepts to use membrane reactors in FTS have been proposed in the literature (Rohde et al., 2005a):

- distributed feed of reactants
- in situ removal of water
- forced-through membrane contactor
- zeolite encapsulated catalysts

The distributed feed of reactants through a membrane allows for better temperature control. Furthermore, the methane selectivity can be influenced, because it depends on the H_2/CO-ratio. Thus, a distribution of H_2 in a stream of CO can lead to an increase in the yield of heavy products (Rohde et al., 2005a).

The group of Schaub from the University of Karlsruhe in Germany investigated in situ water removal with membranes. Water produced during FTS may negatively influence the reaction by reoxidation of catalysts, increasing water/gas shift activity and decreasing partial pressures of the educts. The in situ removal of water requires highly

selective membranes for effective removal of water without loss of educts (Rohde et al., 2005a,b; Unruh, 2006).

In the literature, two approaches for application of forced-through membrane contactors were described. Khassin et al. (Khassin et al., 2003, 2005a,b) use thermally conductive contactor modules (plug-through contactor membrane, PCM). Synthesis gas enters the inner void space and flows through the membrane with a thickness of 2.5 mm. To enhance the thermal conductivity, metallic copper was added during the membrane production. Thus, high space-time-yields at flat temperature profiles can be achieved. Bradford et al. (Bradford et al., 2005) coated a monolithic membrane module with a catalyst layer. The synthesis gas was fed from shell side to the alumina carrier material and forced through the membrane to the catalyst. The membrane was impermeable for the produced hydrocarbons, which can be withdrawn from the tube side.

He et al. presented another membrane application for FTS using encapsulated catalysts. This concept is based on a combination of a FT catalyst and an acidic zeolite. Educts are diffusing through the zeolitic membrane to the catalyst where the reaction takes place. The products also have to pass the zeolite where hydrocracking and isomerization occurs. This leads to a sharper chain length distribution in the product (He et al., 2005).

In the field of membrane reactors for FTS, further research activities are expected. This effort will be focused on the development of new membrane materials and reactor configurations (Rohde et al., 2005a).

2.3 Reactors with monolithic honeycomb catalysts

Roy et al. (2004) and Cybulski and Moulijn (2006) reviewed the state of knowledge about monolithic honeycomb catalysts, covering the catalyst preparation, multiphase flow in the structures, reactor modeling and application in gas and gas-liquid processes. This chapter summarizes the relevant aspects of monolithic honeycomb catalysts.

2.3.1 Monolith loop reactor

Monolithic honeycomb catalysts, which have been used in exhaust gas cleaning for many years, consist of a large number of identical, parallel channels with a cell density of 25 up to 1200 cpsi (channels per square inch). Regarding its characteristic dimension of about

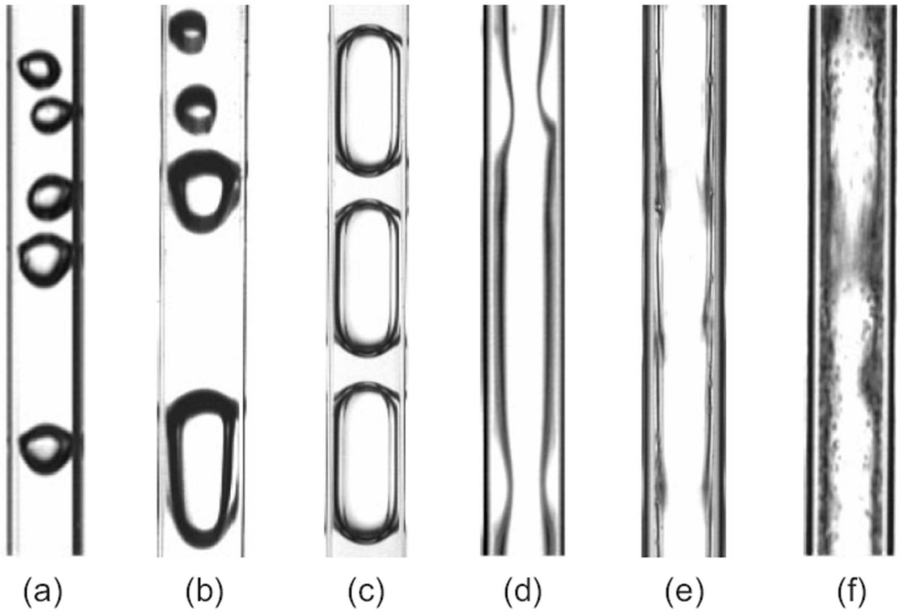

Figure 2.5: Flow regimes in honeycomb MRs; a) bubbly flow, b) transition bubble to slug flow, c) slug or Taylor flow, d) transition slug to film flow, e) film flow, f) churn flow (Bauer et al., 2005b).

1 mm, honeycombs can be classified as mini-structured between conventional fixed beds and μRs (Liu, 2002). However, since the characteristic dimension of honeycombs is at the edge of microtechnology as defined by Klemm et al. (2003), it can also be classified as micro-structure. The main advantages of structured honeycomb catalysts are low pressure drop, high geometric surface area, high mass-transfer coefficients, and short diffusion lengths. The thickness of the catalyst layer can be adjusted to achieve catalyst effectiveness factors close to 1. The external mass transfer is positively influenced by the large surface area and can further be increased by choice of the optimal flow regime inside the capillaries (Figure 2.5) (Simmons et al., 2003). In contrast to fluidized bed catalysts, there is no need for catalyst separation and little danger of catalyst attrition. The low radial heat transfer can be seen as drawback in some applications (Kapteijn et al., 1999; Roy et al., 2004; Kapteijn et al., 2005).

The slug flow regime ("Taylor flow regime") is of particular interest because of the high achievable mass transfer coefficients combined with a low pressure drop. This flow regime is characterized by elongated gas bubbles separated from each other by liquid slugs and from the channel wall by a thin liquid film. Due to friction at the channel walls,

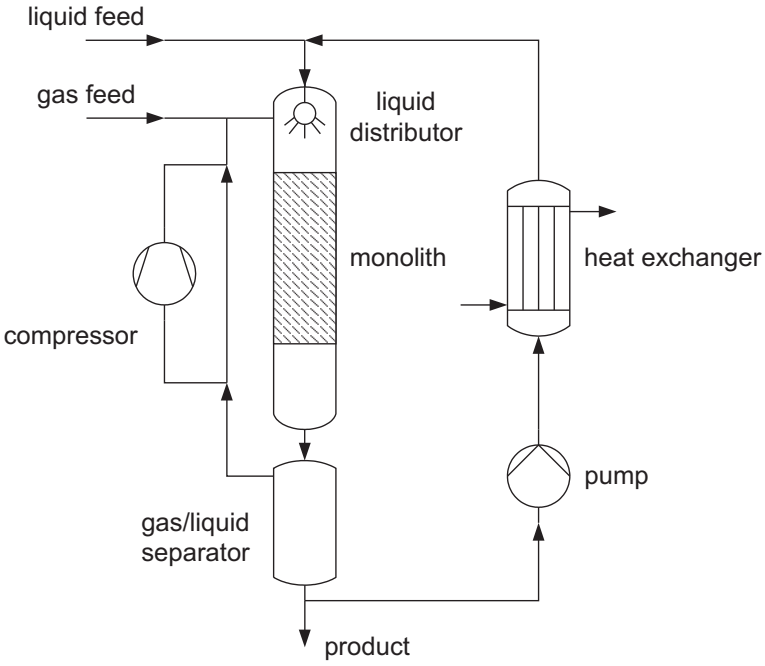

Figure 2.6: Loop reactor concept (redrawn from Heiszwolf et al. (2001b)).

circulation within the liquid slugs occurs that enhances the gas-liquid mass transfer. The back mixing along the channel length is diminished by the presence of gas bubbles, which segregates the liquid phase in isolated liquid slugs (Kreutzer, 2003). Depending on the physical properties of the gas and liquid phase slug flow occurs up to a gas and liquid superficial velocity of $1\,\mathrm{m\,s^{-1}}$ for the nitrogen/water-system and $0.1\,\mathrm{m\,s^{-1}}$ for the nitrogen/squalane-system at 20 bar and 20 °C (Bauer, 2007).

Due to the poor radial heat conductivity of honeycombs, these reactors have to be operated adiabatically. For this reason, Moulijn and coworkers from the TU Delft in The Netherlands suggested to limit the adiabatic temperature rise by recycling of liquid product, while the reaction heat will be removed in the external recycle (Heiszwolf et al., 2001a; de Deugd et al., 2003b) (Figure 2.6). The MLR consists of a tubular reactor for the monolithic catalyst, a gas-liquid separator, a pump and a heat exchanger. The MR is operated in gas-liquid two phase flow. Gas and liquid will be separated in the gas-liquid separator. Subsequently, the liquid will be recycled by the pump and the reaction heat will be removed by the heat exchanger in the liquid recycle. Because of the low pressure drop in the MR, the liquid can be recirculated at high flow rates. The gas phase can also be recycled. One advantage of the MLR arise from the separated heat

and mass transfer section. This allows to scale heat and mass transfer separately, which is an additional degree of freedom in design compared to conventional fixed-bed and fluidized-bed reactors. Further advantages are, that (I) catalyst and product remain separated, (II) no attrition of the catalyst occurs, (III) high gas to liquid mass transfer could be achieved in the slug flow regime and (IV) simple reactor construction as well as (V) energy-effcient operation (Heiszwolf et al., 2001b,a).

The application of catalytically active honeycombs for FTS was first investigated by the Holmen group from the Norwegian University of Science and Technology (NTNU), Trondheim (Hilmen et al., 2001). Continuative, de Deugd investigated ceramic honeycombs with a cobalt catalyst in the gas phase (de Deugd et al., 2003c; de Deugd, 2004; Kapteijn et al., 2005). For the first time, Holmen et al. (Hilmen et al., 2005) carried out experiments with recirculation of liquid to achieve a better temperature control and to prevent reactor runaway. In the cobalt-based honeycomb catalyst employed, a two-phase flow in the film regime was obtained by recirculation of the liquid. However, the suggested concept with liquid recycle to achieve slug flow in the honeycomb channels has not yet been investigated in these laboratories.

2.3.2 Preparation of monolithic honeycomb catalysts

The monolithic honeycomb structure can be prepared from ceramic, metal or plastics (Heck et al., 2001). According to Avila et al. (2005) one can distinguish between two different types of ceramic monoliths, (I) low surface area monoliths and (II) high surface area monoliths, whose preparation paths are illustrated in Figure 2.7.

Low surface area monoliths are typically extruded from ceramic materials like cordierite ($2\,MgO \cdot 2\,Al_2O_3 \cdot 5\,SiO_2$) which are coated by a catalyst layer ("washcoat"). The catalyst layer consists of a porous material such as alumina, titania, silica or carbon which is impregnated with the active phase. The high surface area monoliths are directly extruded from porous material which provides a high internal surface area. This approach allows to achieve higher catalyst loadings in the reactor. Honeycombs can be produced in various geometries, both for small- and large-scale applications (Kapteijn et al., 2001). This work is focussed on the preparation method for low surface area ceramic monoliths.

The preparation of monolithic catalysts, which was reviewed by Nijhuis et al. (2001a), is divided in three preparation steps, (I) the extrusion of the monolithic structure, (II)

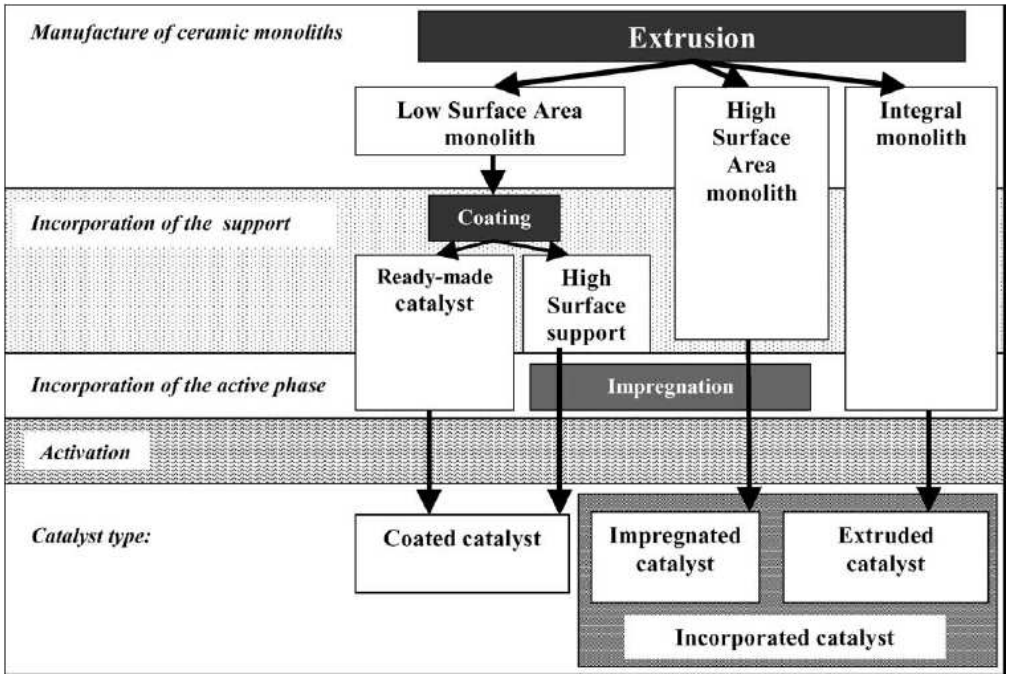

Figure 2.7: Preparation of ceramic monolithic catalysts (Avila et al., 2005).

the incorporation of the porous support and (III) the incorporation of the active phase. The extrusion of the structure will not be discussed here, as it can be obtained ready-made from producers.

The most common method to increase the internal surface area of low surface area monolithic carriers is the "washcoating" by a slurry of porous particles. The advantages of this technique are the small diffusion lengths, the possibility of direct coating of ready-made catalysts and the high catalyst loading. The washcoat quality depends on the solid and liquid properties, the mass fraction of solid in the suspension, the suspension viscosity and the calcination temperature (Nijhuis et al., 2001a; Avila et al., 2005). The slurry for coating consists of a powder with a mean particle diameter of a few micro meters suspended in water. Optionally, binder for increasing the coating strength and acid for changing the pH of the suspension can be added. The monolith carrier is dipped in a slurry of the porous particles for about 1 min. In this time the porous monolithic carrier absorbs water from the suspension and a cake of porous particles develops on the walls. The excess of the slurry is removed gently by pressurized air. Finally, the coated monolith is dried at temperatures right below 100 °C and subsequently calcined. The calcination temperature is typically at least 400 °C. The calcination step is important,

as it binds the washcoat to the monolith walls. Per coating step typically about 10 wt% washcoat can by deposited on the walls. To achieve higher washcoat loadings, the coating procedure can be repeated (Nijhuis et al., 2001a). The adhesion of the coating on the monolithic carrier depends on the particle size of the ceramic powder in the slurry (Agrafiotis et al., 1999). It is suggested, that the particle size is in the range of the macro pores of the carrier, which corresponds to about 5 µm. To further increase the adhesion of the washcoat on the monolith a binder material can be used, with a particle size of about two orders of magnitude smaller. The amount of binder should be about 10 wt% of the total amount of solids. The total amount of solids in the suspension should be about 40 to 50 wt% (Nijhuis et al., 2001a).

The incorporation of the active phase on the monolithic support can be carried out using the same methods applied in conventional catalysts in pellet or powder form. Usually, a high dispersion of the active phase is desired, since the surface area of the active phase and thus the number of active sites increase with smaller cluster sizes. In contrast to small catalyst support particles special attention has to be payed in order to achieve an even distribution of the active phase in the large structure of an monolithic catalyst. Especially for high cell densities the surface tension of the impregnating solution can cause heterogeneous distribution of the active phase within the monolith channels. Several methods for incorporation of the active phase, e. g. impregnation, ion exchange, precipitation and crystallization are described in the literature (Avila et al., 2005; Nijhuis et al., 2001a).

The deposition of the active material on the porous support by the impregnation method will be discussed in more detail in this work. The impregnation method is carried out in three steps. Firstly, the metal precursor is dissolved e. g. in water and the porous support is dipped into this solution. The concentration of the precursor in the solution, affects the loading of the active phase on the support. Subsequently, the impregnated catalyst support will be dried at a temperature right below the boiling temperature of the solvent, to prevent boiling. It should be taken into consideration, that the drying procedure affects the distribution of the active material on the support. It is suggested to start the drying process after impregnating the support. Freeze-drying or microwave drying could help to avoid redistribution of the active phase (Vergunst et al., 2001). The final step is the calcination of the precursor containing support. At temperatures of usually above 400 °C the precursor salt is changing into a metal oxide and the interaction between the active phase and the support increases. The

active phase is permanently fixed on the support. The impregnation procedure can be repeated to increase the active phase loading on the support.

The coating of a monolith with ready-made catalyst can be carried out as described for the porous support. This method usually results in a system with bimodal pore size distribution. The small pores originate from the coated particles, while the large pores originate from the void space between the coated particles. The advantage of this coating method is an even distribution of active material inside the monolith channels. The disadvantage is the often lower binding strength of the particles on the monolith walls. Calcination at high temperatures to bind the particles on the monolith can result in changes in the crystalline structure of both, the porous support and the active material. For this purpose it is supposed to use a binding material. However, the binding material can cover the active phase and block the pores. To avoid this, the used amount of binding material should be as low as possible. Furthermore, if colloidal binder material is used, the binder consists of particles and the complete blocking of the active material is less likely (Nijhuis et al., 2001a).

2.3.3 Assessment of monolith reactors

Theoretical investigations based on correlations for mass transfer, hydrodynamics, pressure drop and intrinsic kinetics showed a high potential for structured catalysts compared to randomly fixed beds (Edvinsson and Cybulski, 1994; Nijhuis et al., 2003; Bauer et al., 2005a).

In addition to modeling studies, several experimental investigations were carried out to evaluate the potential of monolithic catalysts (Table 2.4). During these studies, it was generally assumed that the different catalyst structures had comparable properties. In most cases, the comparability was based on using the same mass of the catalytically active metal in the different geometries. However, it can be suspected that the different catalyst geometries in some of the studies summarized in Table 2.4 had not exactly the same properties. In the literature examples (Broekhuis et al., 2004; Enache et al., 2005; Liu, 2002; Marwan and Winterbottom, 2003; Mazzarino and Baldi, 1987; Nijhuis et al., 2001c,b; Bauer, 2007) monolithic catalysts were compared with commercial or home-made pellets which were used as fixed-bed or, after crushing, as suspended catalyst. In these cases, it is not guaranteed that the pore structures and the distribution of the active metals in different geometries are the same. In the paper by Boger et al. (2004),

Table 2.4: Summary of experimental studies comparing different catalyst geometries in gas-liquid-solid three phase reactors (AMS: α-methylstyrene, MR: monolith reactor, STR: slurry stirred tank reactor, MSR: monolithic stirred reactor, DBC: down flow bubble column, RFPB: radial flow packed bed, RFBR: randomly fixed bed reactor).

Reference	Reaction	Compared reactor types	Catalyst
Broekhuis et al. (2004)	Hydrogenation of glucose to sorbitol	MR, STR	MR: monolith + washcoat + Ru; Powder: commercial
Enache et al. (2005)	Hydrogenation of Pyrolysis Gasoline	MR, RFBR	MR: monolith + washcoat + Pd/Ni;Pellets: commercial
Liu (2002)	Hydrogenation of styrene and 1-octene	MR, RFBR	MR: monolith + 4 wt% NiO/Al_2O_3 washcoat, 70 µm; Pellets: 3.2 mm and 2 sieve fractions, no composition given
Marwan and Winterbottom (2003)	Hydrogenation of Butyne-1,4-diol	DBC (monolithic, packed, slurry)	MR: monolith + washcoat + 1 wt%Pd; Pellets: 16 mm Raschig rings + 1 wt% Pd
Mazzarino and Baldi (1987)	Hydrogenation of AMS	MR, RFBR	MR: commercial 1 wt% Pd on monolith; Pellets: commercial egg-shell Pd/alumina
Nijhuis et al. (2001c,b)	Hydrogenation of AMS, consecutive hydrogenation of benzaldehyde	MR, RFBR	MR: monolith + washcoat + 1 wt% Ni; Pellets: commercial extrudates + 7 wt% Ni
Boger et al. (2004)	Hydrogenation of edible oil	MSR, STR	MR: monolith + washcoat + Pd; Powder: not specified
Hoek et al. (2004)	Hydrogenation of 3-methyl-1-pentyn-3-ol	MSR, STR	MR: monolith + washcoat + binder + Pd; Powder: Si-source + Pd, no binder
Liu et al. (2002)	Dehydrogenation of Ethylbenzene to Styrene	MR, RFPB	MR: extrusion from active material, wall thickness 640 µm; Pellets: crushed monolith, 420–250 µm
Bauer (2007)	Hydrogenation of AMS	MR, RFBR	MR: monolith + washcoat + Pd; Pellets: commercial
Schanke et al. (1998)	Fischer-Tropsch synthesis	MR, RFBR	Base catalyst: commercial alumina + Co/Re; MR: monolith + base catalyst washcoat; Pellets: crushing and sieving of base catalyst

the details of the powder catalyst used were not given. In the paper by Hoek et al. (2004), the same silica source was used for washcoating the monolith and preparing the powder catalyst. However, the use of a binder in case of the monolith may have caused differences to the powder catalyst that was manufactured without binder. In the study of Liu et al. (2002) the monolith was extruded from active material and then crushed into particles. This procedure assures an even distribution of active sites and the same pore structure in both catalyst geometries. On the other hand, the diffusion lengths in powder and monolith were different. Finally, Schanke et al. (1998) prepared monoliths by washcoating of a cordierite carrier with a catalytically active $CoRe/\gamma–Al_2O_3$ powder. The powder catalyst used for comparison, however, was prepared by tabletting of the original catalyst powder and crushing to the desired sieve fractions. During the pressing of tablets, the pore structure of the catalyst may have changed.

3 Modeling and simulation

3.1 Introduction

Multi-tubular fixed-bed reactors (FBRs) are used in the Shell Middle Distillate Synthesis (SMDS). From Sie (1998) it can be derived, that liquid is recycled and the reactor is operated in the trickle-flow regime in the SMDS to control the temperature inside the reactor. Models for FBRs in the trickle-flow regime have been developed for several hydrogenation and oxidation reactions (Dudukovic et al., 1999, 2002). To our knowledge, modeling results for fixed-bed FT reactors in the trickle-flow regime are not yet available in the literature. In the existing models it was generally assumed that liquid is only present in the catalyst pores and that external mass transfer resistances can be neglected (see e.g. Wang et al. (2003b)). Slurry bubble column reactors (SBCs) for FTS have been commercialized by Sasol in the 1980s (Steynberg and Dry, 2004). The SBC has been modeled for FTS using Fe catalyst by van der Laan et al. (1999); Rados et al. (2003) and Wang et al. (2008) and using Co catalyst by Maretto and Krishna (1999) and Krishna and Sie (2000).

An attractive alternative to the established FBR and SBC is the use of honeycomb monolithic catalysts in slug flow regime. However, this flow regime requires high liquid flow rates and consequently recycling of liquid products (Kapteijn et al., 1999). The resulting monolith loop reactor (MLR) concept is considered in our study. Models for honeycomb monoliths are available for several gas-liquid reactions (Edvinsson and Cybulski, 1994; Nijhuis et al., 2003; Bauer et al., 2005a). A modeling study comparing the MLR with simulation results obtained for a commercially sized SBC (Maretto and Krishna, 1999) has been presented by de Deugd et al. (2003a). As a second example of emerging reactor technologies, micro reactors (μRs) are considered. μRs could be especially suitable for modern highly active FTS catalysts and are under development by Velocys (Jarosch et al., 2005). Until now, modeling studies concerning μR for FTS

have not been published.

In the present work a systematic comparison of different reactor technologies for low temperature FTS is carried out. Both commercially established SBC and FBR as well as novel MLR and MR are taken into consideration. The aim is to determine the efficiencies of these reactors and to identify the degree of losses caused by mass and heat transfer resistances. Special attention was paid to the influence of catalytic activity, since future improved catalysts might be required for the development of alternative FT reactor concepts.

3.2 Reactor Models

For comparison of the performance of SBC, FBR, MLR and μR, mathematical models have been developed. Figure 3.1 illustrates the considered reactors schematically. The reactors vary in catalyst volume per channel volume, catalyst volume per reactor volume, characteristic diffusion length (Table 3.1) as well as in the catalyst and reactor geometry. The reactor or channel diameter represents the diameter of one channel or tube in FBR, MLR and μR, while the SBC consists of one single reactor vessel only. The characteristic diffusion length was defined as the ratio of the catalyst volume and its external surface area. For MLR and μR a plate-type catalyst geometry, for FBR and SBC spherical catalyst particles were assumed to be used. The ratio of catalyst and reactor volume depends on both the catalyst fraction in the channel and additional volume for internals like cooling and phase distribution equipment. Values for catalyst volume per reactor volume of FBR and μR, which was supposed to contain catalyst coated walls, were taken from Klemm et al. (2007). The volume of the cooling coils in the SBC was estimated by Maretto and Krishna (1999), while the volume for internals in the MLR was assumed to be negligible. The honeycomb catalyst was supposed to consist of active material only without the use of an inert carrier material. Such fully active monolith honeycombs were already used for FTS by Hilmen et al. (2001, 2005).

All considered reactors are special cases of integral reactors which are operated with gaseous and liquid reactants over solid catalyst. The differences are the heat and mass transfer characteristics and the hydrodynamics. To provide an adequate basis for comparison, all models consist of the same mass and heat balances and differ in the necessary correlations only. The model development is based on general assumptions valid for all

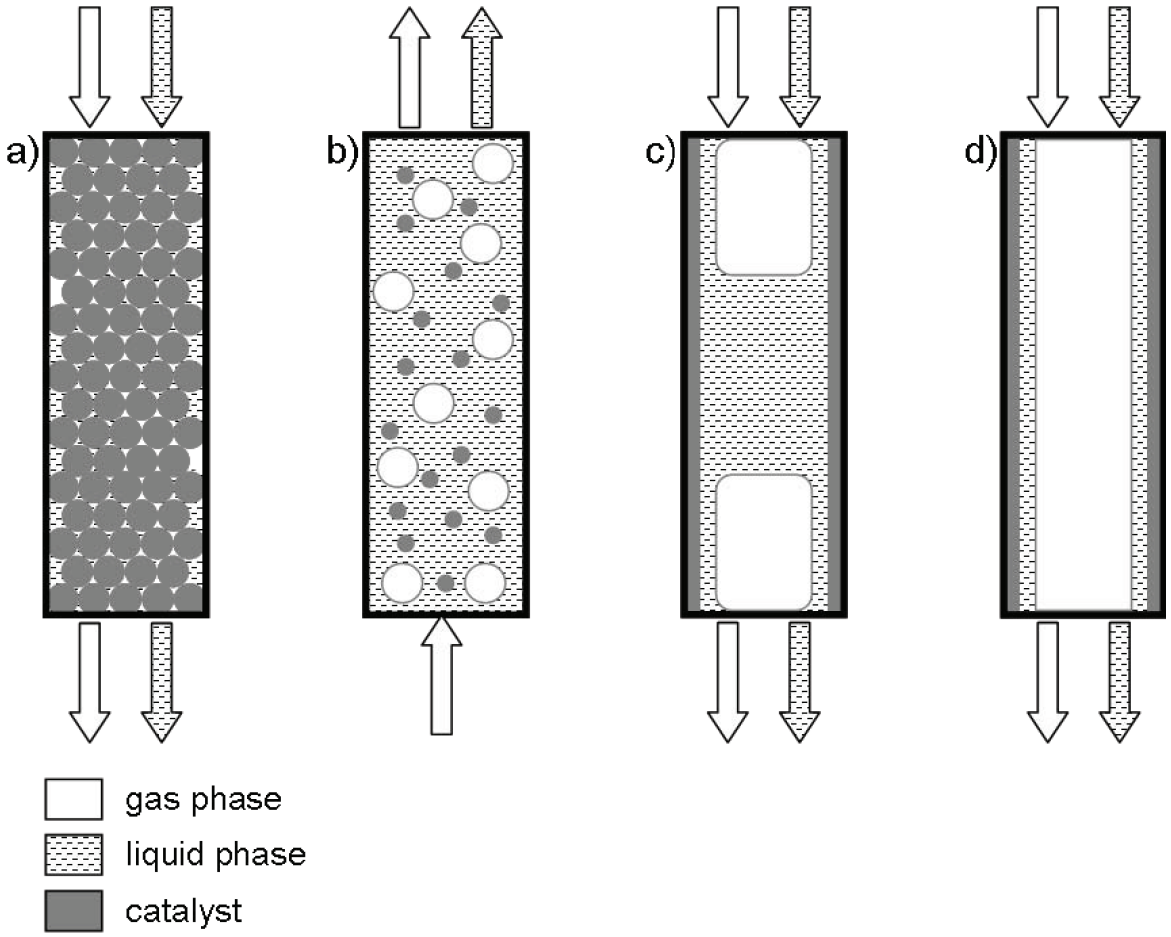

Figure 3.1: Reactors for low-temperature FTS, a) fixed-bed reactor in trickle-flow regime (FBR), b) slurry bubble column reactor (SBC), c) monolith loop reactor in slug flow regime (MLR), d) micro reactor in film flow regime (μR).

Table 3.1: Characteristics of reactors for low-temperature FTS.

Reactor type	FBR	SBC	MLR	μR
Reactor/channel diameter	25 mm	variable	1.1 mm	1 mm
Catalyst diameter/thickness	2 mm	42 μm	170 μm	85 μm
Diffusion length	333 μm	7 μm	85 μm	85 μm
Catalyst volume per channel volume	0.60	0.25	0.25	0.25
Catalyst volume per reactor volume	0.15	0.20	0.25	14.5×10^{-3}

Table 3.2: Model assumptions.

General assumptions	
– ideal gas law and Henry's law applicable	
– no addition or removal of catalyst	
– constant physical properties	
– constant liquid flow rate	
– one single n-paraffin represents liquid phase ($C_{28}H_{58}$)	
– even distribution of gas and liquid over the cross section	
– no radial temperature and concentration gradients	
– no temperature gradients inside the catalyst	
– steady-state conditions	
– liquid phase is saturated with synthesis gas at reactor inlet	
Reactor specific assumptions	
fixed-bed reactor	***slurry bubble column reactor***
– polytropic operation	– polytropic operation
– complete wetting	– no large gas bubbles
– trickle-flow regime	– no LS mass transfer resistances
	– no axial dispersion
monolith loop reactor	***micro reactor***
– adiabatic operation	– polytropic operation
– no axial dispersion	– no axial dispersion
– slug flow regime	– film flow regime

reactors and reactor specific assumptions. In general it was assumed that the model is one-dimensional in axial direction with internal gradients inside the porous catalyst and that the fluid phases are ideally mixed in radial direction in the bulk phase. All general and reactor specific assumptions are listed in Table 3.2. The resulting differential equation systems were numerically solved with Aspen Custom Modeler™.

The physical properties of the liquid phase are taken from de Deugd (2004) where it was assumed that the product consists of a single n-paraffin with a carbon number of 28 ($C_{28}H_{58}$). The Henry and diffusion coefficients are taken from Maretto and Krishna (1999) for 513 K. The heat capacity of the gas phase was calculated to about $30\,\mathrm{J\,mol^{-1}\,K^{-1}}$ for 493 K from Perry and Green (1999). All physical properties which are summarized in Table A.1 are assumed to be temperature independent. The reaction kinetics are based on a simple first order approach with respect to H_2 as suggested by Post et al. (1989) (Equation 3.1), which can be used for limited CO conversions of up to

ca. 60 % (Krishna and Sie, 2000). The activation energy E_A amounts to 120 kJ mol^{-1} and the frequency factor k_0 to 3.107×10^{10} m^3 m$_{cat}^{-3}$ s^{-1}.

$$r_{\mathrm{CO}} = F\, k\, c_{S,\mathrm{H_2}} \tag{3.1}$$

$$k = k_0\, exp\left(-\frac{E_A}{R\,T}\right) \tag{3.2}$$

This reaction rate was varied in our study by a factor F describing the relative catalyst activity. F was varied between 1 and 20 to simulate modern and future catalysts, which would be significantly more active. This possibility of activity enhancement is based on the recent catalyst development reported in the literature. Comparison of the achieved reaction rate in de Deugd (2004) with Post et al. (1989) (catalyst no. 5) at 493 K reveal an at least ten times higher reaction rate. Borg et al. (2007) reported an about 17 times higher reaction rate than reported by Post et al. (1989). The maximum possible enhancement in reaction rate was also estimated using the turn-over frequency (TOF). The reaction rate can be calculated from the TOF by the available Co surface area $a_{\mathrm{Co},av}$, which can be calculated from the Co-cluster size, the Avogadro number N_A and the required surface area per CO atom $A_{\mathrm{CO},req}$ (0.0662 nm^2 atom^{-1}) (Equation 3.3). van Steen and Claeys (2008) reported that the TOF of Co-based FTS catalysts in the temperature range from 473 to 493 K is limited to about 0.1 s^{-1} for Co-cluster sizes above 10 nm. Supposing that the catalyst consists of spherical clusters of Co-atoms with the minimum size of 10 nm only, a maximum possible reaction rate which is about 100 times higher than reported by Post et al. is obtained. In conclusion, the variation of catalytic activity up to a relative enhancement of 20 appears to be reasonable.

$$r_{\mathrm{CO}} = TOF\, \frac{a_{\mathrm{Co},av}}{N_A\, A_{\mathrm{CO},req}} \tag{3.3}$$

The catalyst effectiveness factor was determined by using a pore diffusion model (Equation 3.4). The effective diffusion coefficient D_{eff} was calculated from the diffusion coefficient D, a tortuosity of $\tau_{cat} = 3$ and a catalyst porosity of $\varepsilon_{cat} = 0.5$. The catalyst effectiveness factor was calculated for flat (μR and MR, Equation 3.5) and spherically

shaped catalysts (SBC and FBR, Equation 3.6).

$$0 = D_{\text{eff},\text{H}_2} \frac{d^2 c_{S,\text{H}_2}(y)}{dy^2} + r_{\text{CO}}(y) \tag{3.4}$$

$$\eta_{plate} = \frac{1}{\delta_{cat}} \frac{\int_{y=0}^{\delta_{cat}} r_{\text{CO}}(y) dy}{r_{\text{CO}}(y = \delta_{cat})} \tag{3.5}$$

$$\eta_{sphere} = \frac{3}{\delta_{cat}^3} \frac{\int_{y=0}^{\delta_{cat}} r_{\text{CO}}(y)\, y^2\, dy}{r_{\text{CO}}(y = \delta_{cat})} \tag{3.6}$$

The mass balances comprise axial mass transfer by convection and axial dispersion as well as mass transfer through the phase interfacial surface area. Since complete wetting of the catalyst is assumed, ka_{GS} implies the mass transfer from the gas phase through the liquid film to the catalyst. At reactor inlet Danckwert's boundary conditions were used for all reactor types. The heat balance considers convective heat transfer, the heat transfer to the reactor wall and the reaction enthalpy. The balance equations and corresponding boundary conditions are summarized below.

Mass balances, gas and liquid phase:

$$\begin{aligned} 0 = &- \frac{\partial}{\partial z} u_G\, c_{G,i}(z) + \mathcal{D}_{ax,G} \frac{\partial^2 c_{G,i}(z)}{\partial z^2} \\ &- ka_{GL,i} \left(\frac{c_{G,i}(z)}{He_i} - c_{L,i}(z) \right) - ka_{GS,i} \left(\frac{c_{G,i}(z)}{He_i} - c_{S,i}(z) \right) \end{aligned} \tag{3.7}$$

$$\begin{aligned} 0 = &- u_L \frac{\partial}{\partial z} c_{L,i}(z) + \mathcal{D}_{ax,L} \frac{\partial^2 c_{L,i}(z)}{\partial z^2} \\ &+ ka_{GL,i} \left(\frac{c_{G,i}(z)}{He_i} - c_{L,i}(z) \right) - ka_{LS,i} \left(c_{L,i}(z) - c_{S,i}(z) \right) \end{aligned} \tag{3.8}$$

Boundary conditions, reactor inlet and outlet:

$$\mathcal{D}_{ax,G}\frac{\partial c_{G,i}(z=0)}{\partial z} = u_G^{in}\left(c_{G,i}(z=0) - c_{G,i}^{in}\right) \tag{3.9}$$

$$\mathcal{D}_{ax,L}\frac{\partial c_{L,i}(z=0)}{\partial z} = u_L^{in}\left(c_{L,i}(z=0) - c_{L,i}^{in}\right) \tag{3.10}$$

$$\frac{\partial c_{G,i}(z=L_R)}{\partial z} = 0 \tag{3.11}$$

$$\frac{\partial c_{L,i}(z=L_R)}{\partial z} = 0 \tag{3.12}$$

Boundary conditions, external catalyst surface area:

$$0 = ka_{GS,i}\left(\frac{c_{G,i}(z)}{He_i} - c_{S,i}(z)\right) + ka_{LS,i}\left(c_{L,i}(z) - c_{S,i}(z)\right) + \nu_i\, x_{cat}\,\eta\, r_{\mathrm{CO}}(z) \tag{3.13}$$

Heat balance:

$$0 = -\left(u_L\, c_{p,L}\, \rho_L + u_G\, c_{p,G}\, \rho_G\right)\frac{\partial T}{\partial z} - \frac{4}{d_R}h_{w,ov}\left(T(z) - T_w\right) + x_{cat}\,\eta\, r_{\mathrm{CO}}(z)\,\Delta H_R \tag{3.14}$$

Impulse balance:

$$\frac{dp}{dz} = \left(\frac{dp}{dz}\right)_{fri} + \left(\frac{dp}{dz}\right)_{hs} \tag{3.15}$$

During the production of liquid products from the gaseous educts the molar flow rate of the gas phase and its velocity decrease. Using the simple assumption that the gas phase consists of CO, H_2 and H_2O only, the gas velocity can be calculated as a function of the CO conversion X_{CO} with Equation 3.16.

$$u(z) = u_{in}\frac{3 - 2\,X_{\mathrm{CO}}}{3} \tag{3.16}$$

The pressure gradients, hydrodynamic and heat and mass transfer characteristics are reactor specific and can be described with correlations from the literature. These correlations are summarized in the appendix (section A.1.2 – A.1.5) for each reactor.

The SBC model is based on the work of Maretto and Krishna (1999). For simplification it was assumed, that only small bubbles exist in the SBC, which provide a better mass transfer than large bubbles. However, the differences in mass transfer rates

of large and small bubbles are relatively low (Maretto and Krishna, 1999). The MLR was assumed to be operated in the slug flow regime at a liquid velocity of $0.2\,\mathrm{m\,s^{-1}}$ corresponding to an external liquid recycle ratio of ≈ 275. In contrast to the SBC and MLR, it was assumed that only gas is present at the inlet of the FBR and μR. However, during the reaction liquid product is formed and a liquid film on the catalyst surface develops. For simplification, the simulations were carried out for a constant thickness of this liquid film over the length of the reactor. The average film thickness for MLR and μR was obtained from the liquid phase saturation β_L of $\approx 5\,\mathrm{vol\%}$ calculated from CO conversion, gas and liquid flow rate (Equation 3.17) for a liquid product consisting of a species with n_c carbon atoms. In reality, the thickness of the liquid film will increase with synthesis gas conversion and reactor length. The assumption of a constant film thickness may thus lead to an overestimation of external mass transfer resistances especially in the hot spot region at reactor entrance. The validity of this simplification will be discussed in the results section.

$$\beta_L = \frac{1}{1 + \frac{\dot{V}_{G,in}}{\dot{V}_L} \frac{u_L}{u_{G,in}}} \tag{3.17}$$

$$\frac{\dot{V}_{G,in}}{\dot{V}_L} = \frac{R\,T_{in}\,n_c\,\rho_{n_c}}{X_{\mathrm{CO}}\,p_{in}\,M_{n_c}} \tag{3.18}$$

3.3 Simulation Results

For the simulation study typical gas and liquid velocities were chosen for each reactor. The corresponding flow rates and the reactor diameters can be easily calculated from the velocities. The H_2/CO-ratio in the gas feed was fixed to 2 and the liquid feed was assumed to be saturated with synthesis gas. The temperature of the cooling medium was set equal to the inlet temperature. The maximum temperature inside the reactor was limited to 523 K and the CO conversion at reactor outlet was fixed to 70 %. While typical conversions in industrial reactors are not available, we chose a conversion which on one hand is not too far beyond the validity region of a first-order approach and where on the other hand catalyst deactivation by the product water can be excluded. According to literature data, deactivation and reoxidation of Co-based catalysts occurs at H_2O/H_2-ratios of about 1.5 (Schanke et al., 1996) which corresponds to a conversion of ca. 75 %. To achieve the defined conversion and maximum temperature the reactor

length and inlet temperature were varied. Using the calculated reactor length pressure drop, catalyst volume and reactor volume can be obtained. In the present work we defined the catalyst and reactor productivity P, which represent the daily hydrocarbon production rate per catalyst or reactor volume. With these data, the size of industrial reactors can be extrapolated.

Additionally a reactor efficiency E was calculated by Equation 3.19. This reactor efficiency represents the ratio of the mean achieved apparent reaction rate at the catalyst and the mean reaction rate in the absence of mass transfer resistances at maximum reactor temperature. The difference of the reactor efficiency to unity is caused by losses due to heat and mass transfer resistances. Heat transfer resistances lead to insufficient heat removal and to the development of a temperature profile along the reactor. If the mean reactor temperature is lower than the maximum temperature, the achievable reaction rate decreases. This effect can be quantified by ΔE_T (Equation 3.20). On the other hand one can distinguish between external and internal mass transfer resistances. The efficiency losses due to internal mass transfer resistances can be calculated with the catalyst effectiveness factor η (Equation 3.21). The efficiency losses caused by external mass transfer resistances are given by Equation 3.22. To prove the validity of Equation 3.22 selected simulations were conducted without external mass transfer resistances.

$$E = \frac{\int_z \eta\, r(c_{S,\mathrm{H_2}}(z), T) dz}{\int_z r\left(\frac{c_{G,\mathrm{H_2}}(z)}{He_{\mathrm{H_2}}}, T_{max}\right) dz} \tag{3.19}$$

$$\Delta E_T = \frac{\int_z \eta\, r(c_{S,\mathrm{H_2}}(z), T) dz}{\int_z r\left(\frac{c_{G,\mathrm{H_2}}(z)}{He_{\mathrm{H_2}}}, T\right) dz} - E \tag{3.20}$$

$$\Delta E_{intern} = 1 - \eta \tag{3.21}$$

$$\Delta E_{ext} = 1 - (E + \Delta E_T + \Delta E_{intern}) \tag{3.22}$$

In the following diagrams, the simulation results for the different reactor types as a function of the relative catalyst activity are summarized. Details of operating conditions and simulation results are given in Table A.2 and A.3. The calculated pressure drop is decreasing with increasing catalyst activity for all reactors (Figure 3.2). This can

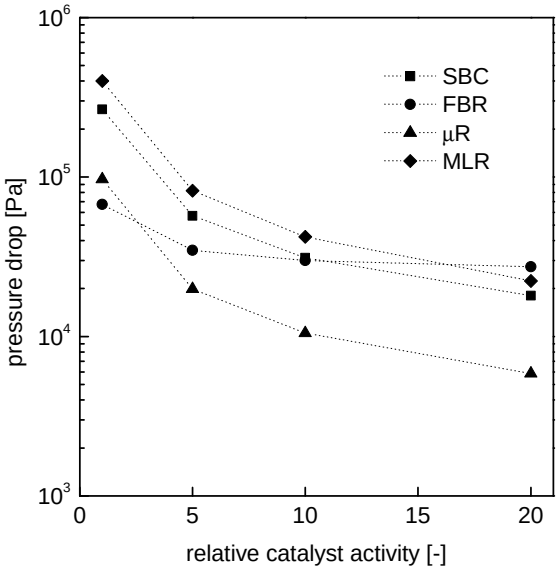

Figure 3.2: Pressure drop as a function of relative catalyst activity.

be explained by the decreasing residence time required for the desired conversion and thus a decreasing reactor length. For the FBR a low influence of catalyst activity on pressure drop is predicted. This can be explained by the very low catalyst utilization in this reactor type as will be discussed later. The surprisingly small pressure drop in FBR may be explained by fact that the static liquid holdup, which can increase the pressure drop significantly, was not considered in this study.

The catalyst productivity increases with increasing catalyst activity (Figure 3.3). SBC and µR achieve the highest productivities, followed by MLR and FBR. Again, the FBR shows the least dependence on the variation of catalytic activity. Analysis of these results is possible by use of the reactor efficiency (Figure 3.4). The reactor efficiency generally decreases with increasing catalyst activity, caused by an increasing role of heat and mass transfer resistances. One can see that the utilization of catalysts is very high for µR and SBC even at high catalytic activities. The value in the range of 0.6 to 0.65 for the MLR is only slightly decreasing with relative catalytic activity. Simulation of the FBR results in much lower reactor efficiencies especially for highly active catalysts.

Figure 3.5 quantifies the efficiency losses for the highest relative catalyst activity of 20. The columns in this Figure represent the reactor efficiency and the efficiency losses caused by lower mean reactor temperature, external and internal mass transfer

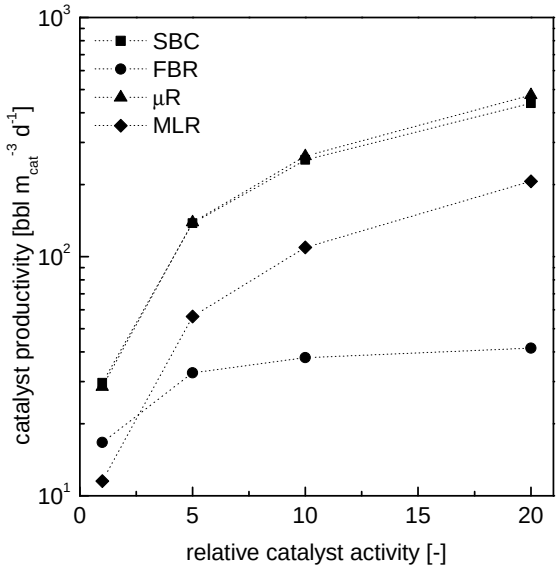

Figure 3.3: Catalyst productivity as a function of relative catalyst activity.

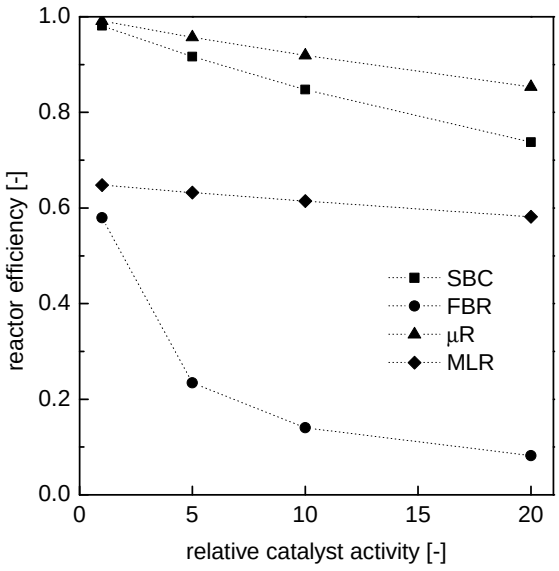

Figure 3.4: Reactor efficiency as a function of relative catalyst activity.

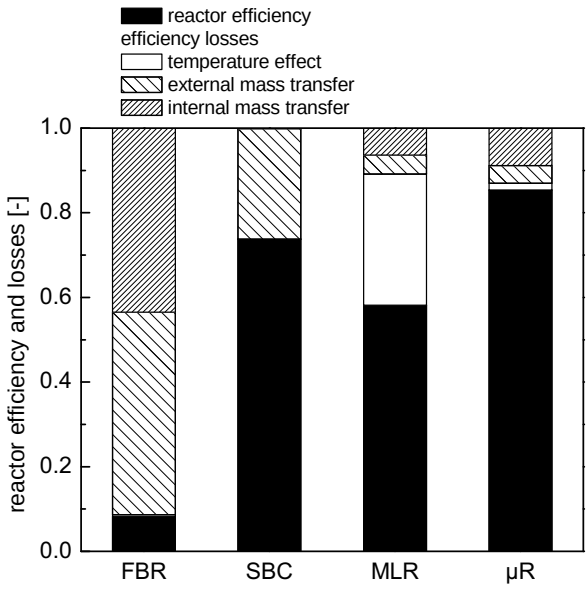

Figure 3.5: Influence of heat and mass transfer resistances on the reactor efficiency for a relative catalyst activity of 20.

resistances (from bottom to top). The SBC is operating completely isothermal. Due to the small catalyst particles used, internal mass transfer resistances are also absent. The deviation of the reactor efficiency from unity can thus be ascribed to external (i.e. gas-liquid) mass transfer resistances. The reactor efficiency for the μR is very high. It is mainly affected by internal mass transfer resistances at the assumed catalyst layer thickness. External mass transfer resistances are of minor importance, while heat transfer resistances are absent as the reactor operates almost isothermal. Given the low influence of external mass transfer resistance for the μR, the accuracy of the simulation results is not much affected by the assumption of a liquid product layer of constant thickness. The MLR is the most efficient reactor if only mass transfer resistances are considered. The main efficiency loss of this reactor type is caused by the adiabatic operation. At the given recycling rate of the liquid product, the inlet temperature has to be chosen considerably lower than the maximum reactor temperature. The observed differences in internal mass transfer resistances between μR and MLR at the same diffusion length can be attributed to the higher mean temperature and thus higher mean reaction rate in the μR. In the FBR the temperature effect is surprisingly small, although this reactor exhibits a significant deviation from isothermal behavior (cf. Table A.2). However, the temperature effect is superimposed by extremely strong internal and external mass

transfer resistances inhibiting the overall reaction rate and reducing the danger of hot-spot formation. As operation of the FBR in the trickle-flow regime with a constant film thickness is only a simplified limiting case, further simulations were carried out. Another limiting case would be a "dry" FBR without formation of a liquid product film and with negligible external mass transfer resistances. However, the performed simulations for this case show a very sensitive behavior of the "dry" FBR. Thermal "run-away" occurs already with a relative catalyst activity of 3, because the heat removal over the reactor wall is not sufficient at the chosen reactor diameter of 25 mm. In contrast to the results obtained in the trickle-flow regime, severe efficiency losses are caused by the deviation from isothermicity even at low relative catalytic activities.

These results clearly indicate the most important efficiency losses for each reactor type and allow the discussion of possible efficiency improvements. The μR is the most efficient reactor and the main losses are due to internal mass transfer limitations. However, a further decrease of catalyst layer thickness is not advantageous as will be discussed later. The already quite efficient SBC is mainly affected by external mass transfer limitation. This behavior can possibly improved by the use of internals giving rise to bubble breakage and an increased gas-liquid mass transfer coefficient. The strongest limitation of the MLR originates from the adiabatic operation. The efficiency losses caused by the lower mean reactor temperature can be reduced by applying a larger recycle of liquid product. However, this necessitates the use of larger recycle pumps requiring higher power. Although the results for the FBR are the least reliable, it is evident that this reactor type suffers from severe mass transfer resistances. The influence of external mass transfer may be reduced by decreasing the catalyst particle diameter. On the other hand, pressure drop would increase at the same time. External mass transfer of the FBR in the trickle-flow regime may be improved by periodic operation (Silveston and Hanika, 2004). However, unsteady-state operation of mega-size commercial FT reactors is hard to imagine.

In Figure 3.6 the reactor productivity including the required volume for the catalyst bed and the internals for cooling and phase distribution is depicted as a function of catalyst activity. Due to the fact that the considered reactors differ strongly in the requirements for internals, the reactor productivity shows different trends than the catalyst productivity. Again, the reactor productivity increases with the catalyst activity. Now, the highest values are obtained for the SBC and the MLR, whereas the productivity for μR and FBR is low. Although the μR allows for the best catalyst utilization,

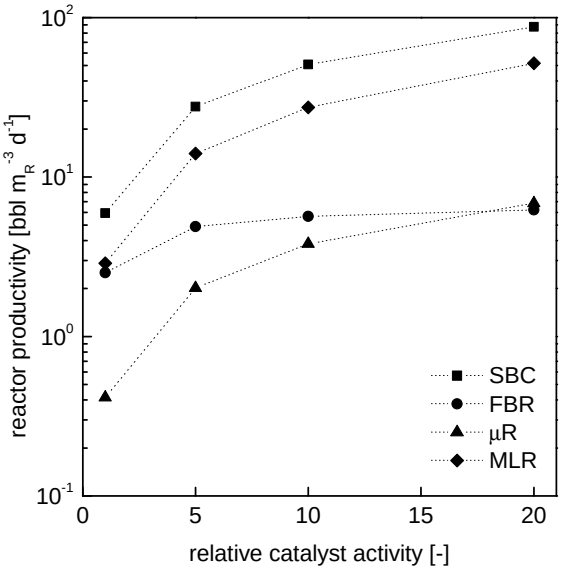

Figure 3.6: Reactor productivity as a function of relative catalyst activity.

it does not offer attractive reactor volumes as the assumed ratio of catalyst and reactor volume is by far too low.

In an attempt to improve the performance of μR and MR, further simulations were carried out with increased thicknesses of the catalyst layers (Figure 3.7). While the ratio of catalyst and reactor volume can be increased with higher layer thicknesses, the efficiency is negatively affected by stronger pore diffusion resistances. We assume that the chosen higher diffusion length of 125 μm for the MLR represents the maximum achievable in a channel of ca. 1 mm as the open frontal area would otherwise become too small. It can be seen that with a MLR of this layer thickness a reactor productivity close to a SBC can be achieved. On the other hand, even an μR with a catalyst layer thickness of 250 μm exhibits only one sixth of the SBC reactor productivity. A further increase of the catalyst layer thickness is not useful since the catalyst effectiveness factor would decrease even more.

A comparison of the MLR to the SBC was already carried out by de Deugd (2004). De Deugd compared the required reactor volume for the MLR and SBC and found that it is about the same. It was stated, that the MLR exhibits several advantages over the SBC. First of all, the MLR offers plug flow behavior due to the slug flow regime, whereas the SBC suffers from backmixing. However, the backmixing behavior in the SBC is controversially discussed as already mentioned. It appears more plausible,

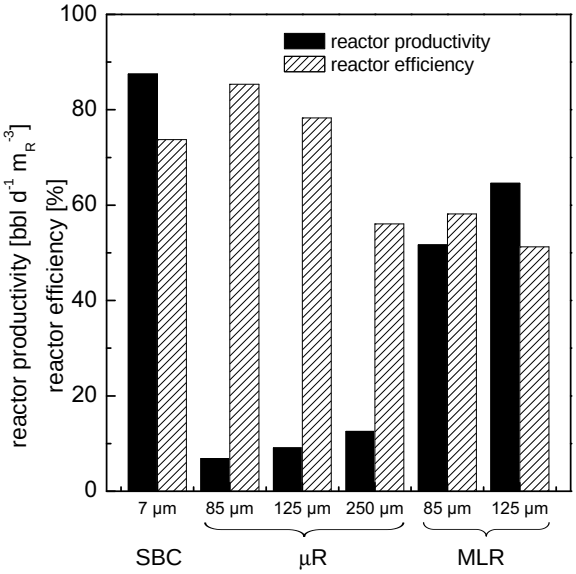

Figure 3.7: Reactor efficiency and productivity for different diffusion lengths in µR and MLR compared to the SBC.

that the residence time distribution of synthesis gas should not significantly differ from ideal plug flow behavior in reactors with a sufficient high length-to-diameter ratio. Furthermore, de Deugd stated, that the adiabatic temperature rise in the MLR increases the productivity, but decreases the selectivity to heavy products. It was also stated, that the process is reaction determined on the one hand and benefits from the enhanced mass transfer rate for more active catalysts on the other hand. Based on these arguments it is surprising, that the MLR do not outperform the SBC with respect to the required reactor volume.

The simulation results presented in this work first of all confirm the results obtained by de Deugd with respect to the comparison of MLR and SBC. The MLR is able to compete with the SBC especially for more active catalysts. Compared to de Deugd this simulation study was extended to SBC, µR and FBR. Furthermore, the reactor efficiency and efficiency losses due to heat transfer and internal and external mass transfer resistances are quantified. It was shown, that for highly active catalysts the SBC suffers from external mass transfer resistances, while the MLR is affected by the adiabatic temperature rise. This explains, that the MLR is not able to outperform the SBC even for more active catalysts. In addition to results from de Deugd it was shown, that the reactor productivity of the SBC and the MLR profits in a similar manner from

more active catalysts. A decision between SBC and MLR will depend on the reduction in mass transfer resistances and on the efforts of catalyst separation in the SBC and the reduction of adiabatic temperature rise and on efforts for the liquid recycle in the MLR.

The required liquid recycle flow rate for an industrial scale MLR plant can be calculated with Equation 3.23. As an example a hydrocarbon production capacity of $\dot{V}_{product} = 47\,300\,\mathrm{bbl\,d^{-1}}$ ($5000\,\mathrm{t\,d^{-1}}$) and a relative catalyst activity of 5 was chosen, as described by Maretto and Krishna (1999) for a SBC. The liquid recycle flow rate was calculated to $41.3\,\mathrm{m^3\,s^{-1}}$, which results in a total reactor cross sectional area of $206\,\mathrm{m^2}$ for a liquid superficial velocity of $0.2\,\mathrm{m\,s^{-1}}$. The power consumption of the liquid pump can be calculated from the pressure drop and the liquid recycle flow rate. With a pressure drop of 82 kPa, the total resulting power consumption of the pumps amounts to approx. 3.39 MW excluding the pressure drop of the tubing. Increasing the relative catalyst activity to 20 will also result in a liquid recycle flow rate of $41.3\,\mathrm{m^3\,s^{-1}}$, but a significantly smaller total pressure drop of 22.3 kPa, which reduces the total power consumption to 923 kW. However, the total liquid recycle flow rate is split over the number of parallel reactors. The feasible volumetric flow rate of one pump will define the number of parallel trains and the reactor diameter. Depending on the process temperature and pressure a liquid flow rate of several cubic meter per second seems to be feasible (e. g. KSB AG, type RDLO).

$$\dot{V}_{recycle} = \frac{u_L\,\dot{V}_{product}}{P_R\,L_R} \tag{3.23}$$

The liquid recycle is reasonable to remove the heat of reaction of ≈600 MW. This huge amount of thermal power can be calculated from the daily production capacity of hydrocarbons, the molar weight for one –CH_2– element in the hydrocarbon chain and the reaction enthalpy of −150 kJ per mole converted CO. In relation to the heat of reaction the power consumption of the pump amounts to about 0.6 % and thus reduces the degree of effectiveness only slightly. Moreover, the heat exchanger in the liquid recycle could be used to produce steam at up to 250 °C, which corresponds to a pressure of ≈40 bar. The required mass flow rate of the cooling water can be calculated with the standard enthalpy of vaporization of $\approx 1.7\,\mathrm{MW\,kg^{-1}}$ at 250 °C to $\approx 350\,\mathrm{kg\,s^{-1}}$. This attractive energy transfer medium can be used to significantly reduce the electric power consumption of the total FT plant. It can be concluded, that, besides the distribution

of gas and liquid over the cross section, the main challenge in applying MLR in FTS is the large liquid recycle flow rate, since the power consumption is high. Nevertheless, it is almost negligible in the overall energy balance of the unit. However, increasing the catalyst activity will further reduce the required reactor length and thus the pressure drop and power consumption for pumping.

3.4 Conclusions

Different reactor types for low temperature FTS were compared. In addition to the commercially established SBC and FBR, novel MR and μR were taken into account. According to our analysis, the SBC is up to one order of magnitude more effective than a FBR operated in the trickle-flow regime both in terms of required catalyst and reactor volume. This drastic difference can be explained by smaller external and internal mass transfer resistances and a completely isothermal operation of the SBC. However, as the separation of the catalyst from the liquid products is still a challenge for SBCs, the search for alternative reactors is justified. The MLR appears to be a quite interesting alternative to the SBC as it offers almost the same productivity per reactor volume using a fixed-bed catalyst configuration. However, this concept requires a large external recycle of the liquid product, which represents the essential challenge for an application on industrial scale. A μR offers a very high efficiency, since mass and heat transfer resistances are negligibly small. On the other hand, a μR with only a thin layer of catalyst applied to the reactor walls provides not enough productivity per unit of total reactor volume to become industrially attractive. Progress in μR for FTS will only be achieved if the ratio of catalyst and reactor volume can be significantly increased.

4 Catalyst Preparation

This chapter describes the preparation and characterization of different catalyst geometries with comparable pore structure and dispersion of active sites in the catalyst layer. For this purpose monolithic honeycomb catalysts are prepared by coating with ready-made catalysts. This method is quite often used by manufacturers of automotive car exhaust catalysts (Heck et al., 2002).

4.1 Catalyst preparation

Powder and monolithic catalysts with approximate contents of 20 wt% Co and 1 wt% Re on γ-Al_2O_3 were prepared (Figure 4.1) as described by Schanke et al. (1998). This allows comparison to previous investigations of monoliths in FTS by the groups of Kapteijn and Moulijn (de Deugd et al., 2003c; Kapteijn et al., 2005) and Holmen (Hilmen et al., 2001, 2005; Storsæter et al., 2005b). Firstly, a base powder catalyst was prepared (step 1). The base catalyst and additional binder material was suspended (step 2) to coat a cordierite monolith carrier by dip-coating (step 3). The suspension was also used to produce the powder catalyst by drying and calcining (step 4). For preparation of the base powder catalyst 139.5 g alumina powder (γ-Al_2O_3, 5 µm, Puralox UF 5/230, Sasol) was suspended in a solution of 174.6 g cobalt nitrate ($Co(NO_3)_2 \cdot 6\,H_2O$) and 4.56 g perrhenic acid (54 wt%, H.C. Starck) in 222 ml of de-ionized water. Subsequently, this suspension was dried at 90 °C and calcined for 4 h at 400 °C in air. The slurry for dip-coating was prepared by suspending 60 g of the base powder catalyst in 54 ml de-ionized water and 34 ml colloidal alumina binder (pseudo-boehmite AlOOH, 20 wt%, 50 nm, pH 7, Alfa Aesar). A pH of 7 in aqueous environment was optimal as will be shown later. The suspension was dispersed with an ultrasound sonotrode for 1 min at 100 W. The resulting slurry contained 45 wt% of solid while 10 wt% of the solid fraction consisted of colloidal binder material.

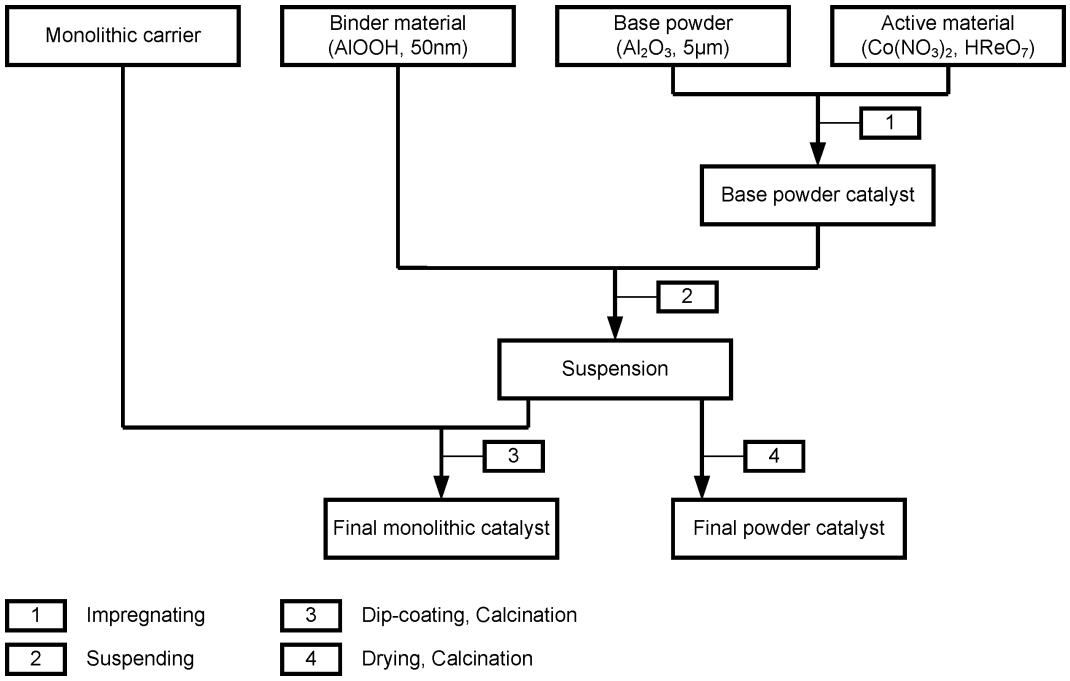

Figure 4.1: Preparation method for powder and monolithic catalysts.

As carrier monoliths (cordierite, 400 cpsi, Corning) with a diameter of 16 mm and a length of 50 mm were used (Figure 4.2). After dip-coating for 1 min, the monolith channels were blown out with pressurized air to remove the excess slurry. The outer surface of the monolith was cleaned to remove the coating. Finally, the coated monoliths were dried for 1 h at 90 °C and calcined for 4 h at 400 °C in air. The coating procedure was repeated to achieve higher washcoat mass fractions, each step followed by drying and calcination. For comparison, monolith samples were also coated with pure alumina washcoats.

The mechanical stability of the washcoats was examined by flow-through tests with water. After 3 h at a velocity of 12 cm s^{-1} followed by 1 h at a velocity of 1 m s^{-1} a loss of only 0.3 wt% was measured. Hence, the washcoat on the monolithic carrier appears to be sufficiently stable.

The final powder catalyst was prepared by using the same slurry as for the dip-coating. The slurry was dried for 6 h at 90 °C, calcined for 4 h at 400 °C and then crushed and sieved to the desired fraction.

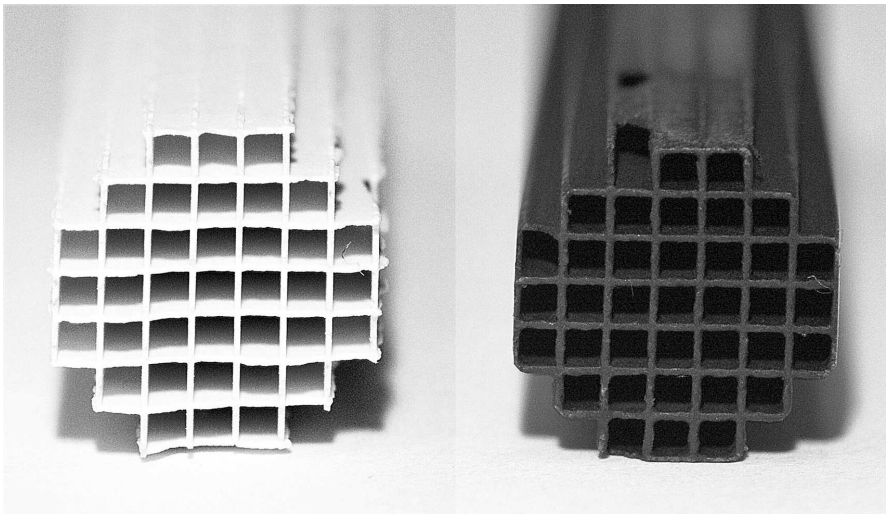

Figure 4.2: Photograph of an uncoated (left) and coated (right) honeycomb monolith.

4.2 Catalyst characterization

The zeta potential of slurries was measured with a Nano-ZS zeta sizer (Malvern Instruments). The resulting catalysts and the main intermediates were analyzed by different methods. The chemical composition of the catalysts was determined by ICP-OES. The pore structure and BET surface area were measured using nitrogen adsorption. XRD (X-ray diffraction) measurements were carried out to determine the phase structures. The distribution and the layer thickness of the washcoat were examined by scanning electron microscopy (SEM).

Temperature programmed reduction (TPR) was performed to receive information about the phases present in the sample (Lemaitre, 1984). The samples were heated with a ramp of $10\,\mathrm{K\,min^{-1}}$ from 50 to 550 °C in a flow ($30\,\mathrm{ml\,min^{-1}_{STP}}$) of 10 % H_2 in Ar at atmospheric pressure.

Pulsed chemisorption measurements with CO were used to determine the active metal surface area, the metal dispersion and the mean cluster size. The pulsed chemisorption was carried out at 50 °C with 10 % CO in He after reducing the catalyst for 1.5 h at 350 °C under pure hydrogen. For both techniques a BELCAT-M (BEL Japan, Inc.) catalyst analyzer was used. The active metal surface area $\tilde{a}_{\mathrm{Co}}$ and the active metal dispersion D_{Co} can be calculated from the measured CO uptake Δn_{CO} (Equations 4.1 and 4.2, Lemaitre et al. (1984)). The mean Co cluster size d_{Co} can be calculated from the Co dispersion by Equation 4.3 (Lemaitre et al., 1984). The parameters used in

Table 4.1: Required parameters for calculation of active metal surface area, dispersion and the mean cluster size from CO chemisorption measurements, (taken from Reuel and Bartholomew (1984): ν_{CO} for 15 wt% Co on Al_2O_3, σ_{Co}).

	Symbol	Dimension	Value
CO uptake	Δn_{CO}	$\mathrm{mol\,g_{cat}^{-1}}$	–
Avogadro number	N_A	$\mathrm{mol^{-1}}$	6.022×10^{23}
Area per surface atom	σ_{Co}	$\mathrm{nm^2\,atom^{-1}}$	0.0685
Stoichiometry factor for CO adsorption on Co	ν_{CO}	–	1.0
Co molar mass	M_{Co}	$\mathrm{g\,mol^{-1}}$	58.93
Co mass fraction on catalyst	$x_{m,Co}$	–	0.186
Co density	ρ_{Co}	$\mathrm{kg\,m^{-3}}$	8900
Geometry factor for spheres	g	–	6
Fraction of active metal surface exposed to reactants	f	–	1

Equations 4.1, 4.2 and 4.3 and typical values are summarized in Table 4.1.

$$\tilde{a}_{Co} = \frac{\Delta n_{CO}\, N_A\, \sigma_{Co}}{\nu_{CO}} \tag{4.1}$$

$$D_{Co} = \frac{M_{Co}\, \Delta n_{CO}}{\nu_{CO}\, x_{m,Co}} \tag{4.2}$$

$$d_{Co} = \frac{g\, f\, M_{Co}}{\rho_{Co}\, \sigma_{Co}\, N_A\, D_{Co}} \tag{4.3}$$

The pore size distribution was measured by N_2 adsorption and Hg intrusion, respectively. The N_2 adsorption allows a high resolution of pore sizes between 0.4 and 400 nm, while the Hg intrusion method allows the measurement of the pore size distribution over a broad range between 2 nm and 200 µm with a more rough resolution.

4.3 Results and discussion

4.3.1 Dip-coating

To optimize the pH conditions for the dip-coating procedure zeta potential measurements were carried out for the base materials by varying the pH with hydrochloric acid between 3.5 and 7. The zeta potential is a reference value for the adhesive forces between particles. Particles with different or low absolute potentials tend to agglomerate, while a suspension with particles with a potential of more than 25 – 50 mV can

be assumed as stable (Hunter, 1991). The results of the measurements are shown in Figure 4.3. The monolithic carrier was crushed to particles to measure its potential. Between pH 3.5 and 7 the potential of the carrier decreases from −20 to −35 mV, while the potential of the base powder decreases from 40 to 20 mV. The colloidal binder material has a potential of 55 mV at a pH of 7. After impregnating the base powder with active material the potential of the base powder catalyst is lower than that of the base powder and decreases between pH 3.5 and 7 from 40 to 0 mV. Adding the binder material to the base powder catalyst leads to an increase in the potential of the final powder catalyst that remains almost constant at 40 mV over the considered pH range. These results reveal that a suspension of the final powder catalyst is stable. Due to the large difference in the potentials of monolith carrier and final powder catalyst at pH 7, a good adhesion between washcoat and cordierite carrier should result. Christiani et al. (2005) analyzed the effect of ageing time in γ-Al_2O_3 slurries for dip-coating and suggested to use a pH of 3.5. However, in contrast to the experiments described in this paper, Christiani et al. used base alumina powder without active metal and colloidal binder. In conclusion, for coating monoliths with the $CoRe/Al_2O_3$ powder catalyst with added AlOOH binder a pH of 7 should be chosen.

The mass of the washcoat on the monolithic carrier was measured gravimetrically. The different curves shown in Figure 4.4 were obtained by repeating the experiments under identical conditions. A comparison of coatings with base alumina powder and powder catalyst shows that higher washcoat mass fractions are achieved using the pure alumina slurry. This can be explained by the higher zeta potential difference between alumina powder and monolithic carrier compared to the powder catalyst Figure (4.3). The high washcoat mass fraction increase during the sixth coating step with alumina powder can be explained by blocking of some channels. In all other cases, the increase of washcoat mass fraction gradually decreases with number of coating steps. Two explanations may be given for this phenomenon. Firstly, if a surface is coated with porous layer, the zeta potential of the whole system will change until eventually the values of the coating are reached. Consequently, the driving force for agglomeration will decrease. Secondly, the surface area of the channel also diminishes with increasing washcoat mass fraction. This leads to a decrease in coating capacity of the capillary and thus in a lower achievable washcoat mass fraction per coating step.

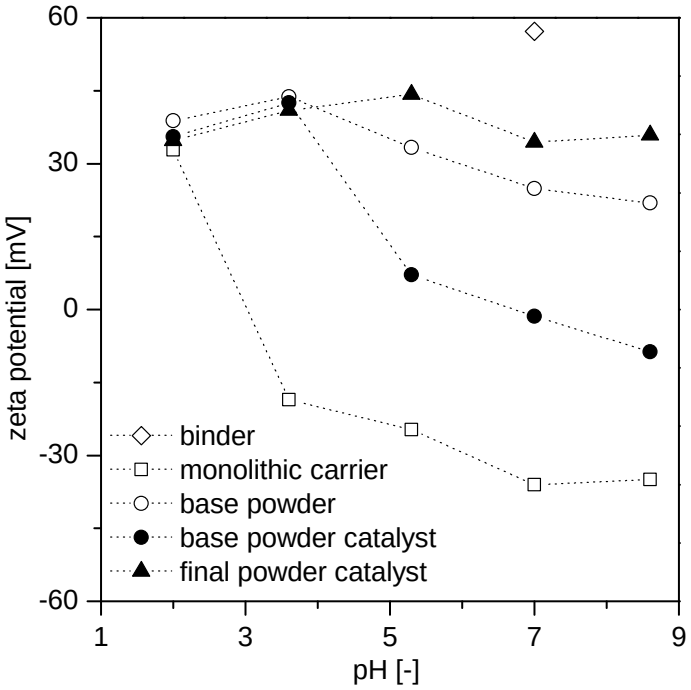

Figure 4.3: Zeta potentials of base materials and catalysts.

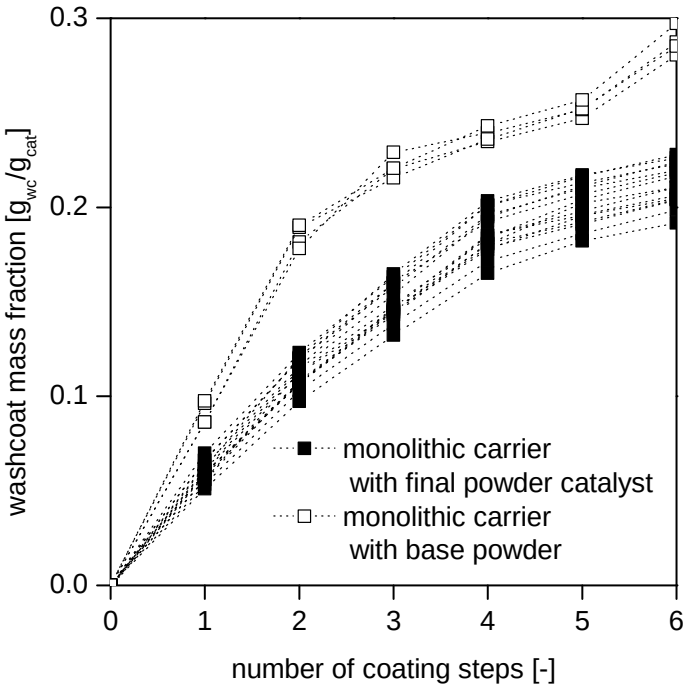

Figure 4.4: Mass fraction of washcoat on monolithic catalysts.

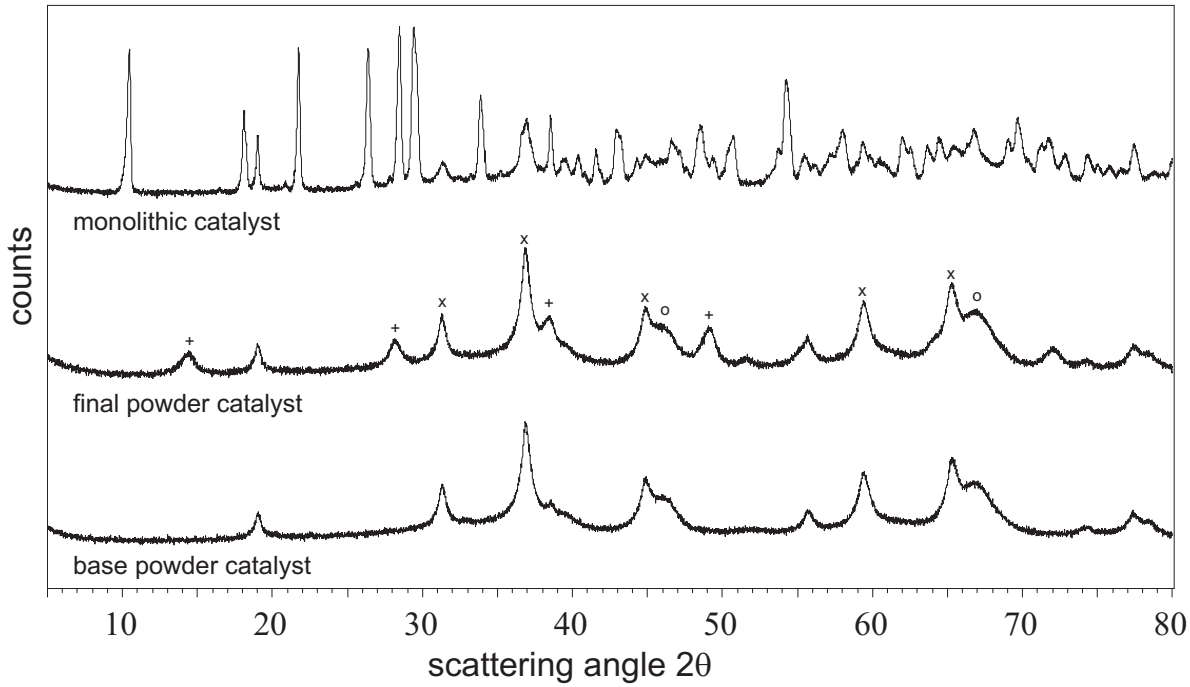

Figure 4.5: XRD pattern for base powder catalyst, final powder catalyst and monolithic catalyst, (+) AlOOH, (x) Co_3O_4, (o) γ-Al_2O_3.

4.3.2 Catalyst composition

The catalyst composition was determined by ICP-OES measurements. According to the elemental analysis, the prepared catalyst had a cobalt content of 18.6 ± 0.9 wt% and a rhenium content of 1.2 ± 0.1 wt% on the γ-Al_2O_3 support. These values are in good agreement with the desired composition of 20 wt% Co and 1 wt% Re.

Figure 4.5 shows the results of XRD measurements for base powder, final powder and monolithic catalyst as a function of the scattering angle 2θ. The characteristic peaks for Co_3O_4, γ-Al_2O_3 and AlOOH are marked exemplary for the final powder catalyst with (x), (o) and (+), respectively. The difference between the base powder and final powder catalyst is the presence of colloidal alumina binder in the final powder catalyst. The results for the monolithic catalyst exhibit more peaks compared to the powder catalyst, since the sample contains high amounts of cordierite. The peaks for Co_3O_4 and γ-Al_2O_3 can not be identified, as the washcoat mass fraction in the sample amounts to about 20 wt% only. The crystal structure is similar to the results obtained by Storsæter et al. (2005b).

Table 4.2: Properties of final catalyst and intermediates (* measured, ** calculated, *** as final powder catalyst, ♯ from data sheet).

Dimension	a_{BET} $m^2\,g^{-1}$	V_{pore} $cm^3\,g^{-1}$	d_{pore} nm	ε –	ρ_{app} $g\,cm^{-3}$
Monolithic carrier*	0.28	0.16	2528	0.26	1.60
Monolithic catalyst*	33.6	0.22	730	0.36	1.65
Base powder*	197 (208)♯	1.00	288	0.64	0.645
Base powder catalyst*	144	0.80	541	0.65	0.806
Final powder catalyst*	167	0.67	325	0.62	0.920
Washcoat**	167	0.46		0.63	0.920***

4.3.3 Pore structure and surface areas

Data describing the pore structure and BET surface area of catalysts and intermediates are summarized in Table 4.2. The washcoat could not be characterized separately, because it is attached to the monolith carrier. The corresponding data were thus calculated from values for the monolith carrier and catalyst using Equations 4.4 to 4.6.

$$a_{wc} = \frac{a_{mcat} - (1 - x_{m,wc})\, a_{mc}}{x_{m,wc}} \tag{4.4}$$

$$V_{pore,wc} = \frac{V_{pore,mcat} - (1 - x_{m,wc})\, V_{pore,mc}}{x_{m,wc}} \tag{4.5}$$

$$\varepsilon_{wc} = \frac{\varepsilon_{mcat} - (1 - x_{v,wc})\, \varepsilon_{mc}}{x_{v,wc}} \tag{4.6}$$

In Equation 4.6 the volume fraction of the washcoat in the catalyst $x_{v,wc}$ is used. This value can be calculated from the mass fraction $x_{m,wc}$ as shown in Equation 4.7, where ρ is the apparent density. From the measured densities and porosities given in Table 4.2, a value of $x_{v,wc} = 0.27$ is obtained.

$$x_{v,wc} = \frac{1}{1 + \frac{\rho_{wc}}{\rho_{mc}} \frac{1 - x_{m,wc}}{x_{m,wc}}} \tag{4.7}$$

The results in Table 4.2 show that the pore volume of the washcoat is smaller than that of the final powder catalyst although the calculated porosities are very similar. This contrasting result may be caused by measurement errors, especially for the monolithic catalyst and thus also for the washcoat.

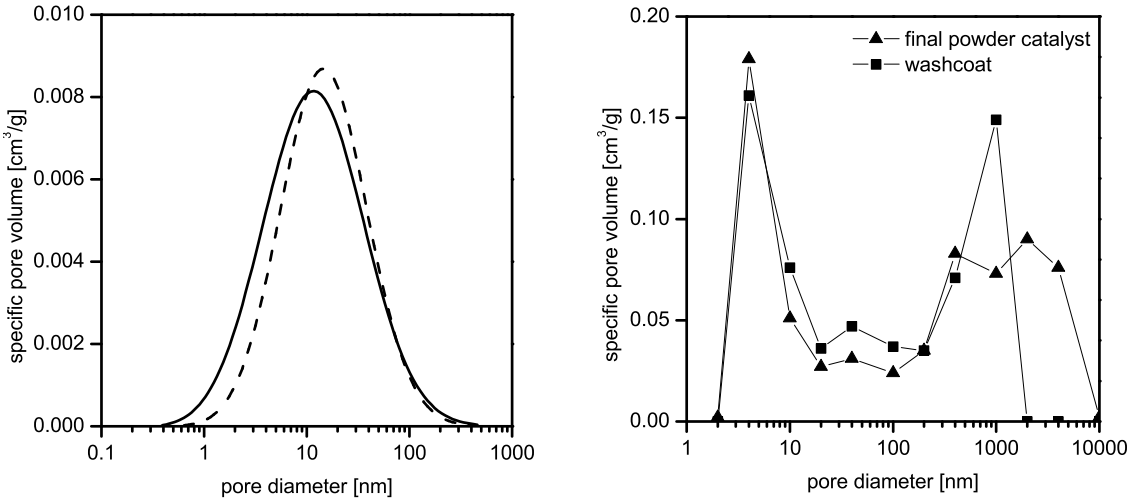

(a) N_2 adsorption (b) Hg intrusion

Figure 4.6: Distribution of specific pore volume in the final powder catalyst and the washcoat.

Table 4.3: Active metal dispersion, active surface area and mean cluster size of final powder catalyst and monolithic catalyst.

	D_{Co} %	$\tilde{a}_{\mathrm{Co}}$ $\mathrm{m^2_{Co}\,g^{-1}_{cat}}$	d_{Co} nm
Final powder catalyst	3.77 ± 0.38	5.09 ± 0.51	26.7 ± 2.69
Monolithic catalyst	3.01 ± 0.08	4.08 ± 0.11	33.2 ± 0.92

As can be seen in Figure 4.6, there are only minor differences in the pore size distributions of final powder and monolithic catalyst. The BET surface area of the washcoat and the final powder catalyst are also very similar (Table 4.2). Thus, it can be concluded, that the monolithic catalyst and the final powder catalyst have comparable pore structure properties. Since the same active catalyst powder was used for washcoating and preparation of the powder catalyst, the distribution of active sites must also be very similar.

The results of TPR measurements of final powder and monolithic catalysts are shown in Figure 4.7. The profile of monolithic catalyst shows smaller peaks for $Co(NO_3)_2$, Co_3O_4 and Re, which may be caused by its longer overall calcination time. The results of the chemisorption experiments obtained with final powder and monolithic catalysts

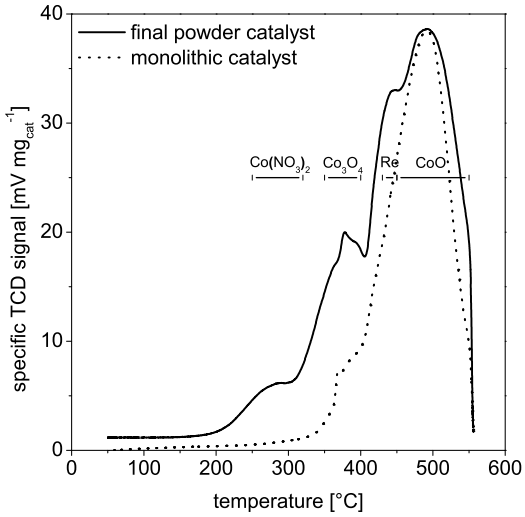

Figure 4.7: TPR profiles of final powder and monolithic catalyst.

are summarized in Table 4.3. In all cases, the small rhenium content was neglected and it was assumed that the reduced catalyst consisted of cobalt metal on alumina. It can be seen that the measured active metal surface area of the final powder catalyst is somewhat higher than for the monolithic catalyst. Consequently, higher metal dispersion and smaller cobalt cluster size are obtained. The results of chemisorption measurements are mainly comparable to literature, although a higher cobalt dispersion of 10.2 % has been reported (Storsæter et al., 2005a). This may be caused by lower cobalt and rhenium contents (12 wt% Co, 0.5 wt% Re) and a different chemisorption method using hydrogen adsorption at 40 °C.

4.3.4 Characteristic diffusion length

The characteristic diffusion length in porous catalysts is usually expressed by the ratio of catalyst volume and its external surface area. If one assumes spherical geometry of the powder catalyst, the resulting diffusion length amounts to one sixth of the mean particle diameter.

In our case, a coated square monolith channel typically shows an about 5 times higher catalyst thickness in the corners ($\approx 225\,\mu m$) compared to the planar walls ($\approx 45\,\mu m$) (Figure 4.8). The characteristic diffusion length of the monolith washcoat was calculated

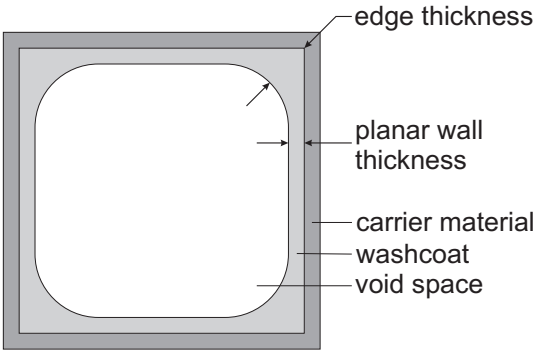

(a) scheme of one coated square monolith channel

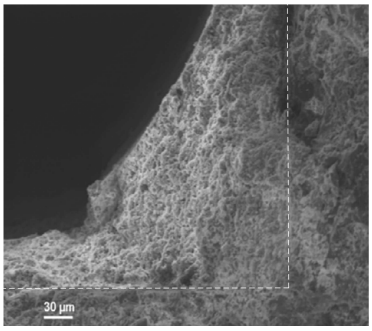

(b) SEM picture of the washcoat thickness in the corners of the channels

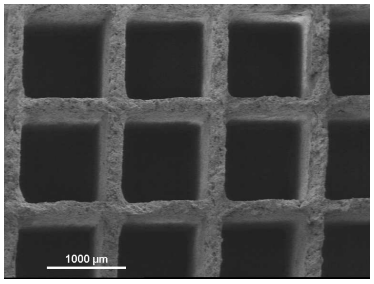

(c) SEM picture of an array of monolith channels

Figure 4.8: Washcoated square monolith channel.

with Equation 4.8. Here, the numerator represents the washcoat volume in one cell of the monolith. In the denominator the external surface area is calculated using the void space of a coated capillary. The open frontal area OFA of an uncoated monolith capillary is typically 0.75 and the diameter of a monolith cell d_{cell} is 1.27 mm for the 400 cpsi monolith used in our study. This calculation accounts for the distribution of the washcoat thickness and should give a reliable value for the characteristic diffusion length.

$$\delta_{wc,char} = \frac{x_{v,wc}\, d_{cell}}{4\sqrt{OFA_{mc} - x_{v,wc}}} \tag{4.8}$$

For the crushed monolithic catalysts, which are also investigated in the STR, it can be expected that the diffusion length of the major fraction is lower than the washcoat layer thickness on the planar walls, i.e. 45 µm. However, it cannot be excluded that part of the crushed catalyst layer, especially from the corners of the square monolith channels has a higher diffusion length. Overall, we assume a characteristic diffusion length of 50 µm for the crushed monolith.

4.4 Conclusions

Monolithic and powder catalysts for FTS based on Co (18.6 ± 0.9 wt%) and Re (1.2 ± 0.1 wt%) on γ-Al_2O_3 have been prepared. The monolithic catalysts were obtained by dip-coating in an aqueous suspension of base powder catalyst and colloidal binder followed by a calcination step. The washcoat thickness was adjusted by repeating this procedure. It was found, that the washcoat mass fraction achieved in each coating step decreases with the number of steps. This can be explained by decreasing surface area during coating and lower differences in zeta potential between the slurry particles and the monolith carrier. After six coating steps a washcoat mass fraction of about 0.20 g_{wc}/g_{cat} was achieved. The final powder catalyst was prepared by drying and calcination of the same catalyst slurry. The composition of the monolithic washcoat and powder catalyst is equal, because the same slurry was used for both preparations. It could also be shown that the pore structure and the internal surface area of the final powder catalyst and the monolith washcoat are very similar. Some differences were found in the reduction behavior and the active metal dispersion by TPR and CO chemisorption measurements, which might be caused by different overall calcination times. The comparability of powder catalyst and monolith washcoat may be further

increased by preparing the final powder catalyst in different layers on a flat support in the same manner as the washcoat. These layers can afterwards be removed from the support, crushed and sieved to the desired fraction.

In conclusion, the present results show that the preparation of powder and monolithic catalysts with identical physical and catalytic properties is challenging. However, the achieved properties of the catalysts are very similar and provide a good basis for a more detailed and systematic comparison of powder and monolithic catalysts used for FTS.

5 Experimental setup and procedure

5.1 Experimental setup

The experimental setup consists of a combination of a fixed-bed reactor and a well-mixed tank reactor for investigating monolithic and powder catalysts. Figure 5.1 and 5.2 present the scheme and an image of the experimental setup. The detailed flow diagram is given in Figure A.3 in the Appendix A.2.

The setup can be operated continuously by feeding CO, H_2 and an internal standard (e. g. CO_2, Ar) in separated lines using Bronkhorst Hi-Tec mass flow controllers. Additionally, the setup can be flushed with N_2. The feed gas mixture is led to the reaction section. After passing the reaction section the product stream is separated by wax (V3) and water (V4) separators to take wax and water samples. The operating pressure is maintained by a back pressure regulator downstream the water separator. The setup is mounted on a vented framework which is covered by plexiglass.

The reaction section can be operated in two modes. For investigation of powder catalysts, the stirred tank (V2) is used by directly feeding the educts via line S3. The streams S1, S2 and S4 are disconnected in this case. For operation in fixed-bed mode, the feed gas mixture is added to the gas recycle stream (S1). Gas and liquid (S2) recycle streams are mixed and supplied to the tubular reactor (V1). In this operation mode the STR is used as phase separator for the gas and liquid phase. Gas and liquid phase can be recycled independently from the STR by means of a compressor and a pump. Since the gas recycle ratio at the chosen conditions is about 100 and the conversion per pass is low, both the MLR and the STR are well mixed.

The stainless steel tubular reactor (22×2 mm) contains a static mixer (Fluitec Georg AG, CSE-X/8G 12.4 mm, 5 elements) at the top and a stainless steel sieve ($\approx$ 500 mesh) at the bottom. The static mixer is used to disperse gas and liquid over the reactor cross section. The sieve fixes the monolithic catalyst inside the tubular reactor. Two

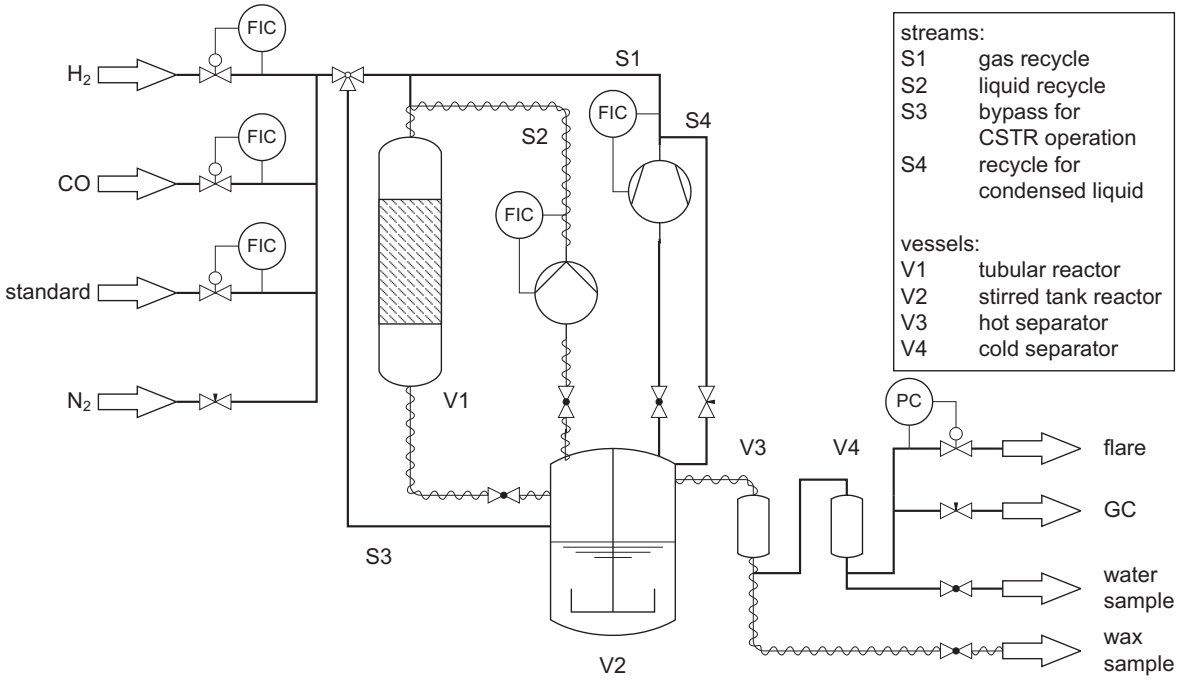

Figure 5.1: Scheme of the monolith loop reactor setup.

internal reactor diameters were used during the experiments (12 mm and 18 mm) at constant length of the catalyst bed of 50 cm. The reactor can be heated up to 400 °C by heating tape from HORST GmbH. Temperature is measured at the reactor wall, in the liquid recycle above the static mixer and directly below the catalyst bed by type K thermocouples.

The STR is home made and consists of a lid and a body (Figure 5.3). The lid is mounted on the framework and is heated by a flexible heating cartridge (hotspring F/4, 4.2×2.2 mm, 295 W) from Hotset GmbH. The lid also provides thread bores (6×G1/4 in, 2×G3/8 in) for the connection to gas and liquid recycle, gas feed, tubular reactor, liquid reservoir, downstream section, thermocouple and manometer. On the top of the lid the stirrer engine (Funrun MRK 46, premex reactor GmbH, 90 N cm, 120 W) is mounted, which can be equipped with home made blade and gas injection stirrers. The body of the stirred tank is equipped with two windows of sapphire glass from SITEC-Sieber Engineering AG (Ø 18 mm). To achieve good mixing and to prevent sedimentation of the catalyst the dead volume is minimized by rounded edges at the bottom. Furthermore the reactor has been equipped with baffles. The body is heated by six heating cartridges from Hotset GmbH (hotrod HHP, 8×130 mm, 250 W). For

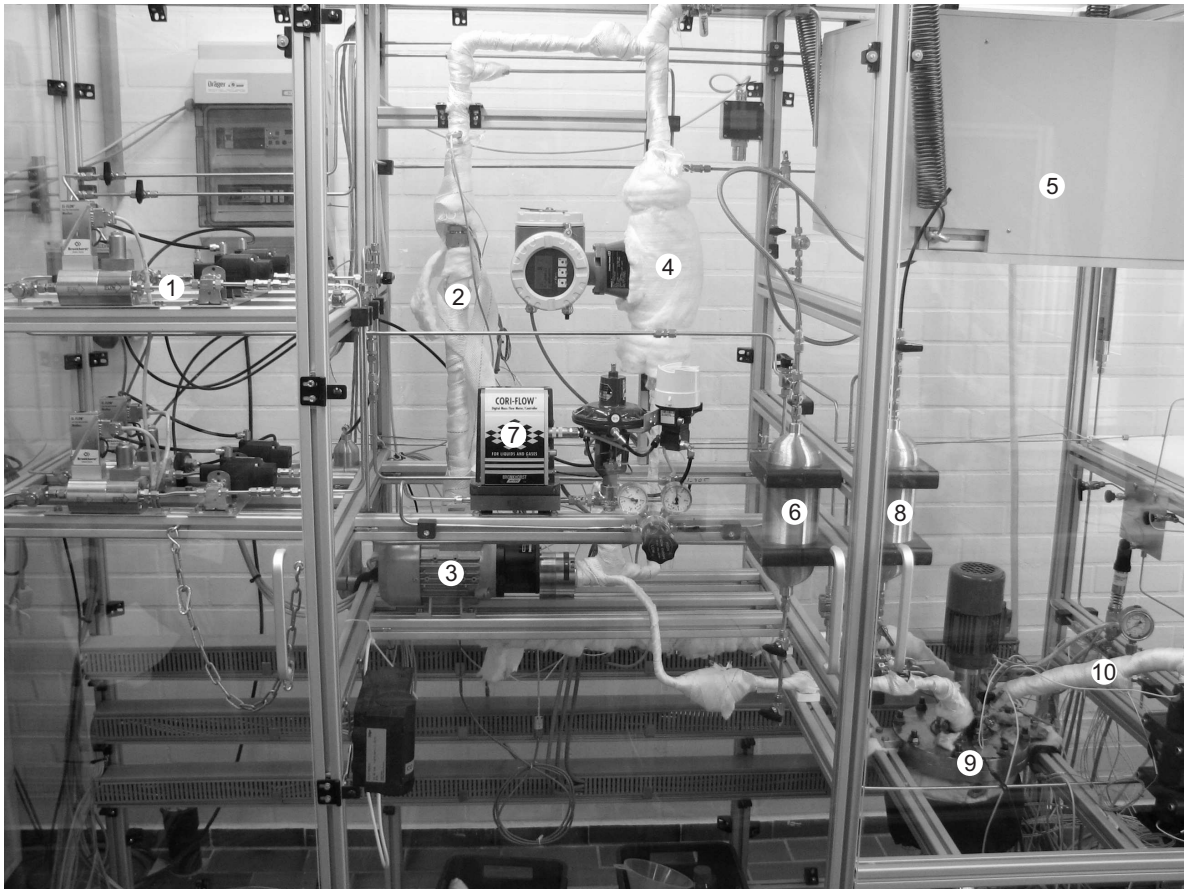

Figure 5.2: Image of the monolith loop reactor setup: (1) gas feed, (2) tubular reactor, (3) liquid recycle pump, (4) liquid recycle mass flow meter, (5) gas recycle compressor, (6) gas reservoir, (7) gas recycle mass flow controller, (8) liquid reservoir, (9) stirred tank reactor and phase separator, (10) heated tubing to wax and water separator.

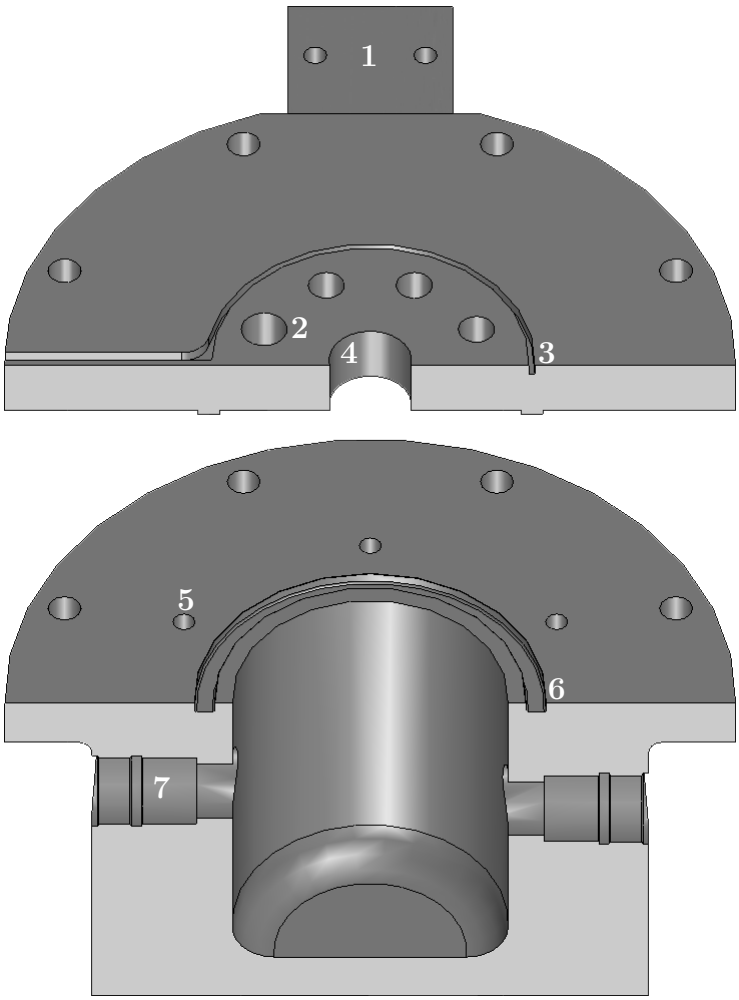

Figure 5.3: Image of the homemade STR (lid: (1) mounting element, (2) thread bores, (3) groove for flexible heating cartridge, (4) thread bore for stirrer engine, body: (5) bore for heating cartridge, (6) sealing groove, (7) window).

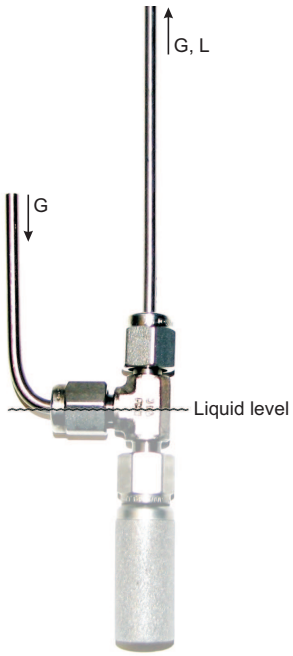

Figure 5.4: Control of liquid level in the STR.

filling and emptying the stirred tank body can be moved vertically by a jack. The lid and the body are sealed by a Chemraz® o-ring (Greene, Tweed & Co. GmbH, Chemraz 9350-605). The STR has a volume of 1 L and can be operated at up to 40 bar and 250 °C. The burst strength calculation for 40 bar and 250 °C revealed, that the maximum equivalent stress in the lid (100 N mm^{-2}) and the body (35 N mm^{-2}) should not exceed the yield stress of 130 N mm^{-2} at the maximum conditions. Additionally, the reactor was successfully pressurized to 40 bar at 20 °C and 30 bar at 175 °C, which proves the mechanical strength at typical operating conditions.

Figure 5.4 shows the principle of controlling the liquid level in the STR as described in Claeys (1997). The device consists of a frit (10 µm) with a 1/8 in tube connection and U-shaped 1/8 in tubing. Due to the continuous operation mode gas flows through the setup entering the U-shaped tubing in the head space of the STR towards the outlet of the setup. The liquid produced during the reaction percolates through the frit. The gas phase sweeps the liquid along to the wax and water separators. This procedure avoids pressure gradients over the frit that would lead to the formation of a filter cake and blocking of pores. Thus the principle is comparable to cross flow filtration, which will be the filtration process of choice for FTS in SBC.

The setup can be fed with CO (0.1 – 5 $L_{STP}\,h^{-1}$), H_2 (0.2 – 10 $L_{STP}\,h^{-1}$) and an internal standard (e. g. CO_2, Ar, 0.02 – 1 $L_{STP}\,h^{-1}$ for Ar) using mass flow controllers (Bronkhorst El-Flow F-230M). The feed can be disconnected by air driven valves. During operation in fixed-bed mode gas and liquid can be recycled independently by a compressor and a pump, respectively. A gear pump (Gather Industrie) transports the liquid phase from the STR and pumps it towards the tubular reactor (approx. 5 – 100 $kg\,h^{-1}$). The mass flow rate is measured by a coriolis mass flow meter (Endress + Hauser, Promass 83F DN 8). The pump is controlled by a frequency converter. In the high pressure section of the pump a pressure transmitter (BD Sensors, DMP331P) is installed, to detect pressure increases caused by blocking. The gas is recycled by a compressor (Haskel, HUAGD-4, 0.05 – 1.5 $kg\,h^{-1}$). In the low pressure section of the compressor an additional gas reservoir (300 mL) and a needle valve is installed. The needle valve reduces the gas flow that can be taken in from the compressor and decreases the pumping frequency. Combined with the reservoir the pressure changes in the stirred tank are reduced. This gas reservoir is cooled to $\approx$ 0 to 5 °C to condense liquid which will be present in the gas phase. The compressor is suspended on springs to reduce vibrations (Thema Federn GmbH). At the outlet of the compressor a gas reservoir (1 L) and a pressure regulator (Tescom, 44-2200) are installed to smooth the pressure for the mass flow controller. The mass flow controller for the gas recycle is a combination of a coriolis mass flow meter (Bronkhorst, Cori-Flow, 0.15–1.5 $kg\,h^{-1}$) and a air driven regulator valve (Badger Meter, RCV RC200). Due to the higher pressure in the high pressure section liquid may condense. Therefore the reservoir at the high pressure section is connected directly to the STR, which allows for transport of the condensed liquid directly back to the STR. Downstream the reactor, the setup was equipped with a wax (500 ml) and a water (300 ml) separator operated at 150 °C and 0 °C to take wax and water samples, respectively. The tubing between reactor and water separator was heated at 150 °C. The operation pressure was maintained by a backpressure regulator (Tescom, 44-1700). The total volume of the plant amounts to approx. 4.25 L in fixed bed mode.

Overflow valves with an opening pressure of 32.5 bar were installed in the gas feed line and at the STR. In addition the supply pressure of all gases is limited to 30 bar to prevent over pressure. To prevent the formation of an explosive gas mixture the setup is mounted in a vented framework which is equipped with CO and H_2 gas detectors. The control software allows the definition of alarm limits for pressure and temperature.

The gas detectors are also connected to the software. If the alarm is released, the power supply to the plant is disconnected and the setup is flushed with N_2.

The setup is computer controlled (Eurotherm Suite Graphics version 3.6.2). The control cabinet and software application was provided by Pro Control BV.

5.2 Analytical setup and procedure

5.2.1 Gas phase analysis

A HP 5890 GC was used to take on-line gas samples after passing the water separator. The GC is equipped with a TCD and a FID in series, a 250 µL sample loop and a HP-PLOT/Q column (Agilent, 30 m × 0.533 mm × 40 µm) to analyze CO, H_2, CO_2 and CH_4. The temperature program starts with 40 °C for 5.5 min followed by a temperature ramp of 20 K min^{-1} up to 200 °C which is maintained for 46.5 min. The split ratio is 12. The adjusted gas flow rates in the GC and supply pressures are given in Table 5.1.

Table 5.1: Gas flow rates and supply pressures for the gas phase GC.

	Gas	flow rate ml min^{-1}	supply pressure kPa
Sample	–	2 – 4	2000
Column	He	1.37	23.5
FID AUX	He	30.1	380
FID	H_2	32.1	120
FID	Air	422	290
WLD AUX	He	5.63	380
WLD Reference	He	16.2	380

Calibration measurements were carried out twice in April 2007 and January 2008 for CO, CH_4 and the internal standard CO_2. The molar fraction of each gas species is varied and the dependence of the molar fraction on the peak area is fitted with a linear function intersecting the coordinate origin (Equation 5.1). The number of data points, the range of molar fraction y_i, the slope of the linear function m_i and the coefficient of determination R^2 is given in Table 5.2. The presented data shows, that the calibration

is reproducible over the mentioned time span.

$$x_{n,i} = m_i \, A_{i,peak} \tag{5.1}$$

For collecting and analyzing the GC data as well as for controlling the GC a LabView program was developed. This program allows to start sample analysis in a given time interval and to record the detector signal of the TCD and FID with a frequency of 20 Hz automatically. The collected raw data is processed to obtain the peak areas of the analyzed components. Both the raw and the processed data are archived. A typical chromatogram of FID and TCD data is given in the Appendix A.2 Figure A.1.

Under the assumption that no carbon dioxide is formed during the reaction it can be used as internal standard. Ar is not appropriate for use as internal standard with a HP-PLOT/Q column, since the separation of Ar and CO is not possible. CO conversion X_{CO} and methane selectivity $S_{\mathrm{CH_4}}$ can be calculated with Equations 5.2 and 5.3. Here R is the peak area ratio of species CO or CH_4 and the internal standard, and m_i the slope of the calibration curve.

$$X_{\mathrm{CO}} = \frac{R_{in,\mathrm{CO}} - R_{\mathrm{CO}}}{R_{in,\mathrm{CO}}} \tag{5.2}$$

$$S_{\mathrm{CH_4}} = \frac{m_{\mathrm{CH_4}}}{m_{\mathrm{CO}}} \frac{R_{in,\mathrm{CH_4}}}{R_{in,\mathrm{CO}} - R_{\mathrm{CO}}} \tag{5.3}$$

Since the reactants are well mixed in stirred tank and fixed bed mode, the observed reaction rate $r_{obs,\mathrm{CO}}$ can be determined from the conversion X_{CO}, the modified residence time τ_{mod} and the H_2/CO feed ratio $R_{feed,\mathrm{H_2/CO}}$ (Equation 5.5). The modified residence time τ_{mod} is defined by the ratio of catalyst mass to synthesis gas feed rate at standard conditions Equation 5.4. The simplified first order reaction rate constant k_{obs}

Table 5.2: Calibration of the gas phase GC.

Gas	data points –	$x_{n,i}$ –	m_i $\mathrm{V^{-1}\,min^{-1}}$	R^2 –
CO	26	0.16, 0.22, 0.36	7.32	0.9957
CO_2	14	0.024, 0.041, 0.054, 0.078	6.05	0.9993
CH_4	10	0.099	10.13	0.9899

can be calculated from the observed reaction rate, the catalyst density ρ_{cat} and the CO concentration in the liquid phase (Equation 5.6). The activation energy can be derived from the rate constants at different temperatures (Equation 5.7).

$$\tau_{mod} = \frac{m_{cat}}{\dot{V}_{SG,in,STP}} \tag{5.4}$$

$$\tilde{r}_{obs,\mathrm{CO}} = \frac{X_{\mathrm{CO}}}{\tau_{mod}} \frac{p_{STP}}{(1 + R_{feed,\mathrm{H_2/CO}})\, R\, T_{STP}} \tag{5.5}$$

$$k_{obs} = \frac{\tilde{r}_{obs,\mathrm{CO}}\, \rho_{cat}}{c_{L,\mathrm{CO}}} \tag{5.6}$$

$$E_A = \frac{R}{\frac{1}{T_2} - \frac{1}{T_1}}\, ln\left(\frac{k_1}{k_2}\right) \tag{5.7}$$

5.2.2 Wax phase analysis

The wax phase is analyzed with a HP 5890 Series II Plus GC, equipped with an autosampler, a FID and a DB-2887 column (Agilent, 10 m × 0.530 mm × 3 µm). The injection volume is 2 µL. The GC is supplied by H_2 (29.3 mL min^{-1}, 133 kPa) and air (349 mL min^{-1}, 250 kPa) for the FID and He as carrier gas (1.71 mL min^{-1}, 220 kPa) and FID dilution (AUX) gas (10.9 mL min^{-1}, 220 kPa). The split ratio is 20. The temperature program starts at 30 °C with a heating rate of 20 K min^{-1} up to 350 °C. The total temperature program takes 120 min. The data is collected and processed with the GC ChemStation software (Agilent, Rev.B.03.01). The heavy waxy products derived from the wax separator still contain squalane and are present in solid state. For analysis, the heavy products are diluted in cyclohexane (≈ 14 wt % wax) and heated to ≈ 70 °C in a homemade Aluminum jacket for the autosampler, to keep it in liquid state for injection.

The analysis of the wax phase allows the calculation of the chain growth probability α. It is stated in ASTM (2002) that the relative mass specific response factor of each n-paraffin must not deviate from unity by more than ± 10 %. On this basis a chain growth probability α (Equation 5.8) can be calculated from the peak areas A of species with i and j carbon atoms in the chain. If data over a range of hydrocarbon species is available,

α can be calculated from the slope of the curve in the ASF-plot (see Equation 2.7).

$$\alpha^{i-j} = \frac{A_i\, j}{A_j\, i} \tag{5.8}$$

5.3 Experimental conditions and procedure

Prior to catalytic measurements the feed gas mass flow controllers were calibrated by the manufacturer at 40 bar and 20 °C. The calibration was checked at 30 bar and 20 °C with N_2 for the H_2 and CO and with Ar for the Ar controller. The deviation of the set point in the control software and the measured value was quantified for usage as correction factor.

Catalytic measurements were carried out to compare reaction rate and methane selectivity obtained with monolithic and powder catalysts during FTS. The powder catalyst was crushed and sieved to the desired fraction. The monolithic catalyst was investigated both as fixed and suspended catalyst bed. In the latter case the monolithic catalyst was crushed to allow the use in the STR. In order to avoid separation of the washcoat layer and the inert cordierite carrier, the crushed material was not sieved but completely used for the catalytic measurements. For the monolithic catalyst in fixed bed operation mode the mass of active catalyst material was limited to ≈ 10 g because of the dimensions of the reactor. In the STR ≈ 14.5 g of active catalyst material (powder or washcoat) were used. In case of the crushed monolith the total solid fraction consists of inert carrier material and active catalyst. This leads to a mass fraction of about 18.6 wt% solids in the suspension compared to about 4.1 wt% in the case of powder catalyst where no inert solid was present.

The reduction of the catalyst was performed with 10 % H_2 in N_2 at 350 °C for ≈ 36 h after heating in N_2 with 1 K min^{-1}. The monolithic catalyst was reduced in situ and the powder catalyst in an external oven. The hydrogen flow rate was set to 48 $\mathrm{ml_{STP}\,min^{-1}}$ corresponding to ≈ 4.62 mol of H_2, which exceeds the stoichiometric required H_2 amount for the reduction of 15 g catalyst by a factor of ≈ 70. After reduction the powder catalyst was cooled down in N_2 to room temperature, covered with squalane ($C_{30}H_{62}$, CAS no.: 111-01-3) under N_2 flow to prevent reoxidation and directly transferred to the STR which is filled to ≈ 450 mL. Squalane was chosen as starting solvent as it is a good solvent for FT products and inert in FTS (Claeys, 1997). Subsequently, the setup

was immediately purged with N_2 to remove O_2 to prevent catalyst reoxidation. Afterwards the setup was pressurized and purged continuously with the desired synthesis gas mixture at room temperature, until the feed gas composition was reached in the setup. The stabilization of the gas mixture in the setup was examined and quantified by the GC. A stable composition was assumed to be achieved, if ten gas phase samples differed in less then 1 % standard deviation. The measured feed gas composition was used in the calculation of conversion and selectivity. Subsequently, the catalyst was activated under synthesis gas flow for 24 h at 160 °C and 170 °C within the experimental setup. During the activation procedure gas and liquid phase were recycled in the monolith experiment. The mild reduction conditions with only 10 % H_2 and the long activation phase at relatively low temperatures was chosen to prevent catalyst damage.

The start-up procedure for operation in stirred tank and fixed-bed mode are different. In case of the STR operation mode the start-up procedure is presented in the discussion of the activation procedure. In the case of the fixed-bed mode of operation the STR was also filled initially with squalane. The liquid level in the STR decreased after the pump was started, due to filling of the tubing of the liquid recycle. To maintain the liquid level an additional reservoir was also filled with ≈ 1 L of squalane. After filling the setup with catalyst and liquid the setup was purged with N_2 carefully, to eliminate O_2 which could be hazardous under reduction conditions. For this purpose the gas compressor recycles the gas phase from the STR via the shortcut from the gas reservoir at the high pressure section back to the STR. This method allows the purge of the complete gas recycle and is also applied to the subsequent purge with feed gas mixture. The reduction procedure was carried out as described followed by pressurizing and purging continuously with feed gas mixture. After achieving a stable gas composition the setup was started up in fixed-bed mode. First the compressor was started and the gas recycle was pressurized. Due to higher pressure in the gas recycle the pressure in the setup decreases during this time. After achieving the operating pressure again, the desired gas recycle flow rate is set followed by the start of the liquid recycle pump. The liquid temperature was previously set to at least 150 °C to reduce the liquid viscosity. After starting the pump the liquid recycle was unstable. This can be caused by various reasons. Firstly, in the beginning gas and liquid phase will be present in the tubing disturbing both, the pump and the mass flow controller. Secondly, the liquid level in the STR decreases, which causes the transport of gas into the liquid recycle. Additionally, the temperature of the liquid decreases, due to the lower temperature of the steel tubing, which will increase the

viscosity. These reasons hinder the operation of the pump. To simplify the start-up of the pump a valve can be opened in the high pressure section of the pump. The pressure difference between the STR and the ambience will force liquid through the pump, which induces a continuous liquid flow and greases the pump. Simultaneously, liquid is added to the STR from the liquid reservoir to maintain the liquid level in the stirred tank. The amount of additional liquid should be slightly higher than required for achieving the desired liquid level inside the STR, since the liquid level is controlled as described before. If the STR contains too much liquid it will be removed and transported to the wax separator by the continuous gas flow. Consequently, liquid will be present in the wax separator which can be controlled by taking samples. Due to the small diameter of the tubing between STR and wax separator of 1/8 in it may take a few hours to remove the excess of liquid from the STR. It is recommend that the cooling aggregates and the heat tracing are activated as soon as possible.

To shut down the setup, the heating of the tubular reactor, the pump and compressor (in this order) were shut off and the temperature in the STR is set to 70 °C. At this temperature the products remain in liquid state and it is possible to clean the stirred tank without the risk of burning. After achieving a lower temperature the setup is depressurized and afterwards purged with N_2 to remove the hazardous CO and H_2. Subsequently, the STR is opened and cleaned under temperature. Finally, the wax and water separator and the tubular reactor are emptied. The internals of the STR are cleaned and the heating system is shut off.

In general the experiments were carried out at temperatures of 190 and 200 °C at a modified residence time of $12\,000\,\mathrm{kg_{cat}\,s\,m^{-3}_{SG,STP}}$ and a H_2/CO ratio of 2. In both operation modes the STR was equipped with a stirrer. In the stirred tank mode a gas injection stirrer was used to disperse the gas phase into the suspension, while in fixed-bed mode a blade stirrer was used to increase the heat transfer to the reactor wall. The flow rates of gas and liquid inside the monolithic honeycomb channels were adjusted to achieve the advantageous slug flow regime. Bauer (2007) investigated the flow regimes in mini-channels for different gas-liquid systems at 20 °C and 20 bar. It is stated that slug flow was achieved for gas and liquid superficial velocities smaller than $0.1\,\mathrm{m\,s^{-1}}$ for the squalane-nitrogen system. The maximum gas and liquid superficial velocities increase to $1\,\mathrm{m\,s^{-1}}$ for the lower viscous water-nitrogen system. Since the viscosity of squalane decreases with increasing temperature, the maximum gas and liquid superficial velocities for achieving slug flow are between 0.1 and $1\,\mathrm{m\,s^{-1}}$. To assure the slug flow regime inside

the monolith channels and to prevent catalyst abrasion the gas and liquid superficial velocity was adjusted to $\approx 0.05\,\mathrm{m\,s^{-1}}$. The required mass flow rates are estimated from the density of the gas and liquid phase. The liquid phase was assumed to consist of squalane, whose density was extrapolated according to data from Fandino et al. (2005). The measured mass flow rate for the gas phase was converted to a volumetric flow rate, assuming a molar mass of $10\,\mathrm{g\,mol^{-1}}$, which approximately corresponds to the feed gas mixture. At the top and the bottom of the monolithic bed an inert bed of glass beads with a length of 2.5 cm and a particle diameter of 1.25 – 1.55 mm was used to ensure an even gas-liquid flow distribution over the cross section.

Regularly, (approx. every two days) wax and water samples were taken. The samples were weighed and the composition of the wax samples was analyzed. As no fresh squalane was fed to the setup during the experiment the initially added squalane is substituted by liquid products over time. Thus, the sample composition represents an integral composition over the total experimental time up to the sampling time. Since the sampling is coupled with a pressure loss in the setup of ≈ 0.5 bar the experiment is slightly disturbed. To minimize the disturbance the sampling frequency was kept es low as possible.

During the experiments gas samples were analyzed online every 2 h. This allows the monitoring of CO conversion and CH_4 selectivity over time on stream. It was assumed that steady state had been reached, when the standard deviation of conversion and selectivity of the last ten samples is below 1.0 %. Steady state condition in the gas phase during the measurements was achieved after approx. 125 – 150 h.

The mass balance was carried out by weighing the liquid in the setup before and after the campaign as well as the wax and water samples. The total amount of feed gas was calculated from the mass flow controller data. The volumetric flow of the exhaust gas was calculated by Equation 5.9 under the assumption, that the molar flow rate of CO_2 as internal standard between inlet and outlet is constant.

$$\dot{V}_{out} = \dot{V}_{in} \frac{A_{in,\mathrm{CO_2}}}{A_{out,\mathrm{CO_2}}} \tag{5.9}$$

The composition of the exhaust gas was estimated from the feed gas composition for each campaign using the mean CO conversion and CH_4 selectivity. The exhaust gas was assumed to consist of CO, CO_2, H_2 and CH_4.

6 Results and Discussion

6.1 Introduction

In this chapter the experimental results obtained with powder and monolithic honeycomb catalysts will be discussed. In total 7 experimental campaigns were conducted between April 2007 and January 2008 with approx. 3170 h on stream. The experiments were carried out with two different catalyst batches. Table 6.1 summarizes the experimental campaigns. Within the campaigns different experiments were carried out by varying operation conditions.

This chapter provides the results and discussion of the conducted experiments. The first two sections deal with the experimental setup in particular. First of all, the sampling system and the effect of the sampling procedure on the sample composition will be discussed. Subsequently, the evolution of the loop-reactor setup in fixed-bed operation mode will be presented. The following sections present the results of the comparing measurements for powder and monolithic honeycomb catalysts with respect to the achieved reaction rate and methane selectivity. Finally, the influence of internal and external mass transfer on reactor performance in the slurry stirred tank reactor (STR) is discussed.

6.2 Results and discussion

6.2.1 Product segregation in the sampling system

The experimental setup consists of a wax and a water separator operated at 150 and $\approx 5\,^{\circ}\mathrm{C}$, respectively. Due to the different temperatures between the STR and the separators the original product mixture will be segregated. Heavy products will be enriched in the reactor and the wax separator, while light products will be enriched in the water separator and the exhaust gas. This segregation allows no conclusion

Table 6.1: Overview of conducted experiments (* Modified residence time in $kg_{cat}\,s\,m^{-3}_{SG,STP}$).

Campaign		I	II	III	IV
Catalyst type		monolith	powder	monolith	powder
Catalyst batch		1	1	1	1
Total time on stream	h	573	399	331	684
H_2/CO feed ratio	–	2	2	2	2
Modified residence time	*	4000	12000	3250	12000
Catalyst mass	g	4.04	14.2	3.75	13.3
Solid mass	g	19.25	14.2	20.11	13.3
Particle size/catalyst thickness	µm	120	50–140	120	500–1000
Characteristic diffusion length	µm	120	16	120	16
Diameter of tubular reactor	mm	12		12	
Flow rate H_2	$L_{STP}\,h^{-1}$	2.42	2.84	2.77	2.65
Flow rate CO	$L_{STP}\,h^{-1}$	1.21	1.42	1.38	1.33
Flow rate CO_2	$L_{STP}\,h^{-1}$	0.47	0.19	0.19	0.19
Deviation in mass balance	%	–	7.3	7.2	1.0
Deviation in mass balance	g	–	142	192	18
Campaign		V	VI	VII	
Catalyst type		crushed monolith	powder	monolith	
Catalyst batch		2	2	2	
Total time on stream	h	384	312	485	
H_2/CO feed ratio	–	2	2	2	
Modified residence time	*	12000	12000	12000	
Catalyst mass	g	14.6	14.3	10.1	
Solid mass	g	66.7	14.3	50.8	
Particle size/catalyst thickness	µm	< 120	50–140	120	
Characteristic diffusion length	µm	50	16	120	
Diameter of tubular reactor	mm			18	
Flow rate H_2	$L_{STP}\,h^{-1}$	2.91	2.86	2.13	
Flow rate CO	$L_{STP}\,h^{-1}$	1.46	1.43	1.01	
Flow rate CO_2	$L_{STP}\,h^{-1}$	0.19	0.19	0.19	
Deviation in mass balance	%	0.22	0.25	6.2	
Deviation in mass balance	g	4.5	4.0	135	

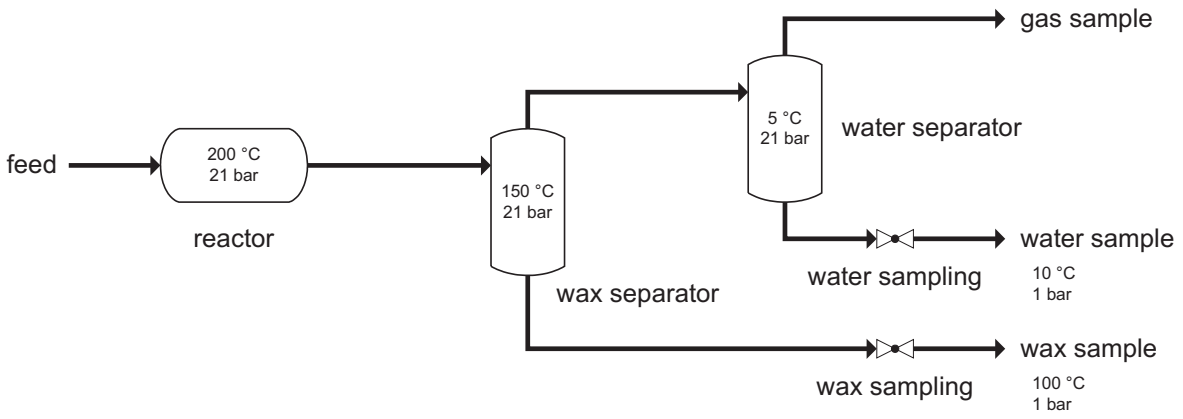

Figure 6.1: Scheme of the sampling system.

from the measured gas or wax phase analysis on the total product composition without further investigation. For this purpose the described phenomenon is modeled in Aspen Custom Modeler® using the Aspen Properties® physical properties database and the Redlich-Kwong-Soave equation of state with Kabadi-Danner modification according to de Deugd (2004). The equilibrium composition in the three phase gas-liquid-water system was calculated using the physical property submodel "Props_flash3" assuming equilibrium. The product mixture was assumed to consist of CO, H_2, H_2O, squalane and paraffins with a chain length of up to 30 carbon atoms. Olefins are neglected, since physical properties such as the vapor pressure are similar to paraffins. The aim of this model is to describe the segregation behavior in the present experimental setup and to provide a method to utilize the wax phase data for determining the chain growth probability.

Figure 6.1 illustrates the sampling setup including the operation conditions. The operating conditions of the phase separators and the sampling procedure are chosen according to the experimental setup and procedure. In the reactor the product distribution is calculated with a typical chain growth probability of $\alpha = 0.777$ for the used catalyst according to results of campaign VI, which will be presented later. The product mixture is transported to the wax separator where a gas-water-liquid three phase system develops. The liquid hydrocarbon and water phase were taken as samples. During sampling the temperature decreases and also the pressure decreases to ambient pressure in the sample. This results in partial evaporation of water and hydrocarbons. The gas phase in the wax separator is transported to the water separator. Since the temperature

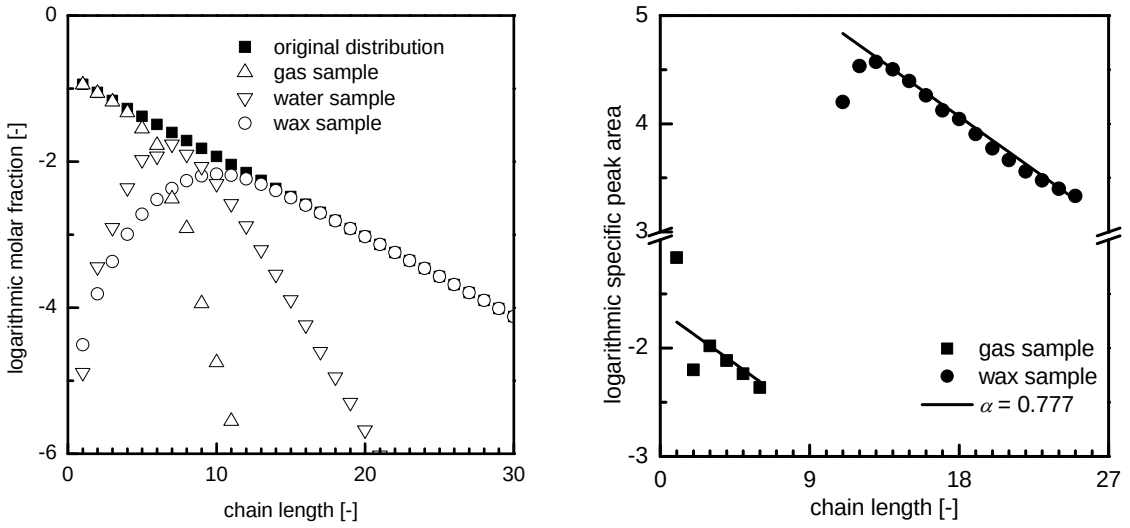

(a) Simulation results

(b) Experimental results (campaign VI, 200 °C, crushed monolithic catalyst)

Figure 6.2: Product segregation in the sampling system for $\alpha = 0.777$.

is smaller in the water separator water and lighter hydrocarbons will condense and a gas-water-liquid three phase system will also develop. The sampling procedure of the liquid hydrocarbon and water phase causes a decrease in pressure and an increase in temperature, which leads to partial evaporation of the sample. The gas phase in the water separator is directly transported to the GC and analyzed. The presented model assumes equilibrium. This assumption is realistic for the phase separators, since the residence time is high. However, during sampling equilibrium may not be achieved and differences between experimental and calculated data will occur.

Figure 6.2a displays the simulation results of the product segregation. It is obvious, that significant segregation of the products in the samples occur, which results in deviations from the original product distribution. The segregation is caused by decreasing vapor pressures with increasing chain lengths of the hydrocarbons. This leads to an enrichment of light hydrocarbons in the vapor phase and heavy hydrocarbons in the liquid phase depending on the temperatures in the wax and water separator. The liquid phase of the wax separator mainly consists of heavy hydrocarbons with a maximum for the species C_9 to C_{11}. Lighter hydrocarbons are mainly present in the gas phase and are transported to the water separator. For heavier hydrocarbons the product distribution converges with the original distribution, since the vapor pressure of these species

is too low at the given temperature. In the sample of the gas phase in the water separator heavy hydrocarbons are present in a proportionally low amount, leading to an underestimation of the chain growth probability. The water sample contains medium hydrocarbons in the range of C_7. Lighter hydrocarbons are mainly present in the gas phase, while heavier hydrocarbons are already separated in the wax separator.

Figure 6.2b presents measured product distributions for the gas and wax sample. Comparing the simulation results with the measured product distributions, deviations are observed for the gas phase composition. This could mainly be attributed to the fact, that equilibrium is assumed in the model, whereas it may not be reached in the experiment. The deviation for CH_4 and C_2 can be explained by the deviance of real and ideal ASF distribution. However, comparing the simulated and measured wax phase composition good agreement can be observed. Both results exhibit a maximum for C_{11} in the model and C_{13} in the wax sample, respectively. For increasing chain lengths the distribution converges with the original distribution. The curves for the measured product distributions in gas and wax phase are shifted in vertical direction, since different GC systems are applied using different peak area definitions, e. g. $V \times min$ or counts $\times$ s. However, the specific peak area of one species is proportional to its molar fraction in the sample.

It can be concluded from the simulation results, that the presented model is able to describe the segregation of the products and that the chain growth probability could by determined from samples of the wax phase, while gas and water samples are not significant. It is suggested to identify the chain growth probability with data for species following the maximum in the distribution of the wax sample to achieve reasonable values.

6.2.2 Evolution of the loop-reactor setup

The loop-reactor setup presented in chapter 5 is the result of revisions of two preliminary experiments in fixed-bed operation mode. To support the comprehensibility of the revisions discussed in this section, Figure 6.3 again displays the scheme of the experimental setup. The main challenge in operating the setup in fixed-bed mode is the gas recycle. Since the phase separator operates at temperatures of 200 to 240 °C the vapor pressure of the produced liquid hydrocarbons, water and Squalane causes that the gas recycle contains liquid components in the range of ≈ 0.1 vol %. This will lead

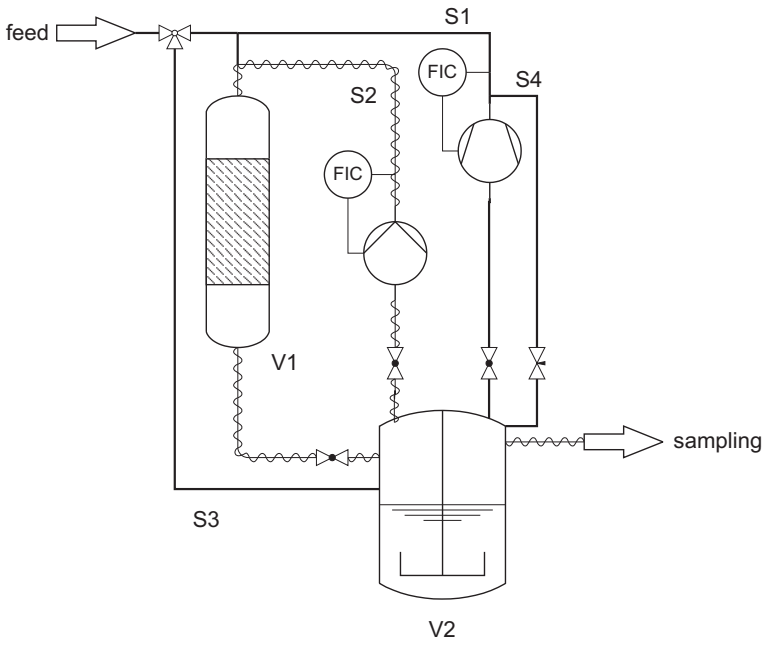

Figure 6.3: Scheme of the experimental setup ((S1) gas recycle, (S2) liquid recycle, (S3) bypass for CSTR operation, (S4) recycle for condensed liquid, (V1) tubular reactor, (V2) stirred tank reactor, detail of Figure 5.1).

to condensation in the high pressure section of the gas recycle, as the pressure is higher and the temperature is lower than in the phase separator. The condensation rate of liquid exceeds the liquid production rate. This results in a continuous removal of liquid from the phase separator.

The first approach to reduce the condensation in the high pressure section of the gas recycle was the insertion of a reservoir previous to the gas compressor and the recycling of condensed liquid from the high pressure section back to the phase separator via stream S4 (Figure 6.3). The aim was to reduce the liquid content in the gas phase by the additional reservoir. The temperature of this reservoir at room temperature was significantly lower than in the phase separator and the gas velocity is reduced. It was expected, that entrained liquid will condense and flow back to the phase separator before entering the gas compressor. The remaining liquid will condense in the high pressure section. It was desired to continuously recycle the condensed liquid back to the phase separator. The experimental campaign following the described improvements revealed, that condensation of liquid in the gas recycle is significantly reduced. However, a continuous feeding of the condensed liquid to the phase separator was not possible.

The main reason could be blocking of the needle valve in stream (S4) by waxy products. The following second approach aims at improving the liquid condensation before the gas compressor. For this purpose, the reservoir in the low pressure section was furnished with cooling coils. Furthermore, the diameter of the tubing between the reservoir and the phase separator was increased from 1/4 in to 1/2 in. This enhancement was expected to reduce the liquid content in the gas recycle significantly, but it is still necessary to discontinuously recycle condensed liquid. However, the improvement was successful, as the time span between recycling condensed liquid could be increased from 1 to 4 days.

The discontinuous recycling of condensed liquid also affects the pressure in the setup. The pressure in the phase separator and the high pressure section of the gas recycle will equalize, which results in an increasing pressure in the phase separator and a decreasing pressure in the gas recycle. The pressure increase in the phase separator will cause a pressure release by the back pressure regulator, as the adjusted pressure is exceeded. This will cause an undefined loss of material, which could cause the relatively high deviation in the mass balance. After recycling the condensed liquid the pressure in the high pressure section increases again and thus the pressure in the phase separator and the whole system decreases, as the total gas volume was reduced by the pressure release. To prevent this pressure drop the outlet of the setup can be closed, until the original pressures are reached.

During recycling the condensed liquid it was furthermore observed, that instabilities in the liquid recycle stream appear. Possible explanations could be the lower temperature and different composition of the condensed liquid. The lower temperature of this liquid will reduce the temperature in the phase separator, which increases its viscosity. Furthermore, the fraction of light hydrocarbons and water in the condensed liquid is higher than in the liquid of the phase separator, as the waxy products are condensed before entering the gas compressor. Recycling the light components will cause evaporating of these components. The liquid phase in the phase separator will be in a turbulent gas-liquid flow and gas can enter the liquid recycle. This could cause instabilities in the liquid recycle flow rate.

In Figure 6.4 the conversion and selectivity for the monolithic catalyst in fixed bed mode (campaign VII) are displayed. Deviations in conversion and selectivity were found and marked in this figure. These deviations are caused by the discontinuous recycling of fresh liquid to the phase separator at the marked times. A possible explanation could be, that the fresh liquid dilutes the produced wax and thus enhances mass transfer and conversion for a short time period.

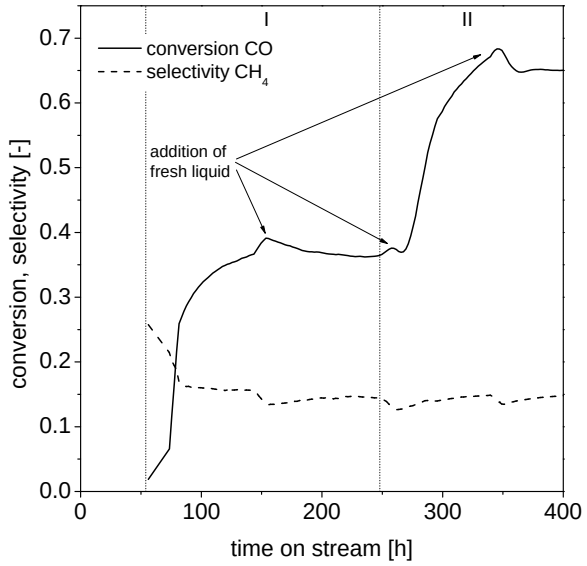

Figure 6.4: CO conversion and CH_4 selectivity over time on stream, campaign VII: monolithic catalyst in fixed-bed operation mode.

A further challenge is the adjustment of the temperatures in the setup to achieve the desired temperature in the tubular reactor. The temperature of the liquid is directly measured in the phase separator, before the liquid recycle mass flow controller and at the inlet and outlet of the tubular reactor. The temperature for the liquid recycle mass flow controller is limited to 200 °C. The mass flow controller and the liquid pump contribute significantly to the heat losses in the liquid recycle, as both devices could not be isolated completely. To achieve 200 °C at the reactor inlet and outlet, the liquid in the phase separator has to be heated to 220 °C which results in a temperature of 209 °C directly before the mass flow controller. This temperature exceeds the specified maximum. The large liquid flow rate from the outlet of the tubular reactor has to be heated from 200 to 220 °C in the phase separator, which requires a shell temperature of the phase separator of 252 °C. These big differences between minimum and maximum temperature of 52 K could only slightly be influenced by improved insulation of the present setup. However, it could be reasonable to implement an additional heat exchanger at the top of the tubular reactor which is supplied by a heating circulator or by electrical heating. It should be possible to heat the recycled liquid from 200 °C up to 220 °C depending on the flow rate, which significantly will increase the reaction and hydrocarbon production rate and buffers the heat losses in the liquid recycle.

Table 6.2: Results for comparison of monolithic honeycomb and powder catalyst in STR and tubular reactor (* $1 \times 10^{-4}\,\mathrm{mol_{CO}\,kg_{cat}^{-1}\,s^{-1}}$, ** $1 \times 10^{-7}\,\mathrm{mol_{CO}\,m_{Co}^{-2}\,s^{-1}}$).

Catalyst		Powder		Crushed Monolith		Monolith	
Campaign		VI		V		VII	
Metal surface area	$\mathrm{m_{Co}^2\,g_{cat}^{-1}}$	5.09		4.08		4.08	
Temperature	°C	190	200	190	200	190	200
CO conversion	–	0.319	0.509	0.268	0.393	0.363	0.650
CH_4 selectivity	–	0.127	0.124	0.133	0.138	0.145	0.147
Mass specific reaction rate	*	3.96	6.31	3.32	4.87	4.51	8.07
Area specific reaction rate	**	0.778	1.24	0.814	1.19	1.11	1.98
Activation energy	$\mathrm{kJ\,mol^{-1}}$	110		81.8		138	

6.2.3 Comparison of catalyst geometries

In this section powder catalyst is compared to monolithic honeycomb catalyst investigated in both STR and tubular reactor. Table 6.2 summarizes the results of the catalyst comparison. The operating conditions were already presented in Table 6.1 in the introduction to this chapter.

Comparison of powder and monolithic catalysts reveals that the methane selectivity in all experiments with catalyst batch 2 ranges from 12.4 to 14.7 %. These values are somewhat higher than for comparable catalysts reported by de Deugd (2004), while Rytter et al. (2007) report comparable values for small pores and large diffusion lengths. The powder catalyst shows the lowest methane selectivity, followed by the crushed monolithic catalyst and the monolithic catalyst used in fixed bed operation mode. However, these differences are relatively small. The differences to the lower CH_4 selectivity of 10.2 to 11.1 % in campaign II (see Table 6.4) may be explained by the different catalyst batch used.

Differences in synthesis gas conversion and reaction rate are observed, comparing powder and crushed monolithic catalyst. These differences are more pronounced at the higher reaction temperature of 200 °C. One reason to explain these differences could be the different active metal surface areas for monolithic and powder catalysts. Taking this into account, using a modified, area-specific reaction rate, a better agreement between powder and crushed monolithic catalysts is obtained at 190 °C. Investigations reported in the literature (de Deugd, 2004) show a 3 to 4 times higher reaction rate for monoliths.

However, these results were obtained in absence of a liquid phase and are thus not directly comparable, as discussed by Hilmen et al. (2005).

The higher reaction rate of the monolithic catalyst in fixed bed operation mode compared to the crushed monolithic catalyst could be caused by external mass transfer resistances in the STR. To test this hypothesis the mass transfer coefficients in the STR and the MR have been estimated. Based on literature correlations (Pangarkar et al., 2002; Kreutzer, 2003) the overall mass transfer coefficient ka_{ov} for STR (Equation 6.1) and MR (Equation 6.5) under reaction conditions was estimated. For $ka_{GL,STR}$ a typical value was taken from measured data reported in the literature for a representative hydrocarbon mixture (Soriano, 2005). The density, viscosity and surface tension of the liquid phase as well as the Henry coefficient for CO were calculated with literature correlations for Sasol wax (Soriano, 2005).

$$\frac{1}{ka_{ov,STR}} = \frac{1}{ka_{GL,STR}} + \frac{1}{ka_{LS,STR}} \tag{6.1}$$

$$ka_{LS,STR} = \frac{6\,D\,x_{cat}}{d_P^2}\left(2 + 0.3\,Re_{\varepsilon}^{0.75}\,Sc^{0.33}\right) \tag{6.2}$$

$$Re_{\varepsilon} = \left(\frac{\varepsilon\,d_P^4\,\rho_L^3}{\eta_L^3}\right)^{\frac{1}{3}} \tag{6.3}$$

$$ka_{GL,STR} = 0.1\,\mathrm{s}^{-1} \tag{6.4}$$

$$ka_{ov,MR} = ka_{GLS,MR} + ka_{GS,MR} = \frac{4\,D}{\delta_f\,d_{ch}} \tag{6.5}$$

$$\delta_f = d_{ch}\,\frac{0.66\,Ca^{\frac{2}{3}}}{1 + 3.33\,Ca^{\frac{2}{3}}}$$

$$Ca = \frac{\eta_L\,u_{TP}}{\sigma_L} \tag{6.6}$$

The influence of the internal and external mass transfer on the observed reaction rate can be analyzed using the time constants for mass transfer ka_{ov}^{-1}, the observed reaction rate k_{obs}^{-1} and the intrinsic reaction rate k_{int}^{-1} inside the catalyst, as well as the catalyst effectiveness factor η (Equation 6.7, Losey et al. (2001)). From the measured conversion and inlet molar flow rate of CO the observed reaction rate can be obtained. The

simplified first order reaction rate constant k_{obs} can be calculated from the observed reaction rate, the catalyst density and the CO concentration in the liquid phase assuming equilibrium. The gas phase was assumed to be ideally mixed and to consist of CO, H_2 and H_2O only. The effect of internal mass transfer can be estimated using the Thiele modulus ϕ (Equation 6.8).

$$\frac{1}{k_{obs}} = \frac{1}{k a_{ov}} + \frac{1}{\eta\, k_{int}} \tag{6.7}$$

$$\eta = \frac{\tanh\ \phi}{\phi} \tag{6.8}$$

$$\phi = \delta_{char}\ \sqrt{\frac{k}{D_{\text{eff}}}} \tag{6.9}$$

These simple calculations show that mass transfer resistances obviously influence the observed reaction rate (Table 6.3). Comparison between crushed monolithic catalyst in STR and monolithic catalyst in fixed-bed reactor with the same active metal surface area show a higher influence of mass transfer on the observed reaction rate in the STR. At comparable intrinsic reaction rates the observed reaction rate in MR is significantly higher. These differences are more pronounced at the higher reaction temperature of 200 °C. The time constants for powder catalyst in the STR are summarized in Table 6.3 as well. These results also show a higher influence of mass transfer resistances on the observed reaction rate compared to the monolithic catalyst in FBR. Furthermore, very similar intrinsic reaction rates as calculated for the monolithic catalysts are obtained.

The results in Table 6.3 also show, that the powder catalyst in the STR is not influenced, while the monolithic catalyst in FBR mode is slightly affected by internal mass transfer. However, these estimations are rough and based on several assumptions and are thus only suitable for qualitative analysis. Especially, the analysis of the data for the crushed monolithic catalyst is challenging, as the particle size distribution is difficult to describe and the large particles could sediment at the bottom of the STR.

The influence of mass transfer resistances on the observed reaction rate can also be seen from the apparent activation energies, which were calculated from the first order reaction rate constants k_{obs}. The results range from 81.8 kJ mol^{-1} for the crushed monolithic catalyst, over 110 kJ mol^{-1} for the powder catalyst to 138 kJ mol^{-1} for the monolithic catalyst. The influence of internal and external mass transfer resistances for

Table 6.3: Comparison of time constants for mass transfer, observed and intrinsic reaction rate for monolithic honeycomb and powder catalyst.

			190 °C	200 °C
Monolithic catalyst	k_{obs}	s^{-1}	0.0160	0.0342
	ka_{ov}	s^{-1}	0.1410	0.1420
	η	–	0.955	0.902
	k_{int}	s^{-1}	0.0190	0.0500
Powder catalyst	k_{obs}	s^{-1}	0.0156	0.0285
	ka_{ov}	s^{-1}	0.0737	0.0740
	η	–	0.999	0.998
	k_{int}	s^{-1}	0.0197	0.0463
Crushed monolithic catalyst	k_{obs}	s^{-1}	0.0127	0.0198
	ka_{ov}	s^{-1}	0.0378	0.0381
	η	–	0.989	0.975
	k_{int}	s^{-1}	0.0193	0.0425

powder catalyst in the STR will be discussed in more detail in the following section.

Besides the CO conversion and the CH_4 selectivity the composition of the wax phase is of interest, regarding the achievable chain growth probability with the applied catalyst. The wax samples taken during the experiments still contain a high amount of squalane, which is the liquid solvent. A typical chromatogram of the wax phase is presented in Figure A.2 in the Appendix. Figure 6.5 shows the product distribution and the ASF-plot for the wax phase for the crushed monolithic and powder catalyst in the STR and the monolithic catalyst in the FBR. Figure 6.5a displays the GC peak area as a function of the chain length. It can be seen, that the product distribution of the crushed monolithic and the powder catalyst is comparable. As discussed previously, the short chain hydrocarbons are depleted in the wax sample, due to the higher vapor pressure. The maximum is reached for the hydrocarbon species C_{13}. The chain growth probability can thus be estimated based on the distribution of the C_{13+} species using the ASF-plot (Figure 6.5b). In the ASF-plot the peak area of each species is divided by the number of carbon atoms to calculate the specific peak area, as the sensitivity of the FID is proportional to the species mass in the sample and molar fraction is required for the determination of the chain growth probability. From the slope of the linear fitted curve the chain growth probability can be estimated by inverse function of the common

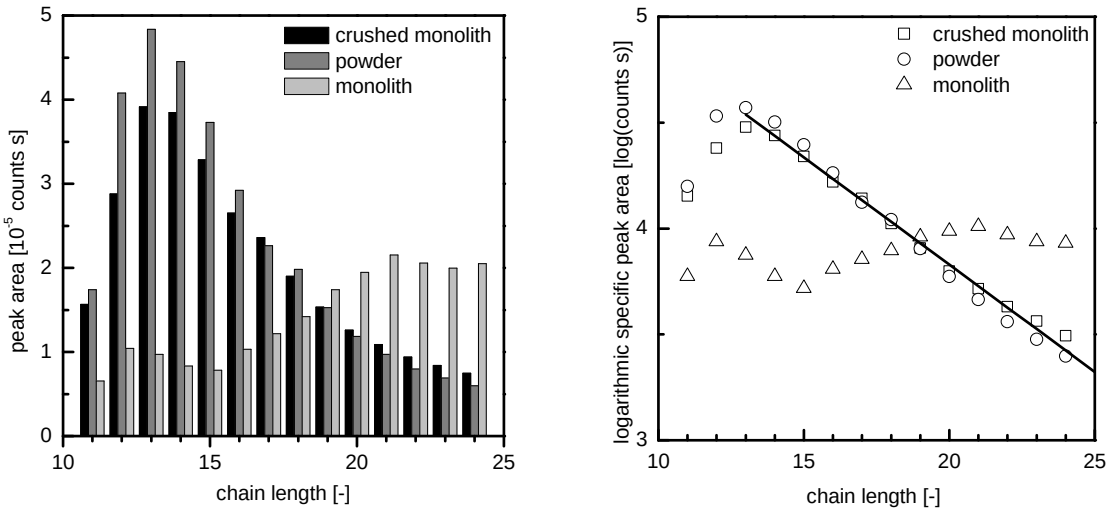

(a) Product distribution

(b) ASF plot (line: $\alpha = 0.791$)

Figure 6.5: Product distribution in the wax phase and determination of the chain growth probability.

logarithm. Since the product distribution of the crushed monolithic and powder catalyst is comparable, the estimation of the chain growth probability is based on a mean value of both samples each with two injection runs. The dependence of the specific peak area on the chain length for crushed monolithic and powder catalyst is fitted with an accuracy of more than 99 %, while the standard deviation between the four data sets is less than 2 %. The estimated chain growth probability amounts to $\approx$ 0.791. In case of the monolithic catalyst in the tubular reactor the analysis of the wax sample is more complicated. The product distribution shows two maxima for C_{12} and C_{21}, which was not expected. Accordingly, the estimation of the chain growth probability is uncertain. A linear fit in the ASF-plot for C_{13+} species is not possible. Explanations for the unusual product distribution could be a higher content of the solute squalane on the one hand. On the other hand an enhanced loss of lighter hydrocarbons can occur. During the recirculation of the gas phase, light hydrocarbons condense in the gas recycle as described. The condensed liquid was discontinuously transported back to the phase separator, where it evaporates again. This causes a pressure increase in the setup and thus a loss of gas due to pressure control. At this time, light hydrocarbons are enriched in the gas phase and are consequently lost in the exhaust gas. The measurement of the CO conversion is not affected by this circumstance, since the conversion is monitored every

Table 6.4: Influence of stirrer speed on CO conversion and CH_4 selectivity, campaign II.

Experiment		III	IV	V	VI
T	°C	200	200	200	200
p	bar	21	21	21	21
n	min^{-1}	1000	500	1500	1000
TOS	h	254.5	312.75	350.75	398.75
X_{CO}	–	0.560	0.515	0.538	0.542
$S_{\mathrm{CH_4}}$	–	0.102	0.111	0.109	0.109
$\tilde{r}$	$10^{-4}\,\mathrm{mol_{CO}\,kg_{cat}^{-1}\,s^{-1}}$	6.95	6.38	6.67	6.72

2 h over an adequate time period, while the evaporation of the light hydrocarbons occurs in a relatively short time. In general conclusion, considering the uncertainty of the estimation procedure, the chain growth probability achieved in the STR is comparable for both investigated catalysts between 0.75 and 0.8.

6.2.4 Effect of internal and external mass transfer in STR

Campaign II was performed to study the influence of external mass transfer for powder catalyst in the STR at 200 °C. For this purpose the stirrer speed was varied between 500 and 1500 min^{-1} at 200 °C for powder catalyst with a characteristic diffusion length of 16 µm. At this small diffusion length internal mass transfer resistances can be neglected. Table 6.4 and Figure 6.6a display the relevant results. Decreasing the stirrer speed from 1000 to 500 min^{-1} results in a decrease of conversion from 0.56 to 0.515 (experiments III and IV in campaign II). Further increase of the stirrer speed shows a slightly increase in conversion. The conversion before changing the stirrer speed could not be reached again. These results indicate external mass transfer limitations at a stirrer speed below 1000 min^{-1}. However, the influence of stirrer speed on conversion and methane selectivity is relatively low.

In contrast to the experimental results simple estimations show a significant influence of external mass transfer resistances on the observed reaction rate constant in campaign II at 200 °C. With an overall mass transfer coefficient of $ka_{ov,STR} = 0.0740\,\mathrm{s}^{-1}$ at a specific power input of $\varepsilon = 2\,\mathrm{W\,kg}^{-1}$ and a catalyst effectiveness factor of $\eta = 1$ (see Table 6.5) the intrinsic reaction rate constant amounts to $k_{int,STR} = 0.0602\,\mathrm{s}^{-1}$,

while the observed reaction rate constant $k_{obs,STR} = 0.0332\,\mathrm{s}^{-1}$ is significantly smaller. This may be explained by the fact, that the enhancement in mass transfer rate by increasing the specific power input is very limited. Figure 6.6b illustrates, that the intrinsic reaction rate constant could not be reached even by significant increase in specific power input. This corresponds well to the experience, that the achievable relative velocity between the liquid phase and fine catalyst particles is limited, since especially the small particles are entrained in the liquid flow. It can thus be concluded, that the intrinsic kinetics cannot be directly measured with the STR used in the present study. The influence of external mass transfer on the observed reaction rate constant is also estimated for SBCs. This estimation is rough, since small and large bubbles contribute to the external mass transfer differently. Furthermore, a correlation for mass transfer between liquid phase and solid catalyst is not available. For the border cases of small and large bubbles, the range of the observed reaction rate constant is shown in Figure 6.6b. The ratio between intrinsic and observed reaction rate constant for small bubbles in the SBC is comparable to the reactor efficiency discussed in Figure 3.5. The results also show comparable observed reaction rate constants for STR and SBC, which supports the STR as reasonable model system for the SBC.

Campaign IV was conducted to study the influence of internal mass transfer on CO conversion and CH_4 selectivity. Therefore catalyst with a particle size between 500 and 1000 µm was used which results in a mean characteristic diffusion length of 125 µm compared to 16 µm in campaign II. The characteristic diffusion length influences the catalyst effectiveness factor as shown in Figure 6.7. However, after finishing the campaign catalyst attrition was observed, which leads to smaller catalyst particles.

Table 6.5 compares the reaction rate and methane selectivity for different diffusion lengths at 200 °C and 21 bar. The results show, that an increase in average catalyst particle diameter from 95 to 750 µm leads to a significant decrease in reaction rate. The catalyst with a particle size between 500 and 1000 µm achieves only 25.8 % of the reaction rate of the smaller particle fraction. From the observed reaction rate constant $k_{obs,STR} = 6.33 \times 10^{-3}\,\mathrm{s}^{-1}$, the catalyst effectiveness factor $\eta = 0.868$ and the overall mass transfer coefficient $ka_{ov,STR} = 0.0278\,\mathrm{s}^{-1}$ for the large particles the intrinsic reaction rate constant $k_{int,STR} = 9.45 \times 10^{-3}\,\mathrm{s}^{-1}$ can be calculated. This estimation reveals an approx. 6.4 times smaller intrinsic reaction rate constant for large particles, which can only partly be explained by the catalyst effectiveness factor of 0.868. The big differences between the theoretical and measured catalyst effectiveness factors may be

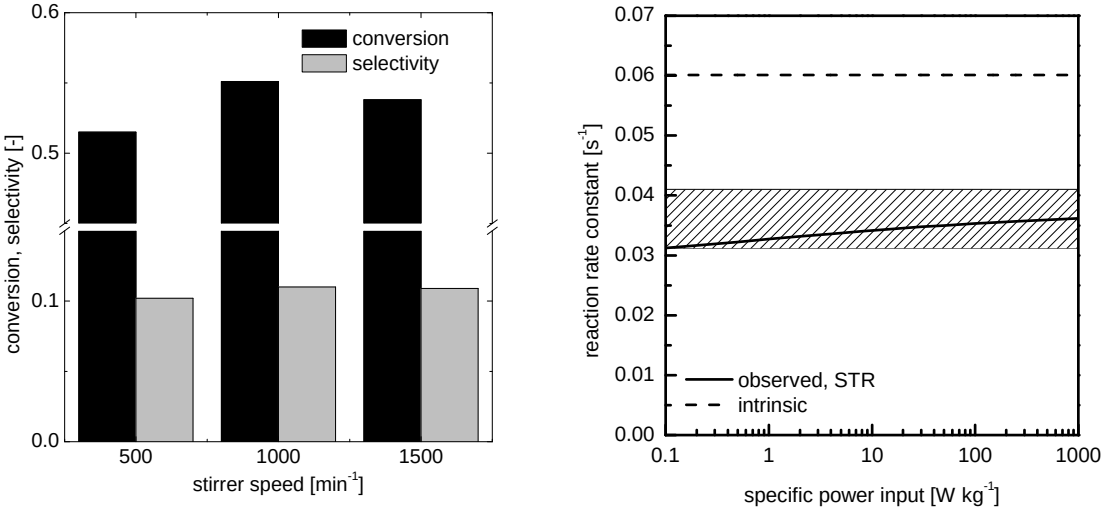

(a) Influence of stirrer speed on CO conversion and CH_4 selectivity

(b) Influence of specific power input on the observed reaction rate constant (shaded: SBC)

Figure 6.6: Influence of external mass transfer resistances for powder catalyst in the STR (campaign II, powder catalyst, 16 µm diffusion length, 200 °C).

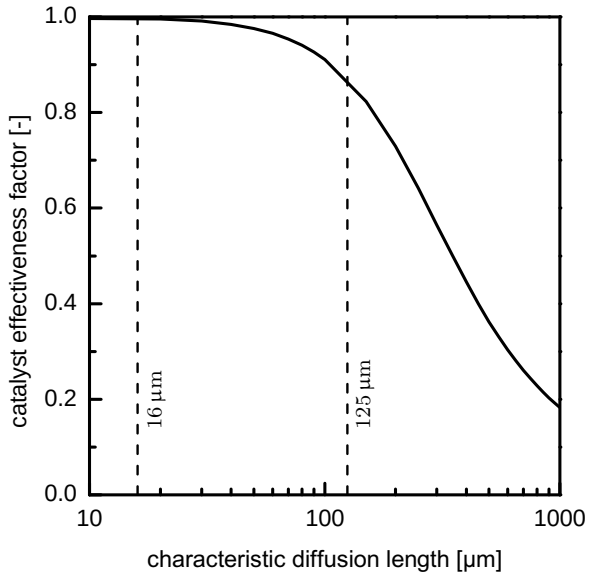

Figure 6.7: Catalyst effectiveness factor for different characteristic diffusion lengths ($D_{\text{eff}} = 2 \times 10^{-9}\,\text{m}^2\,\text{s}^{-1}$, $k = 0.06\,\text{s}^{-1}$ from campaign II, 200 °C).

Table 6.5: Influence of internal mass transfer resistances for powder catalyst in the STR.

		Powder catalyst	
Campaign		II	IV
T	°C	200	200
p	bar	21	21
n	min^{-1}	1000	1000
d_P	µm	50 – 140	500 – 1000
$d_{P,mean}$	µm	95	750
δ_{char}	µm	16	125
X_{CO}	–	0.560	0.144
$S_{\mathrm{CH_4}}$	–	0.102	0.151
$\tilde{r}$	$10^{-4}\,\mathrm{mol_{CO}\,kg_{cat}^{-1}\,s^{-1}}$	6.95	1.79
ϕ	–	0.088	0.685
η	–	0.997	0.868

explained by sedimentation of the large particles at the bottom of the reactor, which are less supplied with educts and thus constrict the observed reaction rate. In conclusion the STR is not appropriate for investigation of internal mass transfer resistances with large particle diameters. However, these rough estimations show that internal and external mass transfer influence the observed reaction rate significantly. Due to the complex multiphase system, the influences of each mass transfer aspect could not be quantified exactly.

The methane selectivity increases with increasing diffusion length. This could be explained by an increase in H_2/CO-ratio inside the catalyst, due to the different diffusion coefficients of H_2 and CO. For a CoRe catalyst on narrow pore γ-Al_2O_3 Rytter et al. (2007) reported an increase in CH_4 selectivity from 10 to 16 % when increasing the particle size from 46 to 638 µm.

Figure 6.8 shows the CO conversion and CH_4 methane selectivity over time on stream for campaign II. The results show an interesting behavior upon temperature changes. Increasing the temperature from 180 °C to 190 °C and further to 200 °C results in a strong increase in conversion. After passing a maximum the conversion decreases again. The methane selectivity is on the other hand not affected by the temperature. With the available results, it is not possible to explain this behavior at this stage of investigation.

During this work two different batches of catalyst were produced using the same

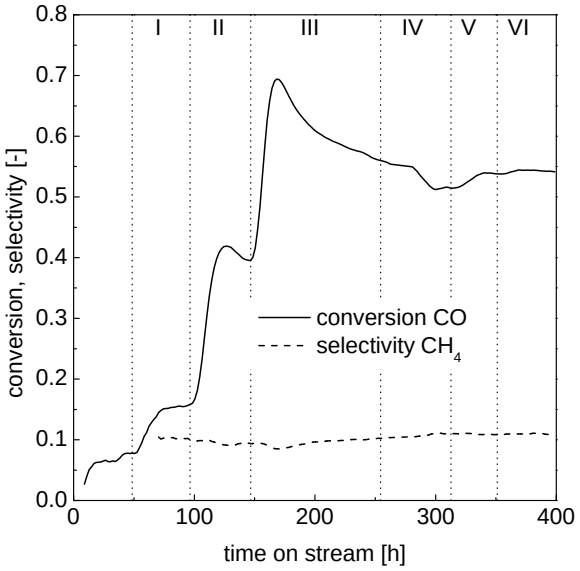

Figure 6.8: Conversion and selectivity over TOS (campaign II, powder catalyst, 16 µm diffusion length).

preparation method. A comparison between campaign II and VI allows for the evaluation of the reproducibility of the preparation method. The comparison of the mass specific reaction rates reveal, that the catalyst used in campaign VI achieves approx. 90 % of the reaction rate of the catalyst in campaign II. The CH_4 selectivity in campaign IV is slightly higher than in campaign II. Thus it can be concluded, that the catalyst preparation method is reproducible.

6.3 Conclusions

Previous to experiments a model was developed to simulate the segregation of the involved species in the reactor and wax and water separator and while sampling performed at different temperatures and pressures. It was observed by simulation, that segregation of the hydrocarbon products occurs, which could be verified with experimental data. It was possible to develop an adequate method for determining the chain growth probability from wax phase analysis.

The aim of the experiments was the investigation and comparison of powder and monolithic honeycomb catalysts in a MLR setup. Preliminary experiments revealed challenges in operating the setup in fixed-bed mode. The gas recycle stream contains

evaporated liquid, which will condense in the high pressure section and consequently cause instabilities in operation of the liquid recycle. In two steps the setup was improved to minimize the amount of evaporated liquid in the gas recycle stream.

First experiments were conducted to investigate the influence of internal and external mass transfer on the reaction rate and methane selectivity in the STR. It was observed, that external mass transfer resistances constrain the reaction rate in the STR. Especially for small catalyst particles the relative velocity between particle and fluid phase is small, since the particles are entrained in the liquid flow. This results in a large stagnant film thickness, which can hardly be decreased even at high specific power input. It was also observed, that internal mass transfer resistances affect the apparent reaction rate and the methane selectivity. The methane selectivity increases, while the observed reaction rate decreases for increasing characteristic diffusion lengths. The increase in methane selectivity corresponds well to literature (Rytter et al., 2007), whereas the strong decrease in reaction rate could not be explained by internal mass transfer resistances only. Most probably also sedimentation of the particles occurred, resulting in a reduced accessible catalyst amount and thus a smaller observed reaction rate. In conclusion, the STR applied in this work is not viable for directly measuring the intrinsic reaction kinetics.

During catalytic measurements with powder and crushed monolithic catalysts in the STR, comparable methane selectivities and reaction rate constants could be observed. Larger deviations at higher reaction temperatures are probably caused by pore diffusion effects in a fraction of the crushed monolithic catalyst with higher diffusion length and sedimentation of catalyst particles. Measurements with monolithic catalysts in fixed bed operation mode show higher reaction rate and activation energy at similar methane selectivities compared to powder catalyst. This reaction rate enhancement is most probably caused by the advantageous external mass transfer characteristics of the monolithic catalyst in the slug flow regime that was for the first time experimentally realized. In conclusion, the results obtained with the monolithic catalyst reveal that structured catalysts are a very promising alternative to suspended powder catalysts.

The discussed setup and experiments represent the first step in the research on MLRs for FTS. It was shown, that investigations in monolithic honeycomb catalysts with recirculation of liquid and gas phase are possible in principle. However, the experiments also reveal challenges for future investigations. The main challenge is the condensation of liquid in the gas recycle, which causes an unsteady operation of the MLR. Although,

the measurement of CO conversion and CH_4 selectivity is not affected, the product composition is influenced by this fact. Furthermore, the temperature of the monolith reactor can not be increased to more than 200 °C in the present setup, since the temperature of the liquid recycle is limited. An increase in reaction temperature by means of an additional heat exchanger at the top of the tubular reactor will lead to an increased production rate of liquid products, which also supports the steady operation of the setup.

7 Conclusions and future work

7.1 General conclusions

A simulation study was performed for comparing the established SBC and FBR with the novel MLR and μR for low temperature FTS. The obtained results confirm the current advantages of the SBC technology compared to FBRs. However, it was also found, that the novel MLR and μR technology offer advantages against the SBC. The achieved catalyst productivity is comparable, combined with the absence of required separation of the catalyst from the product. The challenges of the low catalyst amount in the μR and the large liquid recycle in the MLR are solvable. Especially the MLR can be seen as a promising reactor technology in the near future, since the reactor productivity is high and the liquid recycle is feasible in a large scale plant with the current state of the art.

In order to perform catalytic measurements comparable monolithic honeycomb and powder catalysts were prepared. To achieve a high degree of comparability the monolithic catalyst was prepared by dip-coating of ready-made CoRe on γ-Al_2O_3 catalyst onto a cordierite honeycomb carrier. The powder catalyst was made from the same slurry for the dip-coating procedure. It was discovered, that both catalysts have a comparable pore structure. However, differences in the distribution of the active material were observed. The preparation method was found to be reproducible, which could be verified by catalytic measurements with different catalyst preparation batches. In conclusion, the achieved properties of the catalyst are similar and provide a good basis for a detailed and systematic comparison of powder and monolithic honeycomb catalysts for FTS.

For investigation of powder and monolithic honeycomb catalysts an experimental setup was built according to the loop reactor concept. The continuously operated setup consists of a tubular and a stirred tank reactor and is equipped with independent gas and liquid recycle lines. Moreover, analytical systems were developed for analyzing the gaseous and liquid components present in FTS. The analyzing method of the liquid

waxy products was supported by modeling and simulation of the product segregation in the sampling systems. It was revealed, that product segregation occurs. However, the sample of the wax phase taken from the wax separator allows reliable estimations of the chain growth probability.

During catalytic measurements in the STR it was found, that internal and external mass transfer affect the reaction rate and methane selectivity. The most important result of these experiments is, that external mass transfer constrains the reaction rate in the STR. This could be explained by the small relative velocity between catalyst particles and surrounding liquid, since the catalyst particles are entrained in the liquid flow. In conclusion, the STR applied in this work is not viable for directly measuring of the intrinsic reaction kinetics.

Comparing experiments between monolithic catalyst in fixed bed operation mode and powder catalyst in the STR show a higher reaction rate at comparable methane selectivity for the monolithic catalyst. This enhancement in reaction rate is most probably caused by the advantageous external mass transfer characteristics of the monolithic catalyst in slug flow regime. From the results it can be concluded, that structured catalysts are a very promising alternative to suspended powder catalysts in large scale low temperature FTS.

7.2 Future work

In addition to the presented results more detailed research is required for deeper understanding of the interaction between the intrinsic characteristics, such as flow regime, mass transfer and reaction mechanism. In this chapter, some of the research challenges for future work will be pointed out.

The presented model is based on empirical correlations to describe hydrodynamic and mass transfer characteristics for the considered reactor. This method is suitable, as it allows a sufficient accuracy with low efforts. However, the assumptions simplify the model strongly. An improvement could be the modeling of the MLR depending on the operation time and considering the liquid recycle. A further improvement would be the implementation of microkinetics, to calculate the change of product composition and its effect on the physical properties of the gas and liquid phase. The single improvement steps can be verified by a comparison with experimental data. Finally it could be possible, to design a MLR in pilot plant scale. However, especially the consideration of the real product composition is complex and requires extensive efforts.

The preparation method of the catalyst reveals comparable pore structures of the monolithic honeycomb and powder catalyst. However, the deviations in the active metal distribution should be improved. A possible reason for the differences could be the different overall calcination time of both catalyst types. An improvement could be the preparation of the final powder catalyst in different layers on a flat support in the same manner as the washcoat. These layers can afterwards be removed from the support, crushed and sieved to the desired fraction. Furthermore, the calcination time and temperature could be optimized. The catalyst raw component Re_2O_7 melts at 296 and boils at 360 °C. Especially long calcination times at the applied temperature of 350 °C could result in a depletion of the final Re content. A reduction of the calcination temperature towards 300 °C under reducing atmosphere could prevent evaporation of Re_2O_7. Finally, the long time stability of the catalysts should be investigated.

The main challenge concerning the experimental setup is the condensation of liquid in the gas recycle stream. Further effort should be invested in reducing the condensation to achieve high stability during experiments. Furthermore, the operation temperature of the tubular reactor should be increased, to achieve higher reaction and hydrocarbon production rates. This could be accomplished by the implementation of a heat exchanger at the top of the tubular reactor. Moreover, the analytical system should be improved to quantify C_{2+} hydrocarbons in the gas phase.

With respect to future experiments for the monolithic honeycomb catalyst it is suggested, to vary the gas and liquid flow rates for optimizing the operation conditions and to investigate the film flow regime. Besides the study of the influence of the hydrodynamics on the external mass transfer, the effect of internal mass transfer could by examined by changing the washcoat layer thickness. It would also be interesting to evaluate the influence of the presence of a liquid phase on the methane selectivity and reaction rate by experiments with and without liquid recycle.

In long term perspective the scale-up of the MLR would come in focus. For this purpose long time stability experiments are necessary for the catalyst evaluation. Furthermore, scale-up of the reactor setup is supposed to be feasible based on the presented results and experience. This aim could be achieved by designing a pilot scale MLR operating with single pass of the gas phase. The reactor length should be designed to several meters to achieve the desired conversion of about 70 %. The reactor diameter is limited by the feasible liquid recycle and gas feed flow rate. Investigations towards gas-liquid distribution over the cross sectional area can be conducted separately. In conclusion the MLR has the chance to become industrially applicable in a medium term perspective.

A Appendix

A.1 Modeling and simulation

A.1.1 Physical properties

Table A.1: Physical properties (Maretto and Krishna, 1999; de Deugd, 2004).

Liquid density	$\mathrm{kg\,m^{-3}}$	665
Liquid viscosity	$\mathrm{Pa\,s}$	6.4×10^{-4}
Liquid surface tension	$\mathrm{N\,m^{-1}}$	0.01
Liquid heat capacity	$\mathrm{J\,kg^{-1}\,K^{-1}}$	2710
Liquid heat conductivity	$\mathrm{W\,m^{-1}\,K^{-1}}$	0.133
Catalyst density	$\mathrm{kg\,m^{-3}}$	650
Diffusion coefficient CO	$\mathrm{m^2\,s^{-1}}$	17.2×10^{-9}
Diffusion coefficient H_2	$\mathrm{m^2\,s^{-1}}$	45.5×10^{-9}
Henry coefficient CO	–	2.478
Henry coefficient H_2	–	2.964

A.1.2 Correlations for FBR in trickle flow

Mass transfer gas-liquid, transition regime (Al-Dahhan et al., 1997)

$$ka_{GL,i} = 0.091 \frac{D_i}{d_h^2} \left[(Re_L We_L)^{0.2} (6 X_G)^{0.25} Sc_L^{0.3} \right]^{3.8}$$

Mass transfer liquid-solid, gaseous reactants (Dudukovic et al., 2002)

$$ka_{LS,i} = 2.922 \frac{(1-OFA)^2}{OFA} \frac{D_i}{d_h} Sc_{L,i}^{1/3} \left[\frac{Re_L}{\beta_L (1-OFA)} \right]^{0.495}$$

Axial dispersion, liquid phase (Lange et al., 1999)

$$\mathcal{D}_{ax,L} = 0.55 \cdot 10^{-4} Re_L^{0.61}$$

Axial dispersion, gas phase (Lange et al., 1999)

$$\mathcal{D}_{ax,G} = 13 \cdot 10^{-4} Re_G^{0.78}$$

Heat transfer to reactor wall $Re_L < 40, d_R/d_P > 15$ (Mariani et al., 2001)

$$h_{w,ov} = \frac{\lambda_L}{d_h} \left[3.87 - 3.77\, exp\left(-\frac{1.37\, d_h}{d_R} \right) \right] Pr_L^{1/3} Re_L^{0.643}$$

Pressure drop (Larachi et al., 1991)

$$\left[\frac{\partial p}{\partial z} \right]_{fri+hs} = \frac{2\, \rho_G\, u_G^2}{d_h \left[X_G \left(Re_L\, We_L \right)^{0.25} \right]^{1.5}} \left[31.3 + \frac{17.3}{\left[X_G \left(Re_L\, We_L \right)^{0.25} \right]^{0.5}} \right]$$

A.1.3 Correlations for SBC

The correlations for the SBC reactor were taken from Maretto and Krishna (1999).
Gas saturation, large bubbles, $x_{cat} > 0.16$

$$\beta_G = \frac{0.3}{OFA} \frac{u_G^{0.58}}{d_R^{0.18}}$$

Liquid saturation

$$\beta_L = 1 - \beta_G$$

Mass transfer, gas-liquid, small bubbles

$$ka_{GL,i} = OFA\, \beta_G \sqrt{\frac{D_i}{2 \cdot 10^{-9}}}$$

Mass transfer, gas-solid

$$ka_{GS,i} = 0$$

Heat transfer to reactor wall

$$St = \frac{h_{w,ov}}{u_{TP}\,\rho_{LS}\,c_{p,L}} = 0.1\,Re_{bubble}\,Fr_{bubble}\,Pr^2$$

$$h_{w,ov} = \frac{0.01\,u_{TP}^4\,\rho_{LS}^2\,c_{p,L}^3\,\eta_{LS}}{g\,\lambda_L^2}$$

Pressure gradient, friction

$$\left[\frac{\partial p}{\partial z}\right]_{fri} = 0$$

Pressure gradient, hydrostatic

$$\left[\frac{\partial p}{\partial z}\right]_{hs} = -(1-\beta_G)\,\rho_{LS}\,g$$

Density and viscosity of suspension

$$\rho_{LS} = \rho_L\left[1 - \frac{\rho_L}{\rho_S}\,x_{cat}\right] + \rho_S\,(1-\varepsilon_{cat})\,x_{cat}$$

$$\eta_{LS} = \eta_L\,(1 + 4.5\,x_{cat})$$

A.1.4 Correlations for MLR

Mass transfer, gas-liquid (Bercic and Pintar, 1997)

$$ka_{GL,i} = \frac{0.133\,u_{TP}^{1.2}}{L_L^{0.5}}\left[\frac{D_i}{5\cdot 10^{-9}}\right]^{0.5}$$

Mass transfer, liquid-solid (Kreutzer et al., 2001)

$$ka_{LS,i} = 20\,\frac{D_i}{d_h}\left[1 + 0.003\,\left[\frac{\Psi_L}{Re_{TP}\,Sc_i}\right]^{-0.7}\right]$$

Mass transfer, gas-solid (Irandoust and Andersson, 1988)

$$k_{GS,i} = \frac{D_i}{\delta_f}$$

Liquid film thickness (Kreutzer, 2003)

$$\frac{\delta_f}{d_h} = \frac{0.66\,Ca^{2/3}}{1 + 3.33\,Ca^{2/3}}$$

Phase interfacial area, gas-solid

$$a_{GS} = \frac{4\,(1-\beta_L)}{d_h}$$

Phase interfacial area, liquid-solid

$$a_{LS} = \frac{4\,\beta_L}{d_h}$$

Liquid saturation (Wallis, 1969)

$$\beta_L = \frac{u_L}{u_L + u_G} = \frac{u_L}{u_{TP}}$$

Heat transfer to reactor wall

$$h_{w,ov} = 0$$

Pressure gradient, friction (Heiszwolf et al., 2001a)

$$\left[\frac{\partial p}{\partial z}\right]_{fri} = -44\,\frac{\rho_L\,u_{TP}^2}{Re_{TP}\,d_h}$$

Pressure gradient, hydrostatic (Heiszwolf et al., 2001a)

$$\left[\frac{\partial p}{\partial z}\right]_{hs} = \beta_L \, \rho_L \, g$$

A.1.5 Correlations for μR

Mass transfer, gas-solid (Lebens et al., 1999)

$$Sh_{GS,i} = \frac{k_{GS,i} \, \delta_f}{D_i} = 3.4145 + \frac{0.267 \, (1.5 \, \zeta_i)^{-1.2}}{1 + 0.2 \, (1.5 \, \zeta_i)^{-0.7}}$$

$$\zeta_i = \frac{L_R \, D_i}{\delta_f^2 \, u_L}$$

Mass transfer, liquid-solid (Burghardt and Bartelmus, 1996)

$$Sh_{LS,i} = \frac{k_{LS,i} \, \delta_f}{D_i} = (1.19 + 0.0072 \, Re_G)^{1.1} \, Re_L^{0.494} \, Ga_L^{-0.22} \, Sc_L^{0.33}$$

Liquid film thickness

$$\delta_f = \frac{d_h}{2} \left(1 - \sqrt{1 - \beta_L}\right)$$

Phase interfacial area, gas-solid

$$a_{GS} = \frac{4 \sqrt{(d_h - 2 \, \delta_f) \, d_h}}{d_h^2}$$

Phase interfacial area, liquid-solid

$$a_{LS} = \frac{4}{d_h}$$

Pressure gradient, friction, only gas phase (Heck et al., 2002)

$$\left[\frac{\partial p}{\partial z}\right]_{fri} = -\frac{26.6 \cdot 10^3 \, \rho_G \, u_G^2}{g \, d_h \, Re}$$

Pressure gradient, hydrostatic, horizontal orientation

$$\left[\frac{\partial p}{\partial z}\right]_{hs} = 0$$

Heat transfer to reactor wall, only gas phase, $Re_G < 2300$ (Schlünder, 1972)

$$h_{w,ov} = \frac{\lambda_L}{d_h} \sqrt[3]{3.66^3 + 1.61^3\, Re_G\, Pr_L\, \frac{d_h}{L_R}}$$

A.1.6 Simulation results

Table A.2: Simulation results for different catalyst activities.

		SBC				FBR			
F	–	1	5	10	20	1	5	10	20
X_{CO}	–	0.700	0.699	0.701	0.700	0.700	0.700	0.700	0.700
u_G	$\mathrm{m\,s^{-1}}$	0.3	0.3	0.3	0.3	0.1	0.1	0.1	0.1
u_L	$\mathrm{m\,s^{-1}}$	0.0022	0.0022	0.0022	0.0022	0.01	0.01	0.01	0.01
T_{max}	K	523.0	523.0	523.0	523.0	523.2	523.1	523.2	523.1
T_{in}	K	523	523	523	523	520.7	518.5	518	517.5
η	–	0.999	0.999	0.999	0.999	0.916	0.749	0.656	0.565
L_R	m	49.8	10.7	5.83	3.38	12.8	6.58	5.68	5.19
Δp	Pa	265813	57112	31118	18041	67406	34672	29934	27356
P_{cat}	$\mathrm{bbl\,d^{-1}\,m^{-3}}$	29.7	138.0	253.7	437.5	16.7	32.6	37.8	41.4
P_R	$\mathrm{bbl\,d^{-1}\,m^{-3}}$	5.930	27.595	50.736	87.495	2.507	4.896	5.672	6.215
E	–	0.981	0.917	0.847	0.738	0.579	0.234	0.140	0.082
ΔE_T	–	0.000	0.000	0.000	0.000	0.017	0.012	0.008	0.005
ΔE_{ext}	–	0.018	0.082	0.151	0.261	0.319	0.503	0.508	0.478
ΔE_{intern}	–	0.001	0.001	0.001	0.001	0.084	0.251	0.344	0.435
		µR				MLR			
F	–	1	5	10	20	1	5	10	20
X_{CO}	–	0.700	0.700	0.699	0.699	0.700	0.700	0.700	0.700
u_G	$\mathrm{m\,s^{-1}}$	0.1	0.1	0.1	0.1	0.1	0.1	0.1	0.1
u_L	$\mathrm{m\,s^{-1}}$	0.01	0.01	0.01	0.01	0.2	0.2	0.2	0.2
T_{max}	K	523.1	523.4	523.3	522.9	523.1	523.1	523.1	523.1
T_{in}	K	523	523	522.5	521.5	508.4	508.4	508.4	508.4
η	–	0.995	0.975	0.952	0.912	0.997	0.983	0.967	0.937
L_R	m	17.9	3.67	1.94	1.08	79.2	16.25	8.36	4.42
Δp	Pa	97072	19903	10521	5857	400219	82116	42245	22336
P_{cat}	$\mathrm{bbl\,d^{-1}\,m^{-3}}$	28.56	139.18	263.28	473.44	11.52	56.21	109.23	206.67
P_R	$\mathrm{bbl\,d^{-1}\,m^{-3}}$	0.4	2.0	3.8	6.9	2.9	14.1	27.3	51.7
E	–	0.991	0.957	0.919	0.854	0.648	0.632	0.615	0.582
ΔE_T	–	0.001	0.005	0.009	0.016	0.346	0.338	0.328	0.310
ΔE_{ext}	–	0.003	0.013	0.024	0.042	0.003	0.013	0.025	0.045
ΔE_{intern}	–	0.005	0.025	0.048	0.088	0.003	0.017	0.033	0.063

Table A.3: Simulation results for different diffusion lengths.

		μR			MLR	
F	–	20	20	20	20	20
δ_{cat}	m	85	125	250	85	125
$V_{cat}/V_{channel}$	–	0.25	0.25	0.25	0.25	0.36
V_{cat}/V_R	–	1.45×10^{-2}	2.10×10^{-2}	4.10×10^{-2}	0.25	0.36
X_{CO}	–	0.699	0.698	0.699	0.700	0.699
u_G	$\mathrm{m\,s^{-1}}$	0.1	0.1	0.1	0.1	0.1
u_L	$\mathrm{m\,s^{-1}}$	0.01	0.01	0.01	0.2	0.2
T_{max}	K	522.9	522.8	522.4	523.1	523.1
T_{in}	K	521.5	521.5	521.5	508.4	508.4
η	–	0.912	0.831	0.584	0.937	0.834
L_R	m	1.08	1.18	1.67	4.42	3.58
Δp	Pa	5857	522	9056	22336	18091
P_{cat}	$\mathrm{bbl\,d^{-1}\,m^{-3}}$	473.4	432.9	306.4	206.7	182.0
P_R	$\mathrm{bbl\,d^{-1}\,m^{-3}}$	6.865	9.091	12.562	51.668	64.606
E	–	0.854	0.783	0.561	0.582	0.512
ΔE_T	–	0.016	0.013	0.007	0.310	0.272
ΔE_{ext}	–	0.042	0.035	0.017	0.045	0.049
ΔE_{int}	–	0.088	0.169	0.416	0.063	0.166

A.2 Experimental

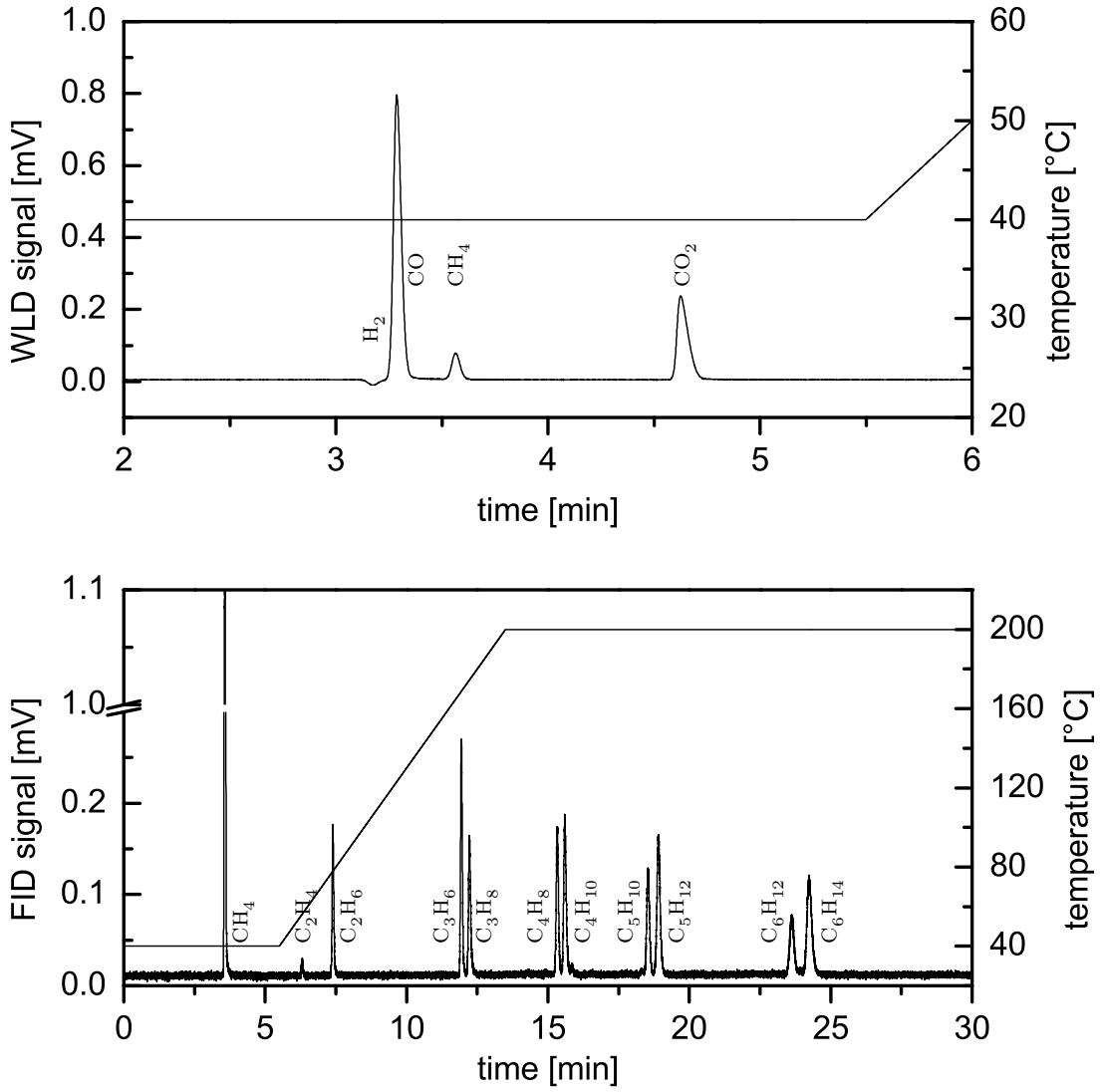

Figure A.1: Typical chromatograms for gas phase analysis (campaign II, 232.5 h TOS, 200 °C, 21 bar, 1000 min^{-1}, 12 000 $\mathrm{kg_{cat}\,s\,m^{-3}_{SG,STP}}$).

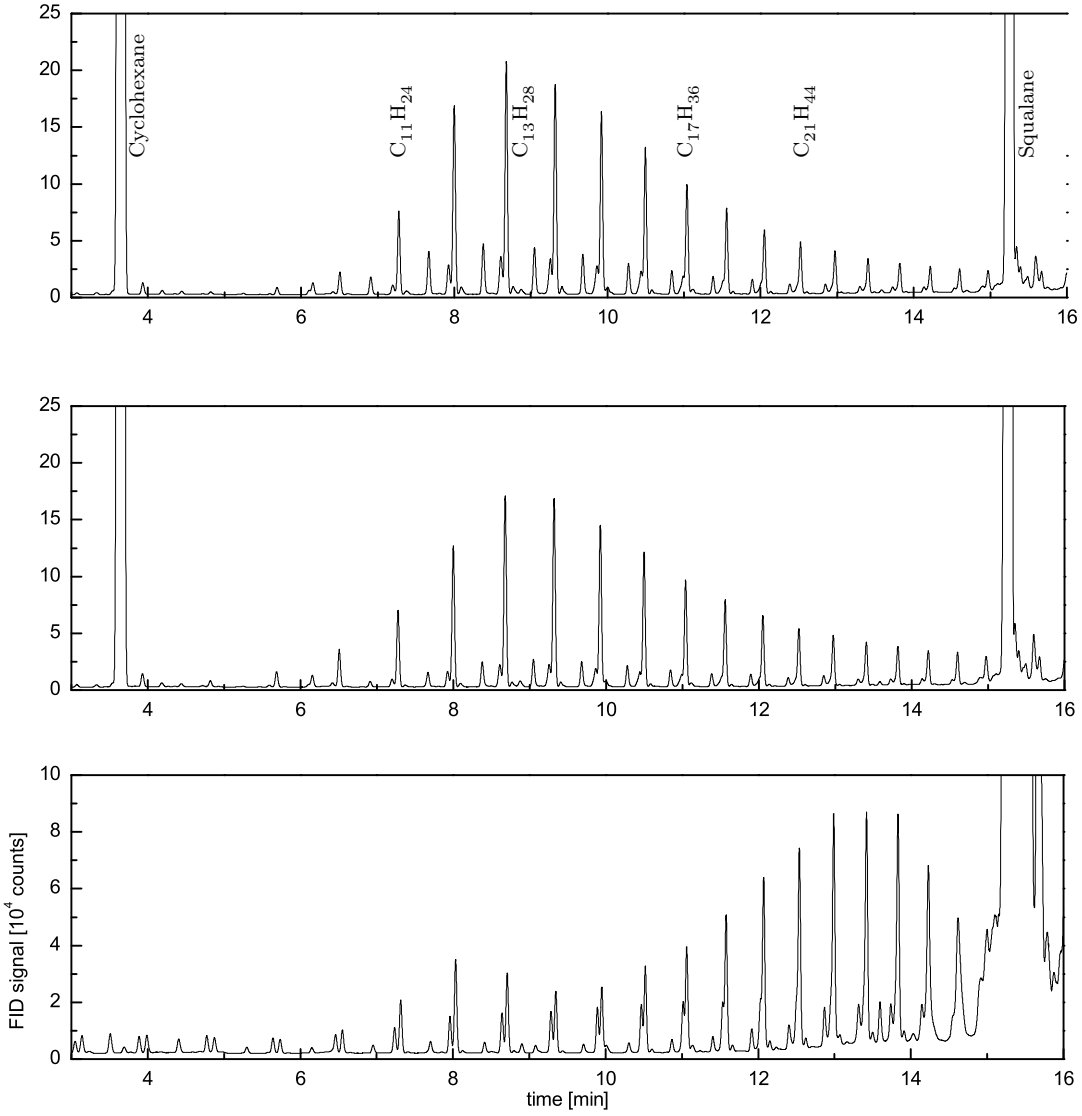

Figure A.2: Chromatograms for the wax phase analysis of powder, crushed monolithic and monolithic catalyst from top to bottom (200 °C, 21 bar, 12 000 $kg_{cat}\,s\,m^{-3}_{SG,STP}$).

Figure A.3 *(facing page)*: Detailed flow diagram of the experimental setup.

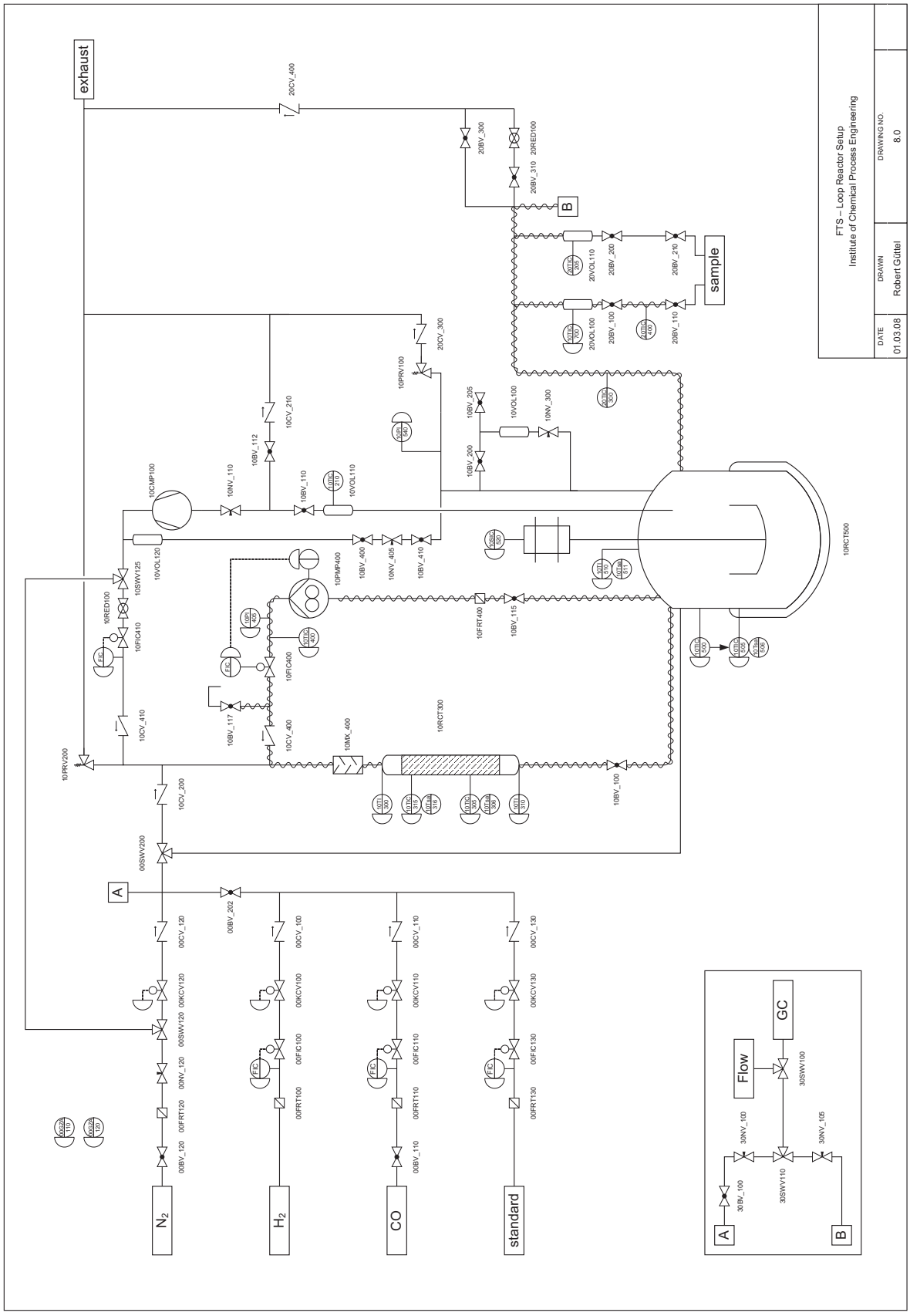
FTS – Loop Reactor Setup
Institute of Chemical Process Engineering
DRAWN Robert Güttel
DATE 01.03.08
DRAWING NO. 8.0
exhaust
sample
N2
H2
CO
standard
A
B
Flow
GC

Bibliography

Agrafiotis, C., Tsetsekou, A., Ekonomakou, A., 1999. The effect of particle size on the adhesion properties of oxide washcoats on cordierite honeycombs. Journal of Materials Science Letters 18 (17), 1412–1224. doi:10.1023/A:1006675524692.

Al-Dahhan, M., Larachi, F., Dudukovic, M. P., Laurent, A., 1997. High-Pressure Trickle-Bed Reactors: A Review. Industrial & Engineering Chemistry Research 36, 3292–3314. doi:10.1021/ie9700829.

Anderson, R. B., 1956. Catalysts for the Fischer-Tropsch synthesis. In: Emmett, P. H. (Ed.), Catalysis. Vol. 4. Van Nostrand-Rheinhold, New York, pp. 29–255.

ASTM, 2002. Standard Test Method for Boiling Range Distribution of Petroleum Fractions by Gas Chromatography. Vol. ASTM D 2887 - 02. ASTM International, West Conshohocken, PA, USA.

Avila, P., Montes, M., Miro, E. E., 2005. Monolithic reactors for environmental applications A review on preparation technologies. Chemical Engineering Journal 109, 11–36. doi:10.1016/j.cej.2005.02.025.

BASF, 1913. Verfahren zur Darstellung von Kohlenwasserstoffen und deren Derivaten. DE293787.

Bauer, T., 2007. Experimental and theoretical investigations of monolithic reactors for three-phase catalytic reactions. Dissertation, TU Dresden.

Bauer, T., Guettel, R., Roy, S., Schubert, M., Al-Dahhan, M., Lange, R., 2005a. Modelling and Simulation of the Monolithic Reactor for Gas-Liquid-Solid Reactions. Chemical Engineering Research and Design 83 (A7), 811–819. doi:10.1205/cherd.04335.

Bauer, T., Schubert, M., Lange, R., 2005b. Prozessintensivierung heterogen katalysierter Gas/Flüssig-Reaktionen mit Monolithreaktoren. Chemie Ingenieur Technik 77 (11), 1683–1692. doi:10.1002/cite.200500143.

Bercic, G., Pintar, A., 1997. The role of gas bubbles and liquid slug lengths on mass transport in the Taylor flow through capillaries. Chemical Engineering Science 52 (21-22), 3709–3719. doi:10.1016/S0009-2509(97)00217-0.

BMWi, 2008. Energiedaten, Nationale und Internationale Entwicklung.

Boger, T., Zieverink, M. P., Kreutzer, M. T., Kapteijn, F., Moulijn, J. A., 2004. Monolithic Catalysts as an Alternative to Slurry Systems: Hydrogenation of Edible Oil. Industrial & Engineering Chemistry Research 43, 2337–2344. doi:10.1021/ie030809v.

Borg, O., Eri, S., Blekkan, E. A., Storsæter, S., Wigum, H., Rytter, E., Holmen, A., 2007. Fischer-Tropsch synthesis over γ-alumina-supported cobalt catalysts: Effect of support variables. Journal of Catalysis 248 (1), 89–100. doi:10.1016/j.jcat.2007.03.008.

Bradford, M. C. J., Te, M., Pollack, A., 2005. Monolith loop catalytic membrane reactor for Fischer-Tropsch synthesis. Applied Catalysis A: General 283, 39–46. doi:10.1016/j.apcata.2004.12.032.

Broekhuis, R. R., Budhlall, B. M., Nordquist, A. F., 2004. Monolith Catalytic Process for Producing Sorbitol: Catalyst Development and Evaluation. Industrial & Engineering Chemistry Research 43, 5146–5155. doi:10.1021/ie0400393.

Burghardt, A., Bartelmus, G., 1996. Hydrodynamics and mass transfer in three-phase cocurrent reactors. Chemical Engineering Science 51, 2733–2738. doi:10.1016/0009-2509(96)00144-3.

Christiani, C., Valentini, M., Merazzi, M., Neglia, S., Forzatti, P., 2005. Effect of aging time on chemical and rheological evolution in γ-Al_2O_3 slurries for dip-coating. Catalysis Today 105 (3-4), 492–498. doi:10.1016/j.cattod.2005.06.020.

Claeys, M., 1997. Selektivität, Elementarschritte und kinetische Modellierung bei der Fischer-Tropsch-Synthese. Dissertation, Universität Karlsruhe (TH).

Cybulski, A., Moulijn, J. A., 2006. Structured Catalysts and Reactors, 2nd Edition. Marcel Dekker Ltd., New York.

Davis, B. H., 2005. Fischer-Tropsch synthesis: Overview of reactor development and future potentialities. Topics in Catalysis 32 (3-4), 143–168. doi:10.1007/s11244-005-2886-5.

de Deugd, R. M., 2004. Fischer-Tropsch Synthesis Revisited; Efficiency and Selectivity Benefits from Imposing Temporal and/or Spatial Structure in the Reactor. Dissertation, Delft University of Technology.

de Deugd, R. M., Chougule, R. B., Kreutzer, M. T., Meeuse, F. M., Grievink, J., Kapteijn, F., Moulijn, J. A., 2003a. Is a monolithic loop reactor a viable option for Fischer-Tropsch synthesis? Chemical Engineering Science 58 (3-6), 583–591. doi:10.1016/S0009-2509(02)00583-3.

de Deugd, R. M., Kapteijn, F., Moulijn, J. A., 2003b. Trends in Fischer-Tropsch Reactor Technology - Opportunities for Structured Reactors. Topics in Catalysis 26 (1-4), 29–39. doi:10.1023/B:TOCA.0000012985.60691.67.

de Deugd, R. M., Kapteijn, F., Moulijn, J. A., 2003c. Using monolithic catalysts for highly selective Fischer-Tropsch synthesis. Catalysis Today 79-80, 495–501. doi:10.1016/S0920-5861(03)00073-7.

Dry, M. E., 1982. Catalytic aspects of industrial Fischer-Tropsch synthesis. Journal of Molecular Catalysis 17 (2-3), 133–144. doi:10.1016/0304-5102(82)85025-6.

Dry, M. E., 1990. The Fischer-Tropsch Process - Commercial Aspects. Catalysis Today 6 (3), 183–206. doi:10.1016/0920-5861(90)85002-6.

Dry, M. E., 2001. High quality diesel via the Fischer-Tropsch process - a review. Journal of Chemical Technology and Biotechnology 77, 43–50. doi:10.1002/jctb.527.

Dry, M. E., 2002. The Fischer-Tropsch process: 1950-2000. Catalysis Today 71, 227–241. doi:10.1016/S0920-5861(01)00453-9.

Dudukovic, M. P., Larachi, F., Mills, P. L., 1999. Multiphase reactors - revisited. Chemical Engineering Science 54, 1975–1995. doi:10.1016/S0009-2509(98)00367-4.

Dudukovic, M. P., Larachi, F., Mills, P. L., 2002. Multiphase Catalytic Reactors: A Perspective on Current Knowledge and Future Trends. Catalysis Reviews - Science and Engineering 44, 123–246. doi:10.1081/CR-120001460.

Edvinsson, R. K., Cybulski, A., 1994. A comparative analysis of the trickle-bed and the monolithic reactor for three-phase hydrogenations. Chemical Engineering Science 49 (24), 5653–5666. doi:10.1016/0009-2509(94)00370-X.

Enache, D. I., Landon, P., Lok, C. M., Pollington, S. D., Stitt, E. H., 2005. Direct Comparison of a Trickle Bed and a Monolith for Hydrogenation of Pyrolysis Gasoline. Industrial & Engineering Chemistry Research 44, 9431–9439. doi:10.1021/ie0502180.

Fandino, O., Pensado, A. S., Lugo, L., Comunas, M. J. P., Fernandez, J., 2005. Compressed Liquid Densities of Squalane and Pentaerythritol Tetra(2-ethylhexanoate). Journal of Chemical & Engineering Data 50, 939–946. doi:10.1021/je049580w.

Fischer, F., Tropsch, H., 1923. Über die Herstellung synthetischer Ölgemische (Synthol) durch Aufbau aus Kohlenoxyd und Wasserstoff. Brennstoff-Chemie 4, 276–285.

Fischer, F., Tropsch, H., 1925. Verfahren zur Gewinnung mehrgliedriger Paraffinkohlenwasserstoffe aus Kohlenoxyden und Wasserstoff auf katalytischem Wege. DE484337.

Fleisch, T. H., 2006. Overview of Syngas Generation from Different Sources and Main Pathways for Syngas Conversion. In: Ernst, S., Jess, A., Nees, F., Perego, C., Rupp, M., Santacesaria, E. (Eds.), DGMK/SCI-Conference "Synthesis Gas Chemistry". Vol. 4 of DGMK Tagnungsbericht. Dresden, Germany, p. 7.

Fox, J. M., 1990. Fischer-Tropsch Reactor Selection. Catalysis Letters 7, 281–292. doi:10.1007/BF00764509.

Frohning, C. D., Kölbel, H., Ralek, M., Rottig, W., Schnur, F., Schulz, H., 1992. Fischer-Tropsch-Synthese. In: Falbe, J. (Ed.), Chemierohstoffe aus Kohle. Georg Thieme Verlag, Stuttgart.

Guettel, R., Kunz, U., Turek, T., 2008. Reactors for Fischer-Tropsch Synthesis. Chemical Engineering & Technology 31 (5), 746–754. doi:10.1002/ceat.200800023.

Guillou, L., Balloy, D., Supiot, P., Le Courtois, V., 2007. Preparation of a multilayered composite catalyst for Fischer-Tropsch synthesis in a micro-chamber reactor. Applied Catalysis A: General 324, 42–51. doi:10.1016/j.apcata.2007.03.006.

Hao, X., Dong, G., Yang, Y., Xu, Y., Li, Y., 2007. Coal to Liquid (CTL): Commercialization Prospects in China. Chemical Engineering & Technology 30 (9), 1157–1165. doi:10.1002/ceat.200700148.

He, J., Yoneyama, Y., Xu, B., Nishiyama, N., Tsubaki, N., 2005. Designing a Capsule Catalyst and Its Application for Direct Synthesis of Middle Isoparaffins. Langmuir 21, 1699–1702. doi:10.1021/la047217h.

Heck, R. M., Farrauto, R. J., Gulati, S. T., 2002. Monolithic Reactors for Environmental Catalysis. In: Catalytic Air Pollution Control, 2nd Edition. Wiley-Interscience, New York.

Heck, R. M., Gulati, S. T., Farrauto, R. J., 2001. The application of monoliths for gas phase catalytic reactions. Chemical Engineering Journal 82 (1-3), 149–156. doi:10.1016/S1385-8947(00)00365-X.

Heiszwolf, J. J., Engelvaart, L. B., van den Eijnden, M. G., Kreutzer, M. T., Kapteijn, F., Moulijn, J. A., 2001a. Hydrodynamic aspects of the monolith loop reactor. Chemical Engineering Science 56 (3), 805–812. doi:10.1016/S0009-2509(00)00292-X.

Heiszwolf, J. J., Kreutzer, M. T., van den Eijnden, M. G., Kapteijn, F., Moulijn, J. A., 2001b. Gas-liquid mass transfer of aqueous Taylor flow in monoliths. Catalysis Today 69 (1-4), 51–55. doi:10.1016/S0920-5861(01)00354-6.

Hilmen, A.-M., Bergene, E., Lindvag, O. A., Schanke, D., Eri, S., Holmen, A., 2001. Fischer-Tropsch synthesis on monolithic catalysts of different materials. Catalysis Today 69 (1-4), 227–232. doi:10.1016/S0920-5861(01)00373-X.

Hilmen, A.-M., Bergene, E., Lindvag, O. A., Schanke, D., Eri, S., Holmen, A., 2005. Fischer-Tropsch synthesis on monolithic catalysts with oil circulation. Catalysis Today 105, 357–361. doi:10.1016/j.cattod.2005.06.032.

Hoek, I., Nijhuis, T. A., Stankiewicz, A., Moulijn, J. A., 2004. Performance of the monolithic stirrer reactor: applicability in multi-phase processes. Chemical Engineering Science 59, 4975–4981. doi:10.1016/j.ces.2004.07.077.

Hunter, R. J., 1991. Foundations of Colloid Science. Vol. 1. Clarendon Press, Oxford.

Irandoust, S., Andersson, B., 1988. Mass transfer and liquid-phase reactions in a segmented two-phase flow monolithic catalyst reactor. Chemical Engineering Science 43 (8), 1983–1988. doi:10.1016/0009-2509(88)87072-6.

Jarosch, K. T., Tonkovich, A. L., Perry, S. T., Kuhlmann, D., Wang, Y., 2005. Microchannel Reactors for Intensifying Gas-to-Liquid Technology. A.C.S. symposium series 914, 258–272.

Kapteijn, F., de Deugd, R. M., Moulijn, J. A., 2005. Fischer-Tropsch synthesis using monolithic catalysts. Catalysis Today 105, 350–356. doi:10.1016/j.cattod.2005.06.063.

Kapteijn, F., Heiszwolf, J. J., Nijhuis, T. A., Moulijn, J. A., 1999. Monoliths in multiphase catalytic processes - aspects and prospects. CATTECH 3, 24–41.

Kapteijn, F., Nijhuis, T. A., Heiszwolf, J. J., Moulijn, J. A., 2001. New non-traditional multiphase catalytic reactors based on monolithic structures. Catalysis Today 66 (2-4), 133–144. doi:10.1016/S0920-5861(00)00614-3.

Khassin, A. A., Sipatrov, A. G., Chermashentseva, G. K., Yurieva, T. M., Parmon, V. N., 2005a. Fischer-Tropsch synthesis using plug-through contactor membranes based on permeable composite monoliths. Selectivity control by porous structure parameters and membrane geometry. Topics in Catalysis 32 (1-2), 39–46. doi:10.1007/s11244-005-9258-2.

Khassin, A. A., Sipatrov, A. G., Yurieva, T. M., Chermashentseva, G. K., Rudina, N. A., Parmon, V. N., 2005b. Performance of a catalytic membrane reactor for the Fischer-Tropsch synthesis. Catalysis Today 105, 362–366. doi:10.1016/j.cattod.2005.06.031.

Khassin, A. A., Yurieva, T. M., Sipatrov, A. G., Kirillov, V. A., Chermashentseva, G. K., Parmon, V. N., 2003. Fischer-Tropsch synthesis using a porous catalyst packing: experimental evidence of an efficient use of permeable composite monoliths as a novel type of the Fischer-Tropsch synthesis catalyst. Catalysis Today 79-80, 465–470. doi:10.1016/S0920-5861(03)00063-4.

Klemm, E., Döring, H., Geisselmann, A., Schirrmeister, S., 2007. Microstructured Reactors in Heterogeneous Catalysis. Chemical Engineering & Technology 30 (12), 1615–1621. doi:10.1002/ceat.200700311.

Klemm, E., Rudek, M., Markowz, G., Schütte, R., 2003. Mikroverfahrenstechnik. In: Dittmeyer, R., Kreysa, G., Keim, W., Oberholz, A. (Eds.), Winnacker Küchler: Chemische Technik, 5th Edition. Vol. 2 of Winnacker Küchler: Chemische Technik. Wiley-VCH, Weinheim.

Kreutzer, M. T., 2003. Hydrodynamics of Taylor Flow in Capillaries and Monolith Reactors. Dissertation, Delft University of Technology.

Kreutzer, M. T., Du, P., Heiszwolf, J. J., Kapteijn, F., Moulijn, J. A., 2001. Mass transfer characteristics of three-phase monolith reactors. Chemical Engineering Science 56 (21-22), 6015–6023. doi:10.1016/S0009-2509(01)00271-8.

Krishna, R., 2000. A Scale-up Strategy for a Commercial Scale Bubble Column Slurry Reactor for Fischer-Tropsch Synthesis. Oil & Gas Science and Technology - Rev. IFP 55 (4), 359–393.

Krishna, R., Sie, S. T., 2000. Design and scale-up of the Fischer-Tropsch bubble column slurry reactor. Fuel Processing Technology 64, 73–105.

Krishna, R., van Baten, J. M., 2003. A strategy for scaling up the Fischer-Tropsch bubble column slurry reactor. Topics in Catalysis 26, 21.

Lange, R., Gutsche, R., Hanika, J., 1999. Forced periodic operation of a trickle-bed reactor. Chemical Engineering Science 54, 2569–2573. doi:10.1016/S0009-2509(99)00004-4.

Larachi, F., Laurent, A., Midoux, N., Wild, G., 1991. Experimental study of a trickle-bed reactor operating at high pressure: two-phase pressure drop and liquid saturation. Chemical Engineering Science 46 (5-6), 1233–1246. doi:10.1016/0009-2509(91)85051-X.

Lebens, P. J. M., Heiszwolf, J. J., Kapteijn, F., Sie, S. T., Moulijn, J. A., 1999. Gas-liquid mass transfer in an internally finned monolith operated countercurrently in the film flow regime. Chemical Engineering Science 54 (21), 5119–5125. doi:10.1016/S0009-2509(99)00265-1.

Lemaitre, J. L., 1984. Temperature-Programmed Methods. In: Delannay, F. (Ed.), Characterization of Heterogeneous Catalysts. Marcel Dekker, Inc., New York.

Lemaitre, J. L., Menon, P. G., Delannay, F., 1984. The Measurement of Catalyst Dispersion. In: Delannay, F. (Ed.), Characterization of Heterogeneous Catalysts. Marcel Dekker, Inc., New York.

Liu, W., 2002. Ministructured Catalyst Bed for Gas-Liquid-Solid Multiphase Catalytic Reaction. AIChE Journal 48 (7), 1519–1532. doi:10.1002/aic.690480715.

Liu, W., Addiego, W. P., Sorensen, C. M., 2002. Monolith Reactor for the Dehydrogenation of Ethylbenzene to Styrene. Industrial & Engineering Chemistry Research 41, 3131–3138. doi:10.1021/ie010730v.

Losey, M. W., Schmidt, M. A., Jensen, K. F., 2001. Microfabricated Multiphase Packed-Bed Reactors: Characterization of Mass Transfer and Reactions. Industrial & Engineering Chemistry Research 40, 2555–2562. doi:10.1021/ie000523f.

Maretto, C., Krishna, R., 1999. Modelling of a bubble column slurry reactor for Fischer-Tropsch synthesis. Catalysis Today 52, 279–289. doi:10.1016/S0920-5861(99)00082-6.

Mariani, N. J., Martinez, O. M., Barreto, G. F., 2001. Evaluation of heat transfer parameters in packed beds with cocurrent downflow of liquid and gas. Chemical Engineering Science 56, 5995–6001. doi:10.1016/S0009-2509(01)00225-1.

Marwan, H., Winterbottom, J. M., 2003. Operating characteristics and performance of a monolithic downflow bubble column reactor in selective hydrogenation of butyne-1,4-diol. Chemical Engineering & Technology 26 (9), 996–1002. doi:10.1002/ceat.200301742.

Mazzarino, I., Baldi, G., 1987. Liquid Phase Hydrogenation on a Monolithic Catalyst. In: Kulkarni, B. D., Mashelkar, R. A., Sharma, M. M. (Eds.), Recent Trends in Chemical Reaction Engineering. Vol. 2. Wiley Eastern Ltd., New Delhi, pp. 181–189.

Meshcheryakov, V. D., Kirillov, V. A., Kuzin, N. A., 1999a. A multifunctional reactor with a regular catalyst packing for Fischer-Tropsch synthesis. Chemical Engineering Science 54 (10), 1565–1570. doi:10.1016/S0009-2509(99)00066-4.

Meshcheryakov, V. D., Kirillov, V. A., Kuzin, N. A., 1999b. A stacked catalyst packing reactor for superexothermal processes in gas-liquid-solid three-dimensional systems. Theoretical Foundations Of Chemical Engineering 33 (5), 508–516.

Nijhuis, T. A., Beers, A. E. W., Vergunst, T., Hoek, I., Kapteijn, F., Moulijn, J. A., 2001a. Preparation of monolithic catalysts. Catalysis Reviews - Science and Engineering 43 (4), 345–380. doi:10.1081/CR-120001807.

Nijhuis, T. A., Dautzenberg, F. M., Moulijn, J. A., 2003. Modeling of monolithic and trickle-bed reactors for the hydrogenation of styrene. Chemical Engineering Science 58 (7), 1113–1124. doi:10.1016/S0009-2509(02)00547-X.

Nijhuis, T. A., Kreutzer, M. T., Romijn, A. C. J., Kapteijn, F., Moulijn, J. A., 2001b. Monolithic catalysts as efficient three-phase reactors. Chemical Engineering Science 56 (3), 823–829. doi:10.1016/S0009-2509(00)00294-3.

Nijhuis, T. A., Kreutzer, M. T., Romijn, A. C. J., Kapteijn, F., Moulijn, J. A., 2001c. Monolithic catalysts as more efficient three-phase reactors. Catalysis Today 66 (2-4), 157–165. doi:10.1016/S0920-5861(00)00621-0.

OPEC, 2007. World Oil Outlook. Tech. rep.

Oukaci, R., Singleton, A. H., Goodwin, J. G., J., 1999. Comparison of patented Co F-T catalysts using fixed-bed and slurry bubble column reactors. Applied Catalysis A: General 186, 129–144. doi:10.1016/S0926-860X(99)00169-6.

Pangarkar, K., Schildhauer, T. J., van Ommen, J. R., Nijenhuis, J., Kapteijn, F., Moulijn, J. A., 2008. Structured Packings for Multiphase Catalytic Reactors. Industrial & Engineering Chemistry Research 47 (10), 3720–3751. doi:10.1021/ie800067r.

Pangarkar, V. G., Yawalkar, A. A., Sharma, M. M., Beenackers, A. A. C. M., 2002. Particle-Liquid Mass Transfer Coefficient in Two-/Three-Phase Stirred Tank Reactors. Industrial & Engineering Chemistry Research 41 (17), 4141–4167. doi:10.1021/ie010933j.

Perry, R. H., Green, D., 1999. Perry's Chemical Engineers' Handbook. McGraw-Hill.

Post, M. F. M., van't Hoog, A. C., Minderhoug, J. K., Sie, S. T., 1989. Diffusion Limitations in Fischer-Tropsch Catalysts. AIChE Journal 35 (7), 1107–1114. doi:10.1002/aic.690350706.

Rados, N., Al-Dahhan, M., Dudukovic, M. P., 2003. Modeling of the Fischer-Tropsch synthesis in slurry bubble column reactors. Catalysis Today 79-80, 211–218. doi:10.1016/S0920-5861(03)00007-5.

Reitzmann, A., Patcas, F. C., Kraushaar-Czarnetzki, B., 2006. Keramische Schwämme - Anwendungspotenzial monolithischer Netzstrukturen als katalytische Packungen. Chemie Ingenieur Technik 78 (7), 885–898. doi:10.1002/cite.200600029.

Reuel, R. C., Bartholomew, C. H., 1984. The stoichiometries of H_2 and CO adsorptions on cobalt: Effects of support and preparation. Journal of Catalysis 85 (1), 63–77. doi:10.1016/0021-9517(84)90110-6.

Riedel, T., 2002. Reaktionen von CO_2 bei der Fischer-Tropsch Synthese - Kinetik und Selektivität. Dissertation, Universität Karlsruhe (TH).

Riedel, T., Schaub, G., 2003. Low-temperature Fischer-Tropsch synthesis on cobalt catalysts - effects of CO_2. Topics in Catalysis 26 (1-4), 145–156.

Rohde, M. P., Unruh, D., Schaub, G., 2005a. Membrane application in Fischer-Tropsch synthesis reactors - Overview of concepts. Catalysis Today 106, 143–148. doi:10.1016/j.cattod.2005.07.124.

Rohde, M. P., Unruh, D., Schaub, G., 2005b. Membrane Application in Fischer-Tropsch Synthesis to Enhance CO_2 Hydrogenation. Industrial & Engineering Chemistry Research 44, 9653–9658. doi:10.1021/ie050289z.

Roy, S., Bauer, T., Al-Dahhan, M., Lehner, P., Turek, T., 2004. Monoliths as multiphase reactors: a review. AIChE Journal 50 (11), 2918–2938. doi:10.1002/aic.10268.

Rytter, E., Eri, S., Skagseth, T. H., Schanke, D., Bergene, E., Myrstad, R., Lindvag, A., 2007. Catalyst Particle Size of Cobalt/Rhenium on Porous Alumina and the Effect on Fischer-Tropsch Catalytic Performance. Industrial & Engineering Chemistry Research 46 (26), 9032–9036. doi:10.1021/ie071136+.

Schanke, D., Bergene, E., Holmen, A., 1998. Fischer-Tropsch Synthesis. WO9838147.

Schanke, D., Hilmen, A.-M., Bergene, E., Kinnari, K., Rytter, E., Adnanes, A., Holmen, A., 1996. Reoxidation and Deactivation of Supported Cobalt Fischer-Tropsch Catalysts. Energy & Fuels 10 (4), 867–872. doi:10.1021/ef950197u.

Schaub, G., 2006. Synthetic Fuels and Biofuels for the Transportation Sector - Principles and Perspectives. OIL GAS European Magazine 32, 34.

Schaub, G., Rohde, M. P., Mena Subiranas, A., 2006. Overview of Syngas Generation from Different Sources and Main Pathways for Syngas Conversion. In: Ernst, S., Jess, A., Nees, F., Perego, C., Rupp, M., Santacesaria, E. (Eds.), DGMK/SCI-Conference "Synthesis Gas Chemistry". Vol. 4 of DGMK Tagnungsbericht. Dresden, Germany, p. 75.

Schlünder, E. U., 1972. Einführung in die Wärme- und Stoffübertragung. Vieweg Verlag, Braunschweig.

Schulz, H., 1999. Short history and present trends of Fischer-Tropsch synthesis. Applied Catalysis A: General 186, 3–12. doi:10.1016/S0926-860X(99)00160-X.

Sie, S. T., 1998. Process Development and Scale up: IV. Case History of the Development of a Fischer-Tropsch Synthesis Process. Reviews in Chemical Engineering 14 (2), 109–157.

Silveston, P. L., Hanika, J., 2004. Periodic Operation of Three - Phase Catalytic Reactors. The Canadian Journal of Chemical Engineering 82 (6), 1105–1142.

Simmons, M. J., Wong, D. C. Y., Travers, P. J., Rothwell, J. S., 2003. Bubble behavior in three phase capillary microreactors. International Journal of Chemical Reactor Engineering 1, A30.

Soriano, J.-P., 2005. Mass transfer characteristics in an agitated slurry reactor operating under Fischer-Tropsch conditions. Master thesis, University of Pittsburgh.

Steynberg, A. P., Dry, M. E., 2004. Fischer-Tropsch Technology. Vol. 152 of Studies in Surface Science and Catalysis. Elsevier B.V., Amsterdam.

Storsæter, S., Borg, O., Blekkan, E. A., Holmen, A., 2005a. Study of the effect of water on Fischer-Tropsch synthesis over supported cobalt catalysts. Journal of Catalysis 231, 405–419. doi:10.1016/j.jcat.2005.01.036.

Storsæter, S., Chen, D., Holmen, A., 2006. Microkinetic modelling of the formation of C1 and C2 products in the Fischer-Tropsch synthesis over cobalt catalysts. Surface Science 600, 2051–2063. doi:10.1016/j.susc.2006.02.048.

Storsæter, S., Totdal, B., Walmsley, J. C., Tanem, B. S., Holmen, A., 2005b. Characterization of alumina-, silica-, titania-supported cobalt Fischer-Tropsch catalysts. Journal of Catalysis 236, 139–152. doi:10.1016/j.jcat.2005.09.021.

Twigg, M. V., Richardson, J. T., 2002. Theory and applications of ceramic foam catalysts. Chemical Engineering Research and Design 80 (A2), 183. doi:10.1205/026387602753501906.

Unruh, D., 2006. Fischer-Tropsch Synthese mit Synthesegasen aus Biomasse - Verbesserung der Kohlenstoffnutzung durch Anwendung eines Membranreaktors. Dissertation, Universität Karlsruhe (TH).

van der Laan, G. P., 1999. Kinetics, Selectivity and Scale Up of the Fischer-Tropsch Synthesis. Dissertation, University of Groningen.

van der Laan, G. P., Beenackers, A. A. C. M., 1999. Kinetics and Selectivity of the Fischer-Tropsch Synthesis: A Literature Review. Catalysis Reviews - Science and Engineering 41 (3-4), 255–318.

van der Laan, G. P., Beenackers, A. A. C. M., Krishna, R., 1999. Multicomponent reaction engineering model for Fe-catalyszed Fischer-Tropsch synthesis in commercial scale slurry bubble column reactors. Chemical Engineering Science 54, 5013–5019. doi:10.1016/S0009-2509(99)00225-0.

van Steen, E., Claeys, M., 2008. Fischer-Tropsch Catalysts for the Biomass-to-Liquid Process. Chemical Engineering & Technology 31 (5), 655–666. doi:10.1002/ceat.200800067.

Vergunst, T., Kapteijn, F., Moulijn, J. A., 2001. Monolithic catalysts – non-uniform active phase distribution by impregnation. Applied Catalysis A: General 213 (2), 179–187. doi:10.1016/S0926-860X(00)00896-6.

Visconti, C. G., Tronconi, E., Lietti, L., Zennaro, R., Forzatti, P., 2007. Development of a complete kinetic model for the Fischer-Tropsch synthesis over Co/Al_2O_3 catalysts. Chemical Engineering Science 62, 5338–5343. doi:10.1016/j.ces.2006.12.064.

Wallis, G. B., 1969. One Dimensional Two-Phase Flow. Mc-Graw-Hill, New York.

Wang, Y., Fan, W., Liu, Y., Zeng, Z., Hao, X., Chang, M., Zhang, C., Xu, Y., Xiang, H., Li, Y., 2008. Modeling of the Fischer-Tropsch synthesis in slurry bubble column reactors. Chemical Engineering and Processing 47 (2), 222–228. doi:10.1016/j.cep.2007.02.011.

Wang, Y., Tonkovich, A. L., Mazanec, T., Daly, F. P., VanderWiel, D., Hu, J., Cao, C., Kibby, C. L., Li, X. S., Briscoe, M. D., Gano, N., Chin, Y.-H., 2005. Fischer-Tropsch Synthesis using Microchannel Technology and Novel Catalyst and Microchannel Reactor. WO2005075606.

Wang, Y., Vanderwiel, D., Tonkovich, A. L., Gao, Y., Baker, E. G., 2002. Catalyst Structure and Method of Fischer-Tropsch Synthesis. US6451864B1.

Wang, Y., Vanderwiel, D., Tonkovich, A. L., Gao, Y., Baker, E. G., 2003a. Catalyst Structure and Method of Fischer-Tropsch Synthesis. US6558634B1.

Wang, Y.-N., Xu, Y.-Y., Li, Y.-W., Zhao, Y.-L., Zhang, B.-J., 2003b. Heterogeneous modeling for fixed-bed Fischer-Tropsch synthesis: Reactor model and its applications. Chemical Engineering Science 58, 867–875. doi:10.1016/S0009-2509(02)00618-8.

Wang, Y.-N., Xu, Y.-Y., Xiang, H.-W., Li, Y.-W., Zhang, B.-J., 2001. Modeling of Catalyst Pellets for Fischer-Tropsch Synthesis. Industrial & Engineering Chemistry Research 40, 4324–4335. doi:10.1021/ie010080v.

Yates, I., Satterfield, C. N., 1991. Intrinsic Kinetics of the Fischer-Tropsch Synthesis on a Cobalt Catalyst. Energy & Fuels 5, 168–173.

Nomenclature

Latin Letters

$\tilde{a}$	$\mathrm{m^2\,kg^{-1}}$	specific surface area
A	$\mathrm{m^2}$	area
a	$\mathrm{m^{-1}}$	specific surface area
c	$\mathrm{mol\,m^{-3}}$	concentration
c_p	$\mathrm{J\,mol^{-1}\,K^{-1}}$	heat capacity
Ca	–	Capillary number, $Ca = \frac{\eta\, u}{\sigma}$
$\mathcal{D}$	$\mathrm{m^2\,s^{-1}}$	dispersion coefficent
D	–	dispersion
D	$\mathrm{m^2\,s^{-1}}$	diffusion coefficent
d	m	diameter
E	–	efficiency
E_A	$\mathrm{J\,mol^{-1}}$	activation energy
F	–	relative catalyst activity
f	–	exposed metal surface area
Fr	–	Froude number, $Fr = \frac{u}{g\, d}$
g	$\mathrm{m\,s^{-2}}$	standard gravity, $9.81\,\mathrm{m\,s^{-2}}$
Ga	–	Galileo number, $Ga = \frac{OFA^3\, d_P^3\, \rho_L^2\, g}{\eta_i^2\,(1-OFA)^3}$
ΔH_R	$\mathrm{J\,mol^{-1}}$	reaction enthalpy
h	$\mathrm{W\,m^{-2}\,K^{-1}}$	heat transfer coefficient
He	–	Henry coefficient
k	$\mathrm{m\,s^{-1}}$	mass transfer coefficient
k	$\mathrm{s^{-1}}$	reaction rate constant
k_0	$\mathrm{s^{-1}}$	frequency factor
ka	$\mathrm{s^{-1}}$	mass transfer coefficient
L	m	length
	–	slope of linear function
M	$\mathrm{kg\,mol^{-1}}$	molar mass
m	kg	mass
n	–	number of moles
N_A	$\mathrm{mol^{-1}}$	Avogadro number, $6.022 \times 10^{23}\,\mathrm{mol^{-1}}$
n_c	–	number of carbon atoms
OFA	–	open frontal area, void fraction

Δp	Pa	pressure drop
P	$\mathrm{bbl\,d^{-1}\,m^{-3}}$	productivity
p	Pa	pressure
Pr	–	Prandtl number, $Pr = \frac{\eta\, c_p}{\lambda}$
$\tilde{r}$	$\mathrm{mol\,g_{cat}^{-1}\,s^{-1}}$	mass specific reaction rate
R	–	peak area ratio
R	$\mathrm{J\,mol^{-1}\,K^{-1}}$	ideal gas constant, $8.3144\,\mathrm{J\,mol^{-1}\,K^{-1}}$
r	$\mathrm{mol\,m_{cat}^{-3}\,s^{-1}}$	volume specific reaction rate
Re	–	Reynolds number, $Re = \frac{\rho\, u\, d}{\eta}$
Re_ε	–	specific Reynolds number, $Re_\varepsilon = \left(\frac{\varepsilon\, d_P^4\, \rho_L^3}{\eta_L^3}\right)^{\frac{1}{3}}$
S	–	selectivity
Sc	–	Schmidt number, $Sc = \frac{\eta}{\rho\, D}$
Sh	–	Sherwood number, $Sh = \frac{k\, d}{D}$
St	–	Stanton number, $St = \frac{h}{u\, \rho\, c_p}$
T	K	temperature
TOF	$\mathrm{s^{-1}}$	turn-over frequency
TOS	h	time on stream
u	$\mathrm{m\,s^{-1}}$	velocity
$\dot{V}$	$\mathrm{m^3\,s^{-1}}$	volumetric flow rate
V	$\mathrm{m^3}$	volume
We	–	Weber number, $We = \frac{\rho\, u^2\, d}{\sigma}$
X	–	conversion
X_G	–	modified Lockhart-Martinelli ratio, $X_G = \frac{u_G}{u_L}\sqrt{\frac{\rho_G}{\rho_L}}$
x_m	–	mass fraction
x_n	–	molar fraction
x_v	–	volume fraction
x_{cat}	–	catalyst volume per channel volume
y	m	internal coordinate inside the catalyst
z	m	axial coordinate

Greek Letters

α	–	chain growth probability
β	–	phase saturation
δ	m	thickness
ε	–	porosity
ε	$\mathrm{W\,kg^{-1}}$	specific power input
η	–	catalyst effectiveness factor
η	Pa s	dynamic viscosity

λ	$\mathrm{W\,m^{-1}\,K^{-1}}$	heat conductivity
ν	–	stochiometric factor
ϕ	–	Thiele modulus
Ψ	–	dimensionless slug length
ρ	$\mathrm{kg\,m^{-3}}$	density
σ	$\mathrm{N\,m^{-1}}$	surface tension
σ	$\mathrm{nm^2\,atom^{-1}}$	area per surface atom
τ_{mod}	$\mathrm{kg_{cat}\,s^{-1}\,m^{-3}_{SG,STP}}$	modified residence time

Subscripts

app	apparent
av	available
ax	axial
BET	Brunauer-Emmet-Teller
$bubble$	bubble
cat	catalyst
$cell$	cell
ch	channel
$char$	characteristic
eff	effective
ext	external
f	film
$feed$	feed
fri	friction
G	gas
GL	gas-liquid
GLS	gas-liquid-solid
GS	gas-solid
h	hydraulic
hs	hydrostatic
in	inlet
int	intrinsic
$intern$	intern
L	liquid
LS	liquid-solid
max	maximum
mc	monolithic carrier
$mcat$	monolithic catalyst
$mean$	mean
obs	observed

out	out
ov	overall
P	particle
$peak$	peak
$plate$	plate
$pore$	pore
$product$	product
R	reactor
$recycle$	recycle
req	required
S	solid
SG	synthesis gas
$sphere$	sphere
STP	standard temperature and pressure
T	temperature
TP	two-phase
w	wall
wc	washcoat

Abbreviations

FT	Fischer-Tropsch
FTS	Fischer-Tropsch synthesis
SBC	slurry bubble column reactor
FBR	fixed-bed reactor
STR	slurry stirred tank reactor
MLR	monolith loop reactor
MR	monolith reactor
μR	micro reactor